
This is the **accepted version** of the article:

Sorbelli, Leonardo; Alba, David M.; Cherin, Marco; [et al.]. «A review on *Bison schoetensacki* and its closest relatives through the early-Middle Pleistocene transition: Insights from the Vallparadís Section (NE Iberian Peninsula) and other European localities». *Quaternary Science Reviews*, Vol. 261 (June 2021), art. 106933. DOI 10.1016/j.quascirev.2021.106933

This version is available at <https://ddd.uab.cat/record/239759>

under the terms of the  IN COPYRIGHT license

1 A review on *Bison schoetensacki* and its closest relatives through the Early-Middle Pleistocene Transition:
2 insights from the Vallparadís Section (NE Iberian Peninsula) and other European localities

3
4 Leonardo Sorbelli^a, David M. Alba^a, Marco Cherin^b, Pierre-Élie Mouillé^c, Jean-Philip Brugal^d, Joan Madurell-
5 Malapeira^{a,*}

6 ^a Institut Català de Paleontologia Miquel Crusafont, Universitat Autònoma de Barcelona, Edifici ICTA-ICP, c/ Columnes
7 s/n, Campus de la UAB, 08193 Cerdanyola del Vallès, Barcelona, Spain

8 ^b Dipartimento di Fisica e Geologia, Università degli Studi di Perugia, Via A. Pascoli, 06123 Perugia, Italy

9 ^c Musée de Préhistoire Régionale de Menton, 06500 Menton, France

10 ^d Aix-Marseille Université, CNRS, Minist. Culture, UMR 7269 Lampea, MMSH, 13094 Aix-en-Provence cedex 2, France

11
12 * Corresponding author.

13 E-mail address: joan.madurell@icp.cat (J. Madurell-Malapeira).

14
15 ABSTRACT

16 The evolutionary history of *Bison* is a matter of debate due to the scarcity of fossil remains from the
17 earliest members of this clade and the close morphological similarities among species. To clarify the
18 taxonomic status of the earliest stouter bison and their relationships to their putative ancestor, *Leptobos*, as
19 well as other primitive forms traditionally referred to subgenus *Bison* (*Eobison*), we carry out a complete
20 revision of the available European fossil record, with a focus on the forms occurring during the Early-Middle
21 Pleistocene Transition. Emphasis is put on the description of the unpublished *Bison* remains from the
22 Vallparadís Composite Section (VCS), including the sites of Cal Guardiola and Vallparadís Estació (Terrassa, NE
23 Iberian Peninsula). VCS fossiliferous layers yielded one of the richest faunal assemblages from the European
24 latest Early Pleistocene and one of the few European fossil sites covering almost entirely the Early-Middle
25 Pleistocene Transition (1.2–0.6 Ma). The collection comprises thousands of ungulates remains, especially
26 abundant fossils of a large *Bison* species. The morphology of the postcranial sample from VCS fits that of
27 *Bison* (*Bison*) *schoetensacki*, i.e., the earliest stout bisons (*Bison* s.s.) recorded in Europe. We studied more

28 than 200 cranial and postcranial elements with a focus on the metapodial remains. Comparisons were
29 performed with all the available fossil record of Pleistocene Eurasian fossil *Bison* species. We confirm the
30 taxonomic validity of *B. schoetensacki* and recognize distinct eco-morphotypes of European bison between
31 the late Early Pleistocene and the beginning of the Holocene based on the size and proportions of the
32 metapodials. Although the appendicular skeleton shows reliable characters for the diagnosis of different
33 species, the great morphological homogeneity recognized within the genus requires a cautious approach in
34 systematic studies based on postcranial material.

35

36 **Keywords:** *Bison*; Bovidae; Early-Middle Pleistocene Transition; Epivilafranchian; Europe; Quaternary.

37

38 1. Introduction

39 The genus *Bison* Hamilton Smith, 1827 includes two extant species, the North American bison (*Bison bison*)
40 and the European bison or wisent (*Bison bonasus*). Additional extinct species are distinguished, but the
41 evolutionary history of this group is still unclear, mainly due to the difficulty in distinguishing early *Bison*
42 remains from those of its putative ancestor. Nowadays, it is commonly accepted that *Bison* originated during
43 the Early Pleistocene from a species of mid-sized bovid *Leptobos* (e.g., Pilgrim, 1947; Brugal, 1985; Masini,
44 1989; Bukhsianidze, 2005; Martínez-Navarro et al., 2007). During the last century, a large amount of *Bison*
45 remains has been discovered from many European Quaternary sites and several species, or sub-species, of
46 this genus, or sub-genus, have been described fueling the debate regarding the evolutionary history of this
47 group of Bovini (Masini, 1989; Sher, 1997; Bukhsianidze, 2005; Maniakas and Kostopoulos, 2018; Kostopoulos
48 et al., 2018) (Fig. 1).

49

50 1.1. The European record of *Leptobos*

51 The genus *Leptobos* includes medium-sized slender bovids from the whole Villafranchian Land Mammal
52 Age (sensu Rook and Martínez Navarro, 2010), being constantly present in the faunal assemblages from the
53 Late Pliocene to most of the Early Pleistocene across Eurasia (from Iberia to northern China). According to

54 the most recent review (Cherin et al., 2019), this genus includes the following species: *Leptobos brevicornis*
55 and *Leptobos crassus* (China), *Leptobos falconeri* (Pakistan), *Leptobos stenometopon* and *Leptobos merlai*
56 (France and Italy), *Leptobos furtivus* (France and, possibly, Italy), *Leptobos etruscus* (France, Italy, and Spain),
57 and *Leptobos vallisarni* (Italy and China). According to Masini et al. (2013), *Leptobos* species from Europe can
58 be divided into two groups or lineages: one includes *L. stenometopon*, *L. merlai*, and *L. furtivus*; and the
59 other includes *L. etruscus* and *L. vallisarni*. The latter group comprises the younger, larger and more derived
60 *Leptobos* species, which have been considered—not without controversy (Bukshianidze, 2005)—as possible
61 ancestors of bison (Masini, 1989). The dispersal of bison from Asia marks the last occurrences of *Leptobos* in
62 Europe, even if the coexistence between early *Bison* and *Leptobos* seems documented in some late
63 Villafranchian Chinese, Greek-Balkan and Eastern Europe localities (Duvernois, 1990; Tong et al., 2016;
64 Agadzhanyan, 2017; Kostopoulos et al., 2018; Lopatin et al., 2019).

65 66 1.2. *Earliest Asian and European bison*

67 The earliest occurrences of *Bison* date to the Late Pliocene-Early Pleistocene of Southeast Asia (Tong et
68 al., 2016). The poorly-known *Bison (Eobison) sivalensis* from India (3.4–2.6 Ma) and *Bison (Eobison)*
69 *palaeosinensis* from China (ca. 2.6 Ma) share some features with the most derived *Leptobos* species and
70 differ in size and cranial morphology from “true” bison of subgenus *Bison* s.s. (Flerov, 1972; Tong et al.,
71 2016). In some areas of Asia, these primitive bison might have been partially coeval and even co-occurring
72 for some time with *Leptobos*, which eventually went extinct by the end of the Villafranchian (Tong et al.,
73 2016).

74 Flerov (1972) erected the subgenus *Eobison* to include the two aforementioned primitive Asian species as
75 well as the poorly-known *Bison (Eobison) tamanensis* from Europe, first described by Verestchagin (1959).
76 Later on, *Eobison* has been widely used, either as a subgenus (Masini et al., 2013) or as a separate genus
77 (Geraads, 1992), to allocate all the Early Pleistocene small-sized bison remains from Europe. However, this
78 taxonomic arrangement has been recently questioned (Bukshianidze, 2005; Kostopoulos et al., 2018), by
79 showing that *Eobison* is a weakly defined taxon and that some forms previously included in this subgenus
80 should be transferred to *Bison (Bison)* (e.g., *Bison deguili*).

81 The earliest record of *Bison* in Europe is represented by *B. (Eobison) georgicus* from Dmanisi (Georgia;
82 1.76 Ma; Burchak-Abramovich and Vekua, 1994; Bukhsianidze, 2005). Other species from Eastern Europe
83 include the above-mentioned *B. tamanensis*, from the Epivilafranchian (ca. 1 Ma) of the Azov Sea area, and
84 whose taxonomic status is uncertain (being considered a species inquirenda by Kostopoulos et al., 2018), as
85 well as *Bison suchovi* from the late Villafranchian of Dolinskoye (Ukraine; Alekseeva, 1967, 1977), whose
86 taxonomic validity has similarly been questioned (Sher, 1997).

87 The earliest records of the genus *Bison* from Europe include: *Bison* sp. from Venta Micena (Spain; ca. 1.5
88 Ma; Moyà-Solà, 1987; Martínez-Navarro et al., 2011); *B. (Eobison)* sp. from Le Riège (France; ca. 1.4 Ma;
89 Ambert et al., 1996); *B. (Eobison) degiulii* from Pirro Nord and Capena (Italy; ca. 1.6–1.2 Ma; Masini, 1989;
90 Masini et al., 2013); and *Bison* cf. *degiulii* from the Mygdonia Basin (Greece; ca. 1.7–1.2 Ma; Kostopoulos et
91 al., 2018). By the end of the Early Pleistocene, the first “true” large bison appear, being represented by the
92 long-legged *Bison (B.) menneri* from Untermaßfeld (Germany; 1.05 Ma; MIS31; Sher, 1997; Bukhsianidze,
93 2020)—recently included in the subgenus *Bison (Poephagus)* by Bukhsianidze (2020)—and the relatively
94 stouter woodland wisent *B. (B.) schoetensacki* from Le Vallonnet (France; ca. 1.2 Ma; Mouillé, 1992), Durfort
95 (France; ca. 1.0; Brugal, 1995), Mauer (Germany; ca. 0.6 Ma; Freudenberg, 1914), Süssenborn (Germany; ca.
96 0.6 Ma; Flerov 1969) and Isernia La Pineta (Italy; ca. 0.58 Ma; Sala, 1986; Peretto et al., 2015). *Bison menneri*
97 and *Bison schoetensacki* are characterized by derived cranial features, large body size, relatively long limbs,
98 and short and swollen horn-cores. During this same period, *Bison* cf. *menneri* and *Bison (Bison)*
99 *voigtstedtensis* have been respectively recorded from Gran Dolina TD8 and Sima del Elefante TE9c (Spain; ca.
100 1.1–0.75 Ma; Huguet et al., 2017; Van der Made et al., 2017). The taxonomic status of *B. voigtstedtensis*,
101 originally described on the basis of cranial material from Voigtstedt (Germany; ca. 0.7 Ma), has been
102 debated, being considered a subspecies of *Bison (Bison) schoetensacki* by some authors (e.g., Fischer, 1965;
103 Sala, 1986; Brugal, 1995; van Asperen and Kahlke, 2017), and a distinct species by others (e.g., Flerov, 1979;
104 Van der Made et al., 2017).

105 Only by the mid-Middle Pleistocene, the well-known steppe bison, *Bison (Bison) priscus*, with the two
106 subspecies *B. priscus priscus* and *B. priscus mediator*, appears in eastern Eurasia (Kahlke, 1999). This massive
107 species exhibits stouter limbs, larger head, and longer horns than earlier bison, but is overall very

108 polymorphic throughout its chronostratigraphic and geographic range (Kahlke, 1999). The steppe bison
109 dispersed across the whole Holarctic, reaching North America through Beringia and giving rise to the
110 American bison lineages in the Late Pleistocene, as demonstrated by fossil and molecular evidence (Shapiro
111 et al., 2004; Froese et al., 2017). In turn, the extant European wisent *Bison (B.) bonasus* appears during the
112 Late Pleistocene as a possible relative of the steppe bison (Soubrier et al., 2016) or, with more uncertainty,
113 to the woodland wisent, with probable introgression from the auroch (*Bos primigenius*), as testified by
114 recent molecular studies studies (e.g., Palacio et al., 2017; Grange et al., 2018).

115

116 2. The Vallparadís Composite Section

117 The Vallparadís Composite Section (VCS) includes the paleontological open-air sites of Cal Guardiola (CGR)
118 and Vallparadís Estació (EVT), located in the Vallès-Penedès Basin (NE Iberian Peninsula; Madurell-Malapeira
119 et al., 2010, 2017; Fig.1). During the excavations carried out between 1997 and 2008, more than 30,000
120 remains of vertebrates from the late Early to Middle Pleistocene sequences were recovered from CGR and
121 EVT. The two sites are characterized by a depositional setting influenced by the dynamics of an alluvial fan
122 system and the geometry of the Miocene paleorelief. The excavated sediments consist of debris-flows and
123 mud-flows resulting from alluvial fan system dynamics with influence of close colluvial processes.

124 Biochronological, magnetostratigraphic, and U-series-ESR data agree indicate that the VCS ranges from
125 before the Jaramillo paleomagnetic subchron (ca. 1.1–1.0 Ma) to the early Middle Pleistocene (ca. 0.6 Ma;
126 Madurell-Malapeira et al., 2010, 2012, 2014, 2017; Minwer-Barakat et al., 2011). The timespan embraced by
127 the VCS can be divided into four different time intervals (Madurell-Malapeira et al., 2010, 2014, 2017;
128 Minwer-Barakat et al., 2011): (1) pre-Jaramillo (layers CGRD1 to CGRD3); (2) Jaramillo subchron interval,
129 (layers EVT9 to EVT12); (3) post-Jaramillo, Matuyama (layers EVT4 to EVT7 and CGRD4 to CGRD8); and (4)
130 early Middle Pleistocene interval (layers EVT2 and EVT3).

131 The timespan comprised between 1.25 and 0.6 Ma was marked by the onset of new asymmetric
132 glacial/interglacial cycles that affected climate (decrease in temperatures and humidity couplet with
133 seasonality with longer and harsher winters) as well as vegetation structure (long alternations between
134 steppe and deciduous forests) in Europe—the so-called ‘Early-Middle Pleistocene Transition’ (EMPT; Head

135 and Gibbard, 2005; Clark et al., 2006). In the older part of the VCS (ca. 1.1 Ma) the pollen and wood analyzed
136 from CGRD2 suggest a warm-temperate and humid paleoenvironment, indicating the presence of a river or
137 river-marsh ecosystem with a variety of plant groups, from aquatic macrophytes to deciduous trees and
138 grasses. The abundance of hippo remains in this layer is consistent with the inferred fluvial/lacustrine main
139 depositional environment, and the high diversity of large-sized ungulates such as deer, horses, and bison
140 suggest the existence of a wide spectrum of different environments in the surroundings, including
141 woodlands and more open and dry areas (Mijarra et al., 2007). Meso- and microwear analyses performed on
142 a large sample of ungulate teeth from VCS indicate that, since 0.9 Ma (MIS22), the paleoenvironments
143 experienced a substantial change, from the predominance of open dry grasslands with a certain seasonality
144 (Layer EVT12, ca. 1.0 Ma; MIS31) to more humid woodlands with, possibly, an even more marked seasonality
145 (Layers EVT7 and CGRD7; ca. 0.86 Ma; MIS21), in agreement with data from other Southern European coeval
146 sites (Strani et al., 2019).

147

148 3. Materials and methods

149 The VCS bovid sample analyzed herein is housed in the Institut Català de Paleontologia Miquel Crusafont
150 (ICP), Sabadell, Spain. The complete list of specimens is reported Table S1. The stratigraphic provenance of
151 the bovid material is unbalanced: 135 specimens come from CGRD7 and EVT7 (0.86–0.78 Ma); 70 from
152 EVT10 and EVT12 (1.07–0.99 Ma); 14 from CGRD2, CGRD3, and CGRD4 (1.1–1.0 Ma), and 4 from EVT3 (<0.6
153 Ma). The descriptions of dental and postcranial features follow the nomenclature used by Masini (1989), Sala
154 (1986), Sher (1997), and Maniakas and Kostopoulos (2017a). Measurement abbreviations are explained in
155 Table 1 and shown in Fig. 2. Measurements are partially modified from Brugal (1985), Masini (1989) and
156 Maniakas and Kostopoulos (2017a). All measurements were taken with a digital caliper to the nearest 0.1
157 mm. Juvenile specimens are not included in the analyses.

158 Throughout this work we use *Bison* s.l. for all members of the genus *Bison*, and *Bison* s.s. for species
159 referred to the subgenus *Bison* (*Bison*), i.e., excluding those commonly attributed to *Bison* (*Eobison*).

160 Comparative material of *Leptobos* spp. from Upper Valdarno and Olivola (Tuscany, Italy), *Leptobos* aff.
161 *vallisarni* from Pietrafitta (Umbria, Italy) and *Bison schoetensacki* (Isernia La Pineta, Italy) studied by us is

162 housed, respectively, in the IGF, MPLB, and MPPPL—see institutional abbreviations below. Other
163 comparative data were taken from the literature.

164 Z-scores were used to compare dental measurements of the described specimens with those from other
165 samples, box plots of the ratio (%) between tooth width and length (W/L%) and bivariate plots of L vs W
166 were employed to assess the size and proportions of the molars among the different *Bison* s.l. populations.
167 Two shape indices were computed for the humerus to distinguish *Bison* from *Bos* and *Leptobos*: Stampfli's
168 trochlea index (Stampfli, 1963), computed as the ratio (%) between DEAW and TWI; and Lehmann trochlear
169 index (Martin, 1987) computed as the ratio (%) between THI and THm (all measurement abbreviations are
170 explained in Table 1). To distinguish *Bison* from *Bos* metapodials we used an index expressed as the ratio (%)
171 between DEW and DDW (Delpech, 1972). A shape index for the metacarpals was computed as the ratio (%)
172 between PFWI and PFWIm. To quantify the magnitude of sexual dimorphism in metacarpals we applied, to
173 the samples in which putative males and females were recognized, the equation given by Schertz (1936b):
174 $(x_1 - x_2) / x_1 * 100$, where x_1 and x_2 are the average male and female value, respectively, for the selected
175 variable. To identify sources of significant biometric differences within the VCS sample, we performed (1)
176 univariate ANOVA on eight variables (raw values of Lmax, PEW, PET, DW, DT, DEW, DT) for metacarpals and
177 metatarsals from the two main chronologies of VCS (1.07–0.99 Ma and 0.86–0.78 Ma) and (2) a MANOVA on
178 the complete metapodials (metacarpals and metatarsals analyzed separately) based on five variables (raw
179 values of Lmax, PEW, DW, DEW, DEW/Lmax%). Moreover, biometric differences in teeth were assessed by
180 means of an ANOVA based on the W/L% ratio of M2 and M3 (the scarcity of specimens from different layers
181 prevented us to perform the same analysis on other teeth). Significance level set at 0.05. To assess the
182 stoutness of metapodials, bivariate plots of Lmax vs DEW/Lmax % were employed. Log₁₀ ratio diagrams
183 (Simpson, 1941) were constructed based on the average values of seven selected variables of *Bison* samples
184 from various Eurasian sites. The extant *Bison bonasus* was used as a standard of comparison (y=0; data taken
185 from Reshetov and Sukhanov, 1979). Principal component analyses (PCAs) were performed based on
186 metacarpal and metatarsal bones separately to explore the main morphological differences among different
187 extinct *Bison* forms and series. Two sets of variables were used. The first approach relies on seven Mosimann
188 shape variables (Table 2) obtained by log-transforming the ratio between each measurement and the

189 geometric mean of the seven measurements for each specimen (Jungers et al., 1995). The second approach
190 considers eight variables calculated following Scott and Barr (2014), i.e., adjusting each measurement as the
191 log transformed ratio between the measurement and Scott's (2004) metapodial global size variable (MGSV).
192 $MGSV = ((PEW * PET * DW * DT * ABETI * AETm * DEW * (DETm * DETI)^{1/2})^{1/9}$. For consistency, a second
193 multivariate approach was used with the computation of a MANOVA on seven raw variables (Lmax, PEW,
194 PET, DW, DT, DEW, DET). Significance level set at 0.05.

195 Statistical computations were made with PAST v. 3 (Hammer et al., 2001).

196 Institutional abbreviations: AUTH, Aristotle University of Thessaloniki, Greece; GNM, Georgina National Museum, Tblisi (Georgia);
197 HLMD Hessisches Landesmuseum, Darmstadt (Germany); ICP, Institut Català de Paleontologia Miquel Crusafont, Sabadell (Spain);
198 IGF, Museo di Storia Naturale, Sezione di Geologia e Paleontologia, Università di Firenze (Italy); IPHES, Institut Català de
199 Paleoecología Humana i Evolució Social, Tarragona (Spain); IQW, Senckenberg Research Station of Quaternary Palaeontology,
200 Weimar (Germany); IVPP, Institute of Vertebrate Paleontology and Paleoanthropology, Beijing (China); MCM, Musée Cuvier de
201 Montbéliard (France); MNHN, Muséum national d'Histoire naturelle, Paris (France); MPLB: Museo Paleontologico Luigi Boldrini" di
202 Pietrafitta (Italy); MPPPL, Museo di Paleontologia e Preistoria Piero Leonardi, University of Ferrara (Italy); MPRM, Musée de
203 Préhistoire Régionale, Menton (France); MuPA, Museo Archeologico e Paleontologico, Serravalle del Chienti (Italy); NAS, National
204 Alliance of Shidlovskiy "Ice Age Period" "Ice Age Museum", Moscow (Russia); UNIFE, Prehistoric Sciences section of the Department
205 of Humanistic Studies, University of Ferrara (Italy).

206

207 4. Systematic paleontology

208

209 Order Artiodactyla Owen, 1841

210 Family Bovidae Gray, 1821

211 Subfamily Bovinae Gray, 1821

212 Genus *Bison* Hamilton Smith, 1827

213 Subgenus *Bison* Hamilton Smith, 1827

214 *Bison (Bison) schoetensacki* Freudentberg, 1914

215 Figs. 3–8; Figs. S1–3

216

217 4.1. *Referred specimens*

218 The VCS sample includes a total of 90 cranial (Figs. 3–4) and 130 postcranial (Figs. 4–8; Figs. S1–3)
219 remains. See Table S1 for details.

220

221 4.2. *Description*

222 4.2.1. *Horn cores*

223 *Description*^{3/4} Only a well-preserved apical portion of a horn core (IPS92970; Fig. 4c) and several
224 fragments of a basal part of a second horn (IPS92971) were recovered from EVT7 and EVT10, respectively. In
225 IPS92970 the tip curves markedly upward, the section is subcircular, slightly dorso-ventrally compressed in the
226 basal portion. In dorsal view, the horn core is slightly curved backward along the longitudinal axis. The
227 longitudinal grooves along the surface are quite shallow and more pronounced on the ventral side in the
228 proximal portion. Narrower, shorter, and shallower furrows are present on the dorsal portion of the tip.
229 IPS92971 is severely fragmented. The estimated large diameter and the presence of sinuses on the internal
230 side of some fragments suggest that the remains represent the basal portion of the horn core. Relatively deep
231 furrows are present on the external ventral surface. No further characters are recognizable.

232 *Remarks and comparisons*^{3/4} Bovid horn cores are very variable, also within *Bison*. Early bison species
233 (e.g., *B. menneri*) are characterized by short horns that emerge backward (i.e., inserted caudally) and
234 commonly taper abruptly, whereas the more derived species (e.g., *B. priscus*) have longer, laterally inserted,
235 and more gently tapering horn cores (Sala, 1986). *Bison schoetensacki* shows an intermediate morphology.
236 Even if these features are relatively stable, it must be taken into account that the size, shape, and position of
237 horn cores in *Bison* spp. are strongly influenced by sexual dimorphism and ontogenetic stage. This may cause
238 erroneous taxonomic attributions of fossils, especially based on small samples. The horn cores from VCS are
239 too fragmentary to substantiate a determination to species rank, mainly because their basal portion is not
240 preserved. However, the two available specimens (especially IPS92970) exhibit some features (ventral furrows
241 in the middle portion of the horn core, smaller dorsal furrows on the tip, dorsoventral compression of the horn
242 core, and backward bending of the tip) that have previously been described by Sala (1986) and Brugal (1995)

243 for *B. schoetensacki*. However, at the state of the art, we cannot exclude that similar characters were also
244 present in some species of *Bison* (*Eobison*), for which the morphology of the horn cores is still largely unknown
245

246 *4.2.2. Dentognathic remains*

247 The studied specimens include a large number of isolated teeth, a few fragmentary mandibles, and a
248 maxillary fragment (Figs. 3–4; Table 3). Almost all the specimens come from layer EVT7. The cheek teeth are
249 typically bovine in overall morphology, mesiodistally elongate, moderately hypsodont, and have well-
250 developed styles/stylids.

251 *Description of the upper dentition*³⁴ The P2 is mesially tapering and narrow relatively to length. The
252 parastyle is pointed, the paracone rib is relatively marked, and the metastyle is faint (Fig. 3f). The P3 is
253 mesiodistally elongate (Fig. 3g) whereas the P4 has squarerocclusal contour (Fig. 3h). In the P3 and P4, the
254 parastyle and metastyle are similar in size and somewhat protruding on the labial side (more markedly in the
255 P4). The paracone rib is not particularly protruding. A small fold can be observed in the inner recess on the
256 lingual margin of the P3. In the M1 the mesial lobe is slightly narrower buccolingually than the distal one,
257 whereas in the M2 the two lobes are similar in width, and in the M3 the distal lobe is markedly narrower. The
258 cement is visible in most of the molars, concentrated on the lingual walls and less abundant on the buccal side
259 (e.g., IPS93005). The styles are strong and prominent, with the parastyle and metastyle being the equally
260 developed. The mesostyle, which is somewhat distally oriented, is generally the most developed. In the M3,
261 the metastyle protrudes distally. The entostyle is relatively high and cylindrical in lingual view, and in most
262 cases shows an ovoid occlusal section (only in a few specimens it has an irregular occlusal outline). In most
263 specimens, the cement penetrates deeply between the entostyle and the two lobes, isolating the entostyle
264 from the protocone and the metaconule. In some specimens, the central cavities have a simple crescent-
265 shaped enamel outline, while in other cases the enamel shows a fold in the middle of the distal wall of the
266 central cavities. This “bubaline fold” (after Masini, 1989), if present, is deeper in the distal central cavity. A
267 small enamel islet is present between the two lobes in several specimens (e.g., IPS93032, IPS93018).

268 *Description of the lower dentition*³⁴ Only two p4 are preserved in the entire sample. The parastylid is
269 large and relatively sharp, curved toward the lingual margin. The lingual wall has three vertical grooves of

270 varying depth. The entoconid is well developed and slightly curved distally. The distal margin of the tooth is
271 flat. The molars have cement both lingually and buccally. Like in the upper molars, the cement is concentrated
272 on the lingual inner walls between the protoconid and hypoconid. On the buccal wall, cement is absent in most
273 specimens. The stylids are very prominent; the parastylid and entostylid (especially in the m1 and m2) are
274 similar in size; in the m3, the parastylid is prominent (mesially projecting). The m3 ectostylid, located between
275 the protoconid and the hypoconid, is slightly mesiodistally flattened, with an ovoid occlusal outline; in some
276 teeth, the ectostylid is located on the distal portion of the protoconid, whereas in others it is more shifted
277 distally, between the two lobes. The recess filled by the enamel between the entostylid and protoconid is
278 deeper and generally narrower than that of the hypoconid internal flange. In the less worn m1 and m2, the
279 entostylid and the parastylid are slightly bent distally. In the m3, the labial recess between the hypoconulid
280 and the hypoconid is deep and narrow.

281 *Remarks and comparisons*³ 82 out of 86 dental remains from the VCS were unearthed from layer
282 EVT7, dated to ca. 0.86 Ma. The teeth are relatively homogeneous both in size and shape. This is also confirmed
283 by the one-way ANOVA results performed on the W/L% ratio of M2 and M3 from the two main VCS
284 chronologies, that is, sin-Jaramillo (EVT10 and EVT12) and post-Jaramillo (CGRD7 and EVT7) (Table 4).
285 Generally, their morphology is typically “bisontine”, with a square and buccolingually wide occlusal contour,
286 especially the upper teeth. Decades ago, bison tooth size and shape were considered taxonomically relevant
287 (e.g., Merla, 1949; Flerov, 1969; Sala, 1986). However, based on our experience, we concur with Sher (1997)
288 that tooth morphology is strongly influenced by the degree of wear and, hence, is not particularly diagnostic,
289 especially when working with small samples. Nevertheless, some characters such as enamel penetration in the
290 inner lingual wall of the upper molars, entostyle development, and tooth size overall can give some taxonomic
291 hints. The presence of a “bubaline fold” in the upper molars from the VCS is variable, as in other bovines (e.g.,
292 it is absent in *Proamphibos*, but variably developed in *Leptobos*, and subject to individual variation in *Bos* and
293 *Syncerus*; Merla, 1949), and thus of little taxonomic value. The VCS upper molars are distinctly swollen just
294 above the cervix, as often in *Bison*, but unlike in *Bos* (where this feature is almost entirely absent; Sala, 1986).
295 However, a less-developed swelling is present in some *Leptobos* specimens from Upper Valdarno and Olivola,
296 thus only unequivocally distinguishing *Bos* from *Leptobos* and *Bison*. In contrast, cement is commonly present

297 on the lingual side of the teeth from the VCS (especially in old individuals), and even on the buccal side in some
298 specimens, whereas in *Leptobos* cement is almost entirely absent (Masini, 1989; Demirel and Mayda, 2014).
299 The abundance of cement is very variable among European *Bison* populations (Sher, 1997)—e.g., it is lacking
300 in *B. priscus* from Taubach but present in *B. menneri* from Untermassfeld. The presence of an enamel islet in
301 the upper molars between the protocone and the hypocone distinguishes *B. (Eobison)* spp., *B. menneri* and *B.*
302 *schoetensacki* from *B. priscus* and *Bos primigenius*, where it is rare (Prat, 1968; Sala, 1986) although these
303 islets are relatively common in recent *B. bonasus* populations. The VCS sample displays this character in almost
304 all the teeth with a medium-advanced wear stage, fitting the morphology of *B. schoetensacki* from Isernia and
305 other European sites (Sala, 1986).

306 Average values of tooth length and width for the analyzed *Bison* samples (Table S2) show that there is
307 a general overlap between all the considered species. The L vs W diagram and the box-plots of the ratio W/L%
308 of m3, M1, M2, and M3 (Fig. S1) help us to compare the size and proportions of *Bison* s.l. teeth. The extremely
309 massive *B. priscus* from Taubach features large teeth (especially m3) (Fig. S1a–d) but with low values of W/L%,
310 i.e., teeth are narrow as compared with total length (Fig. S1e–h). *Bison* cf. *priscus* from Westbury shows long
311 and very wide teeth (Fig. S1a–d). The *B. schoetensacki* specimens from Le Vallonnet, Cromer Forest-bed and
312 the few remains from Durfort are characterized by general smaller size (especially the M1s from Durfort; Fig.
313 S1b), but higher values of W/L%, i.e., relatively more squared teeth (Fig. S1e–h). The Isernia m3s and M3s are
314 quite stout and relatively large (Fig. S1a, d, e, h), whereas the Süssenborn specimens are elongated with very
315 low values of W/L%, similar to those of *B. menneri* from Untermassfeld and *B. priscus* from Taubach (Fig. S1a–
316 h). The *B. menneri* remains display a high degree of variation but, generally, are among the narrowest teeth
317 analyzed (Fig. S1). The bovid from Mygdonia basin also shows high variation (see, for instance, the M1 biplot
318 and box-plot; Fig. S1b, f), overlapping with almost every other sample. The *B. (Eobison)* teeth from Pirro are
319 among the shortest and stoutest (Fig. S1). The teeth from VCS appear short and relatively wide, compared
320 with the othersamples examined, showing proportions similar to those of *B. schoetensacki* from Le Vallonnet,
321 Cromer forest-bed, and Durfort (Fig. S1). On the other hand, the VCS teeth differ from those from Isernia and
322 Süssenborn, which feature larger size and more elongated proportions. Some specimens from VCS (e.g., the
323 single M3 from EVT3; IPS93023) display a quite short and stout morphology, similar to that shown by the older

324 remains of *B. (Eobison) degiulii* from the Italian Peninsula. The z-scores computed for the VCS sample (Table
325 S3) show negative values in most instances for the length of the upper molars and the m3 compared with the
326 other *Bison* populations, being similar to the specimens from Venta Micena, Mygdonia basin, and Le Vallonnet.
327 On the contrary, for the width, z-scores are positive in most cases, showing that the VCS sample has relatively
328 wide molars, also compared with the large form of *B. priscus* from Taubach (Table S3, Fig. S1).

329

330 4.2.3. *Vertebrae*

331 *Description*³⁴ An axis (IPS114551), another cervical vertebra (IPS107615), and four fragmentary
332 thoracic vertebrae (IPS92954, IPS92955, IPS92956, IPS118117) were recovered from VCS (Fig. S2; Table S4).
333 The axis is quite high and elongate, and displays a low spinous process directed dorsally. The transverse
334 foramina are small and located on the posterior portion of the lateral expansions. The neural canal is teardrop-
335 shaped in anterior view. The lateral expansions of the anterior articulation are quite prominent and have a
336 circular anterior outline. The anterior part of the neural process and the transverse processes are broken.

337 The cervical vertebra IPS107615 is short and massive, with subcircular neural canal, and robust pre-
338 and postzygapophyses. Most of the spinous and transverse process and part of the vertebral body are
339 missing. Its general morphology indicates that it could be one of the last cervical vertebrae due to the
340 anteriorly prominent prezygapophysis, the enlarged postzygapophysis, the position of the transverse process
341 (directed anter-oposteriorly to dorso-ventrally) and the reduced posterior tuberculum of the ventral crest.

342 The thoracic vertebrae display smaller bodies with subcircular anterior and posterior rib facets. The
343 neural canal is large and slightly compressed dorso-ventrally. The left transverse process is broken in IP92954,
344 and both transverse processes are missing in IPS92956 and IPS92954. In IPS92956, the foramina on the left side
345 are absent, but there is a narrow, deep groove between the transverse process and the posterior rib facet.
346 The spinous process is inclined posteriorly; in IPS92954, it is almost complete (about 400 mm high).

347 *Remarks and comparisons*³⁴ The five vertebrae from VCS have the typical morphology of large bovids.
348 It is noteworthy that the extremely long spinous process of the thoracic vertebra IPS92954 exceeds the height
349 recorded for any species of *Leptobos* and *Bos*. According to Sher (1997), the tallest spinous process recorded

350 for *B. menneri* is ca. 360 mm, whereas in some specimens of *B. priscus* from Siberia it exceeds 600 mm. Apart
351 from this character, no other vertebral features are helpful in distinguishing *Bison* from either *Leptobos* or *Bos*.

352

353 *4.2.4. Scapula*

354 *Description*³⁴ See Fig. 4d and Table S5. IPS107637 is almost complete, although slightly fragmentary
355 and lacking the distal margin, while IPS92922 only preserves the glenoid cavity and a proximal portion of the
356 blade. The glenoid cavity is subovoid, with its major axis oriented antero-posteriorly. The lateral margin of the
357 cavity is slightly concave in distal view. The acromion, partially preserved in both specimens, is not particularly
358 pointed. The spine, almost complete in IPS107637, is relatively sharp in the proximal half and constituted by a
359 flat surface in the distal half (about 80 mm of width), which displays a small, shallow groove that runs along
360 the lateral surface up to the distal margin. The incisura scapulae is straight and relatively deep. The
361 supraglenoidal tubercle (only preserved in IPS92922) is large, displays a rough surface, and slopes dorsally
362 from the edge of the glenoid. There is a narrow groove on the medial surface of the collum scapulae between
363 the glenoid cavity and the supraglenoidal tubercle. The infraglenoidal tubercle is developed postero-ventrally
364 and located on the medial side of the bone, just above the glenoidal margin.

365 *Remarks and comparisons*³⁴ The two scapulae from VCS closely resemble each other in size and shape,
366 and fit well with the morphology of large Bovids, especially *Bison* (eg., glenoid cavity more rounded in *Bos*).
367 The dimensions of the glenoid cavity in the VCS specimens fall within the variation ranges of the smallest
368 species of *Bison* (i.e., *B. menneri* and *B. bonasus*; Table S6).

369

370 *4.2.5. Humerus*

371 *Description*³⁴ Six humeri from the VCS are available (Fig. 5a–b; Table S7). They only preserve the distal
372 epiphysis and, in some cases, part of the diaphysis. The distal epiphysis is massive and has the typical bovid
373 morphology, with a large trochlea divided by a crest shifted toward the lateral margin. The medial margin of
374 the trochlea is proximodistally higher than the lateral, thus the trochlea in anterior view tapers lateralward.
375 The large groove and the crest that separate the two epitrochleae are located slightly lateral to the distal
376 articulation midline. On the lateral margin of the trochlea, a large and bulging trochlear crest is present. The

377 coronoid fossa is a mediolaterally wide. The olecranon fossa is deep, relatively narrow, and medially and
378 laterally delimited by strong crests that slightly converge distally. On the lateral surface of the shaft, at the
379 contact between the diaphysis and distal epiphysis there is a rough half-moon-shaped ridge. The lateral
380 trochlear pit (which is absent on the medial side) is large and deep.

381 *Remarks and comparisons*³⁴ The VCS humeri are morphologically homogeneous, except for the
382 differences in overall size and robusticity, which are attributable to sexual dimorphism. The presumably male
383 specimens IPS50672 and IPS114549 display a larger distal epiphysis than the rest of the sample, which are
384 likely female. The humerus of *Bison* s.s. generally resembles that of *Leptobos* and *B. (Eobison)*, except for the
385 larger distal ends of the former and some small differences in the trochlear elements (see below). The distal
386 epiphysis of the VCS humeri falls within the size variation of *Bison*, in particular *B. schoetensacki* and *B.*
387 *menneri*, being slightly smaller compared to *B. priscus* (Table S8). Several studies have attempted to find
388 diagnostic characters in the humerus, focusing on the distal epiphysis, to distinguish *Bison* from other large
389 bovids such as *Bos*. The humeri of *Bos* and *Bison* are markedly polymorphic (Martin, 1987; Sher, 1997), but
390 according to Martin (1987) the two genera differ in the proportions between the medial and lateral
391 epitrochleae (affected by the position of the trochlear crest), the shape of the trochlear crest, and the shape
392 of the olecranon fossa. In particular, *Bison* has parallel trochlear margins and a smoother outline of the
393 trochlear crest, whereas *Bos* has a higher crest, a deeper trochlear groove, and generally irregular dorsal and
394 ventral edges of the trochlea (Stampfli, 1963; Sala, 1986). However, we concur with Sher (1997) that this last
395 difference is not reliable. The VCS specimens show a wide range of variation in this character (e.g., sharp in
396 IPS50672 and smooth in IPS107620), indicating it has no diagnostic value. The proportions between the lateral
397 and medial epitrochleae, as measured by Stampfli's trochlea-index (Stampfli, 1963), is extremely variable in
398 the VCS sample and the analyzed comparative sample (including *Leptobos*, *Eobison*, *Bison*, and *Bos*), indicates
399 great overlapping (Table S9). The lateral tapering of the trochlea has been proposed as a diagnostic character,
400 as measured by the Lehmann trochlear index (Table S10), although it is proved similarly undiagnostic (Sher,
401 1997). In the VCS sample, this index has the widest range of variation among the analyzed samples (ranging
402 between 62.9 and 76.5), although on average it most closely resembles the values displayed by the smallest
403 taxa (*Eobison* and *B. menneri*; Table S10).

404 4.2.6. *Radius*

405 *Description*³⁴ Radii are among the most common and best-preserved long bones found in VCS (Fig. 406 5c-d and Table S11). The ulna is fused with the radius in all studied specimens except IPS39893 and IPS92916. 407 The lateral tuberosity of the radius, which has an antero-posterior diameter roughly similar to the proximo- 408 distal one, forms an obtuse angle with the distal epiphysis. The dorso-medial and medial portions of the 409 proximal epiphysis form a clearly protruding shelf with a square proximal outline. The posterior contour of the 410 proximal articulation is slightly undulated, forming an obtuse angle with the lateral edge. The outline of the 411 lateral glenoid cavity is dorsally convex, being more or less deep depending on the specimen (e.g., gentle and 412 shallow dorsal convexity in IPS13570, deep and almost angular in IPS48775). Distal to the lateral glenoid cavity, 413 on the lateral part of the posterior portion, there is a wide depression of variable depth and, medially, a rough 414 area. The notch between the two proximal glenoid cavities is wide and shallow (V-shaped in IPS48775). When 415 preserved, the articular surface for the ulna is well visible in the middle of the proximal diaphysis of the radius, 416 being wide and rough. On the anterior surface of the distal epiphysis there is a grooved area for the tensor 417 tendon, parallel to the diaphysis and delimited medially and laterally by blunt crests. The distal epiphysis is 418 inclined posteriorly and shows a circular pit at the medio-distal end, surrounded by radial rugosities. The 419 fissure marking the contact between radius and ulna in the distal diaphysis is well visible (e.g., in IPS107628 420 and IPS92919). The articular surfaces for the scaphoid and semilunar are particularly deep in the anterior 421 portion, edged posteriorly by two pits. Between the ulnar articular surface and the pointed styloid process 422 there is a wide and deep notch. On the medial side of the distal end there is a small bulge for the metacarpal 423 carpal ligament, more developed in the largest specimens (IPS92916, IPS39893, and IPS92918) than in the rest 424 of the sample.

425 *Remarks and comparisons*³⁴ The radii from the VCS show the typical morphology of *Bison*. They can 426 be distinguished from the ones of *Bos* based on several characters, including: the poorly developed lateral 427 tuberosity of the proximal epiphysis, the wide and shallow notch between the two proximal glenoid facets 428 with a smooth posterior outline, and a fissure marking the contact between ulna and radius (Brugal, 1983; 429 Sala, 1986; Gee, 1993; Sher, 1997). These characters are also present in *Leptobos* spp. (Masini, 1989) which 430 nevertheless show smaller and slenderer radii. The VCS radii display stout proportions as showed by the

431 diagram of stoutness (built as the ratio between proximal epiphysis width and total bone length VS the total
432 length; Fig. 9c), especially when compared with *Leptobos* and *Eobison*. The VCS radii are similar in size to those
433 of *B. menneri* and *B. schoetensacki*. The aforementioned index of stoutness indicates that VCS specimens
434 overlap with those of *B. schoetensacki*, being slenderer than those of *B. priscus* (which is characterized by a
435 very stout radius, i.e., wide diaphysis and epiphyses) but slightly more robust than those of *B. menneri* (which
436 displays similarly long radii but with lower width values; Table S12).

437

438 4.2.7. *Ulna*

439 *Description*³⁴ Three almost complete ulnae are available from EVT and CGR (IPS39893, IPS107616,
440 IPS107617; Fig. 5c–d; Table S13), all of them paired with the corresponding radii. The olecranon process is
441 large and square, gently inclined posteriorly with respect to the long axis of the bone. The medial and lateral
442 surfaces of the olecranon are slightly concave. The ulnar shaft is posteriorly concave. The medial articular facet
443 for the radius is subrectangular and concave. The radius lateral articulation is latero-medally wide, divided into
444 two facets by a small crest, one distal to the other. The proximal facet is subtriangular and almost flat, while
445 the distal facet is subcircular and concave. The semilunar notch is large and has a small pointed tip at the distal
446 margin which reaches the medial articulation facet for the radius.

447 *Remarks and comparisons*³⁴ There are no substantial differences between the VCS ulnae and those of
448 *Bos* and *Bison* (Table S14). Even if some authors noted some minor differences between these genera
449 (Bibikova, 1958; Gee, 1993; Brown and Gustafson, 2000), the only clear difference relates to the articulation
450 between the radius and the ulna (Gee, 1993; Sher, 1997): in *Bison*, the lateral articulation with the radius is
451 wide and does not intrude into the postero-proximal part of the radius, whereas in *Bos* this facet is shaped as
452 an elongated triangle that deeply intrudes into the radius. The VCS sample displays the former condition,
453 although with some degree of variation, as already noticed in *Bison* spp. by Sher (1997).

454

455 4.2.8. *Carpal bones*

456 Only very few carpal bones are available from the VCS collection (Fig. S3; Table S15), mostly from layer
457 EVT10 (IPS92960, IPS92961, IPS92962, IPS92963). Morphological description and comparisons of large bovid

458 carpal bones are often neglected in literature (Sher, 1997); moreover, the few studies performed are
459 sometimes contradictory and do not agree on the measurements to be taken (Bibikova, 1958; Stampfli, 1963;
460 Sala, 1986; Sher, 1997). For these reasons, only a short description and comparison are presented for these
461 anatomical elements. The lack of *Leptobos* material precludes comparisons with this genus, while no
462 differences in size or shape were found among *Bison* species.

463 *Pyramidal (carpi ulnare)*³⁴ The laterally S-shaped morphology of the pyramidal, with an elongated
464 distal portion, is typical of *Bos* and *Bison*. According to Sala (1986), the proximal margin of the facet for the
465 unciform in *Bison* has a smaller radius of curvature as compared with *Bos* (Stampfli, 1963; Sala, 1986). This is
466 disproved by the two pyramidal bones from the VCS, which display a quite wide radius of curvature, as well as
467 by the pyramidal of *B. menneri* figured by Sher (1997), who emphasized the high degree of variation in the
468 population from Untermassfeld.

469 *Semilunar (carpi intermedium)*³⁴ The only specimen recovered from VCS is partially broken. Its
470 morphology does not differ from that of *Bison* and *Bos*. Sala (1986) evidenced some differences regarding the
471 proximal and distal facets, which are hard to recognize in our sample due to the fragmentary state of the fossil.
472 The comparison of IPS92961 with the *Bos* and *Bison* spp. semilunars figured by Sala (1986: Figs. 11–12) does
473 not highlight appreciable differences, although the VCS single specimen more closely resembles the *B.*
474 *schoetensacki* sample from Isernia.

475 *Unciform (os carpale IV)*³⁴ According to Sher (1997), this bone is extremely variable in size within a
476 single population of *Bison*. This is confirmed by the two specimens from VCS, which are similar in shape, but
477 differ in size (IPS92962 is about 25% larger than IPS92964). This variation might be due to sexual dimorphism.
478 Their morphology fits well with that described for *Bison* (Sala, 1986), being quite different from the one of *Bos*
479 (i.e., the more rounded shape of the axial edge in the proximal articular facet of *Bison*).

480 *Capitatotrapezoid (os carpale II+III)*³⁴ The poor state of preservation of the single available
481 capitatotrapezoid does not allow a detailed description or comparisons.

482

483 4.2.9. *Metacarpal*

484 *Description*^{3/4} All the VCS metacarpals are stout (Fig. 6a–c; Table 5). The proximal and distal epiphyses
485 have almost the same width. Four specimens (of which two complete: IPS107626, IPS92910 from EVT12) are
486 slenderer than the remaining ones, most probably due to sexual dimorphism (see Section 6.3.). The proximal
487 articular surface displays a D-shaped outline in proximal view. The lateral articular facet is triangular and
488 located on a lower plane than the medial articular facet, being separated from it by a high crest oriented
489 antero-posteriorly. In some specimens the lateral facet is characterized by a small depression on the anterior
490 margin (e.g., IPS92907, IPS92909, IPS92908). The medial facet is larger and subsquare. Its medial outline varies
491 from subcircular to square. The synovial fossette is a variably developed irregular pit located in the middle of
492 the medial facet (not visible or very small in IPS92912, IP92911, and IPS14985). The proximal epiphysis is
493 marked by a bulging ridge that follow the articular surface, interrupted in the posterior margin by a U-shaped
494 small notch that corresponds to the proximal nutrient foramen, which is located at the posterior margin of the
495 crest that separates the two proximal facets. On the lateral margin of the ridge cited above, there is a
496 subrectangular facet for the fifth metacarpal. The postero-proximal nutrient foramen is teardrop-shaped and
497 located in the middle of a deep rough depression. This depression does not extend onto the posterior portion
498 of the diaphysis, which is almost flat. In anterior view, the diaphysis is generally wide and hourglass-shaped,
499 with the narrowest mediolateral diameter located in the distal half of the diaphysis. The vascular groove on
500 the distal portion of the diaphysis shows a great variation, from narrow and shallow to wide and deep; its
501 deepest part is located just proximally to the distal epiphysis, and the groove always stops distally to the
502 midshaft. The distal anterior foramen is always present, although variable in size, located within the vascular
503 groove just above the distal end of the groove itself. The distal portion of the diaphysis displays marked
504 epitrochlear tubercles (sensu Sher, 1997), so that the maximum width between them almost equals that
505 measured across the trochleae. There is a constriction between each tubercle and the distal end of the
506 corresponding trochlea. The intertrochlear margins tend to converge distally. The distal trochlear crests
507 (intercondylar crests) are subparallel to distally convergent. Two deep depressions are present proximally to
508 either side of each trochlear crest. The two outer depressions are larger and deeper than the inner ones. The
509 lateral and medial trochlear pits are deep and marked by radial rugosities.

510 *Remarks and comparisons*³⁴ The metacarpals from VCS are characterized by similar morphologies with
511 some exceptions. Two specimens (IPS107626 and IPS92910) from EVT12 are particularly slender, with
512 narrower diaphysis and epiphyses than most of the sample, although two proximal epiphyses (IPS14102 and
513 IPS14702) from CGR7 show similar dimensions. This is most likely attributable to sexual dimorphism, which is
514 quite common in bovids and normally implies that females have slenderer metapodials than males (Sher, 1997;
515 Brugal and Fosse, 2005; Kostopoulos et al., 2018). The one-way ANOVA test, performed on 8 eight selected
516 variables of the specimens coming from the two main VCS chronologies of VCS (EVT10-EVT12 and CGRD7-
517 EVT7) shows that, except for the maximum length, no significant differences were found (Table 4). It is
518 noteworthy that one of the specimens (IPS14917) from layer CGRD2 displays a pathological bone outgrowth
519 (of unknown etiology) along the medial margin of the distal shaft, which reaches the epiphysis and expands in
520 a large and thick bone outgrowth on the posterior portion of the diaphysis. A similar malformation is also
521 present in one intermediate phalanx (IPS16778) from the same layer and given their corresponding size it
522 might belong to the same individual. A MANOVA between the two main subsamples from VCS (i.e., specimens
523 divided by stratigraphic provenance), performed on five variables, does not evidence significant differences
524 between the two groups (Table 4). The aforementioned metacarpal IPS14917 was not included in the ANOVA
525 and MANOVA because it is the only metacarpal from the pre-Jaramillo layers. Nonetheless, the "stoutness"
526 diagram and the PCA clearly show the overall similarity between this specimen and the rest of the sample
527 (particularly the specimens from EVT7-CGRD7; see below).

528 Given their abundance in the fossil record and distinctive features, metacarpals are the most
529 diagnostic postcranial bones for bovines and thus those most frequently used for taxonomic purposes in the
530 literature (Table S16). *Bison* s.l. is readily distinguished from *Bos* based on the diaphysis distal end (contact
531 between the diaphysis and distal epiphysis; Schertz, 1936a, 1936b; Lehman, 1949; Bibikova, 1958; Stampfli,
532 1963; Ayrolles, 1973; Brugal, 1983, 1985, 1995; Sala, 1986; Gee, 1993; Sher, 1997). Our analysis performed on
533 several samples of Pleistocene large bovids shows that the ratio between DDW and DEW (Delpech, 1972) is a
534 very useful tool to distinguish *Bos* and *Bison/Leptobos*, with the former showing significantly lower values
535 (Table S17). In *Bison*, this area has marked tubercles, so that the width of the bone is roughly equal to, and
536 sometimes even greater, than maximum distal width; on the contrary, in *Bos* the epitrochlear inflation is less

537 pronounced and the distal end gently curves, following the distal margins of the hourglass-shaped diaphysis
538 being quite medio-laterally thinner than the distal epiphysis width. According to our observations, the *Bison*-
539 like distal inflation is also present in the *Leptobos* sample. Despite some minor individual variation, the
540 specimens from VCS resemble the condition of the *Bison/Leptobos* group. According to many authors (e.g.,
541 Schertz 1936a, b; Bibikova, 1958), the medial facet of the proximal articular surface would be quadrangular in
542 *Bos*, and more rounded and medio-laterally developed in *Bison*. However, this feature is very variable (Sher,
543 1997), as shown by the VCS sample, where it ranges from rounded (e.g., IPS13928, IPS13547) to square (e.g.,
544 IPS14072, IPS92913). Nevertheless, the ratio between the diameters of the lateral and medial facets
545 distinguishes *Bison* from *Leptobos*, with the latter displaying a relatively wider lateral facet. The *Bison* sample
546 from VCS overlaps the mean values of the *Bison* s.l. group (Table S18).

547 The VCS metacarpals, despite some variation, are quite heavily built, especially the male specimens.
548 They are more robust than those of *B. menneri*, and longer and stouter than those of *Leptobos* or *B. (Eobison)*
549 spp., but less massive than those of *B. priscus*, and most similar to those of *B. schoetensacki* (Table S16). Our
550 "stoutness" diagram (Fig. 9a) indicates that, despite some overlap, the VCS metacarpals (especially the
551 specimens coming from EVT7, CGRD2, and CGRD7 from EVT12) fall within the variation range of *B.*
552 *schoetensacki* from various localities (Süssenborn, Mauer, Mosbach, Le Vallonnet, Durfort, and Cromer Forest-
553 bed) although some large specimens (IPS107636, IPS107635, and IPS92907) also resemble those of female *B.*
554 *priscus*. The curves established by the Log_{10} ratio diagrams (Fig. 9e-g) confirm these results, as the VCS bison
555 is characterized by a trend that closely resembles *B. schoetensacki* samples.

556 The PCAs highlight the considerable overlap between different *Bison* samples. In the first PCA (Fig.
557 10a, Table S19), PC1 (60% variance) is mostly driven by Lmax (negative scores) and, to a lesser extent, mvDW,
558 mvDEW and mvPEW (negative scores), separating slender with relatively elongated metacarpals, toward the
559 negative values, from stout and short metacarpals at the opposite portion of the diagram, characterized by
560 robust structures. *Bison priscus* and *B. schoetensacki* display the most positive scores, whereas *Leptobos* and
561 *B. (Eobison)* spp. show the most negative values. PC2 (14% variance) is mostly driven by mvDT and mvDW
562 (negative scores) and by mvPET, mvPEW, mvDET and mvDEW (positive scores); thus, the specimens with wide
563 and thick shaft have negative values, while the ones with a narrow diaphysis but robust epiphyses are

564 characterized by positive values. The VCS sample (positive, for PC1 and negative for PC2, in all the male
565 specimens except for IPS14917 ad IPS13928 which have positive PC2 values) is characterized by stout
566 metacarpals with a massive distal epiphysis and relatively large diaphysis. The specimens overlap with the *B.*
567 *schoetensacki* in both PCs. The two VCS female specimens are located at the edges of the *B. schoetensacki*
568 convex hull, close to the Durfort and Süssenborn female specimens and overlapping with the *Eobison* group.

569 The second PCA (Fig. 10b, Table S20), based on Scott and Barr's (2014) method, shows no substantial
570 differences relatively to the first PCA. PC1 (58% variance) is affected principally by reLmax and reDW, and
571 separates long metacarpals with a relatively narrow diaphysis (positive scores) from shorter but stouter
572 metacarpals (negative scores). PC2 (14% variance) is mostly influenced by reLmax and the stoutness of the
573 shaft (reDW and reDT) regarding positive scores, while it is negatively affected by the dimensions of the
574 proximal epiphysis (rePET and rePEW), thus segregating long metacarpals with a wide diaphysis (positive
575 scores) from short metacarpals with a massive proximal epiphysis (negative scores). The VCS specimens display
576 negative scores for both PCs, except for the single female specimen (IPS107626, which displays a positive for
577 PC1), and cluster with the *B. schoetensacki* and *B. priscus* scatter of points. The only exception is IPS13928,
578 which is characterized by an extremely stout distal epiphysis and hence overlaps with the lower range of *B.*
579 *priscus* from UK for PC2. The main convex hull of VCS is bordered below by the single metacarpal from
580 Süssenborn and above by the remains from Le Vallonnet and Mauer/Mosbach. The MANOVA performed
581 among the VCS sample, other species of *Bison* s.l., and *Leptobos etruscus* shows that the Iberian sample is
582 characterized by significant differences from all the others, with the exception of those attributed to *B.*
583 *schoetensacki* (Table S21).

584

585 4.2.10. *Tibia*

586 *Description*^{3/4} A partial tibia (IPS107618) lacking the proximal epiphysis is the most complete specimen
587 from the VCS, whereas the rest of the sample is composed of distal fragments (Fig. 8; Table S22). The medial
588 malleolus is variably developed (from poorly marked in IPS92943 to strongly developed in IPS92942). It extends
589 distally below the trapezoidal process, separating the two articular grooves. The area immediately anterior to
590 the medial malleolus is characterized by a raised tubercle. The anterior malleolar facet is inclined anteriorly.

591 The posterior surface of the distal diaphysis is slightly convex. Between the medial malleolus and the
592 subtriangular process separating the two articular grooves, there is a shallow furrow that extends up to the
593 shaft ending distally to the midshaft (in IPS92942, this furrow is deeper than in the others and delimited by
594 two crests, the medial one being sharper). The lateral margins of the two malleolar facets are concave dorsally
595 and separated by a deep U-shaped notch. The lateral articular groove is antero-posteriorly longer but
596 mediolaterally narrower than the mesial one. The anterior margin of the lateral articular groove is pointed and
597 more anteriorly protruding than the mesial groove. Conversely, the posterior margins of the two grooves lie
598 almost at the same level. The postero-medial corner of the medial groove forms a right angle. In all the
599 specimens but IPS92943, on the posterior margin of the medial malleolus there is a marked a step. The lateral
600 malleolus is more developed than the medial and hosts the anterior and posterior malleolar facets. The
601 subcircular anterior facet is small and slightly concave, while the subtriangular posterior facet is larger and
602 more concave than the anterior one.

603 *Remarks and comparisons*³⁴ The VCS tibiae attest to marked sexual dimorphism, with male specimens
604 (IPS107618, IPS92942, IPS114546) being larger and more robust than female ones (IPS92940, IPS92943). Gee
605 (1993) recognized several diagnostic criteria between the tibiae of *Bos* from *Bison*. However, we found that
606 the most reliable lies in the two facets for the malleolus (Brugal, 1985; Sala, 1986; Sher, 1997). In *Bos*, the
607 facets are often confluent, and the anterior one is quite smaller and flatter than the posterior one. The VCS
608 tibiae depart from this morphology and more closely resemble *Bison*, where the two facets are well separated
609 by a marked notch and the anterior facet is concave to some extent. The size of the distal epiphysis in the VCS
610 sample fits within the variation of *Bison* spp. (Table S23).

611

612 4.2.11. *Astragalus*

613 *Description*³⁴ See Fig. 7a–b and Table S24. The bone is large and stout, and the mediolateral diameter
614 is always larger than half of the maximum proximodistal length. The proximal lateral trochlea is wider and
615 higher than the medial one. The intertrocLEAR notch is narrow and smooth, and ends distally in a deep and
616 rough fossa. The distal trochleae are more similar to each other than the proximal ones, although the lateral
617 one is slightly wider. The distal intertrocLEAR notch is wider and shallower compared to the proximal one.

618 There is a small tubercle between the proximal and distal trochleae along the medial margin of the bone. Most
619 of the posterior surface of the talus is occupied by the wide and subrectangular calcaneal articular facet. This
620 facet is delimited dorsally by a transversal groove. The posterior margin of the calcaneal facet is separated
621 from the distal trochlea and the central tarsal facet by a deep and narrow L-shaped groove. The angle between
622 the two segments of this groove is slightly higher than 90°. The cubonavicular facet is located at the
623 distomedial corner of the calcaneal facet and is delimited laterally by a step, which is less marked in IPS92952
624 and IPS92951 than in the remaining specimens.

625 *Remarks and comparisons* The VCS astragali are homogenous in size and shape, with the only
626 exception of IPS92951, which is slightly smaller and slenderer than the others. The astragalus exhibits several
627 diagnostic features that distinguish *Bison* from *Bos* (Schertz, 1936a; Bibikova, 1958; Stampfli, 1963; Brugal,
628 1985; Sala, 1986; Gee, 1993; Sher, 1997). On the posterior side, the groove that separates the calcaneal facet
629 from the central tarsal facet is less accentuated in *Bos* than in *Bison* (Schertz, 1936a) and the L-shaped angle
630 described by this groove is almost right in *Bos* and obtuse in *Bison* (Brugal, 1985; Sala, 1986). These characters,
631 even if somewhat variable in both *Bos* and *Bison*, can help discriminating them based on large samples. All the
632 VCS specimens display a deep and obtuse groove, thus more closely resembling *Bison*. Furthermore, according
633 to Bibikova (1958), *Bos* would also differ from *Bison* in having a longer and thinner prolongation of the
634 calcaneal facet on the lateral side of the astragalus. However, this feature is highly variable in the VCS sample,
635 with some specimens (e.g., IP92953) displaying the supposedly *Bos*-like condition and others (e.g., IPS92949)
636 being instead *Bison*-like. Gee (1993) evidenced that in *Bos* the posterior lateral margin of the astragulus is
637 curved, whereas it is straight in *Bison*. We found that this character is generally reliable, as further shown by
638 the VCS astragalus sample, which shows very straight margins.

639 *Leptobos* and *B. (Eobison)* somewhat differ from *Bison* s.s. in the ratio between the width of the distal
640 trochlea and the total length of the astragalus (Fig. 9), with the former taxa having smaller and thinner bones.
641 However, the ranges given by the DEW/Lmax of all the species referred to *Bison* s.l. overlap widely, making
642 this feature not particularly diagnostic, especially for isolated remains. Within *Bison* s.s., *B. priscus* has larger
643 (both longer and wider) astragali compared to *B. menneri* and *B. schoetensacki*, but there are not many
644 evidence of differences in stoutness (Fig. 9d; Table S25).

646 4.2.12. *Calcaneum*

647 *Description*^{3/4} See Fig. 8c–d and Table S26. The calcaneum body displays an hourglass-shaped anterior
 648 contour, with a constriction just above the subtentaculum tali and a massive tuber calcanei (particularly
 649 developed in IPS13936, IP92946, and IPS92948). The anterior and posterior edges of the tuber are slightly
 650 convergent toward the proximal end which, in medial view, has subrounded margin. The angle between the
 651 calcaneum body and the subtentaculum tali is almost right. The cubonavicular facet is elongate and shows a
 652 sinuous concavity (oriented postero-medially in the proximal half and posteriorly in the distal). The anterior
 653 and posterior margins of the calcaneum are convergent towards the tuber calcanei. The medial surface of the
 654 anterior process bears a large tuberosity, edged posteriorly by a shallow depression. Posterior to the
 655 subtentaculum tali, there is a very small crest (not visible, probably due by taphonomic damage, in IPS92945).
 656 In distal view, the astragalus facet has a subsquare shape. This articulation expands also on the antero-medial
 657 side of the subtentaculum tali and has a semicircular outline. This articulation forms a right angle with the
 658 curved cubonavicular facet. This facet is delimited on the medial margin of the postero-medial subtentaculum
 659 tali by a subtriangular rough area. The facet for the malleolus is concave, in anterior view is proximodistally
 660 elongated and has a subrectangular shape. The anterior process is pointed and projects distally.

661 *Remarks and comparisons*^{3/4} The VCS calcanei come from EVT7, apart from IPS13936, which comes
 662 from CGR-D2. The EVT specimens are morphologically quite homogeneous, except minor differences in the
 663 development of the tuber calcanei, probably related to sexual dimorphism or age. In contrast, IPS13936 is
 664 much larger. Previous studies tried to find diagnostic features in the calcaneum, especially based on the
 665 relative size of the central tarsal and astragalar articular facets (Bibikova, 1958; Stampfli, 1963; Sala, 1986).
 666 However, the size of these facets is extremely variable even within a single bovine population (Sher, 1997) and
 667 thus lacks any taxonomic value. The average dimensions of the VCS calcanei resemble those of *Bison* spp.
 668 (Table S27). Like other postcranial elements, the calcaneum of *Bison* s.s. is generally larger than in the most
 669 primitive species. However, it has to be noted that the calcaneum of female specimens of *B. priscus* and *B.*
 670 *schoetensacki* is much smaller than that of the males, being similar to that of small-sized species of *Leptobos*
 671 and *B. (Eobison)*.

672

673 4.2.13. Other tarsal bones

674 See Fig. S3 and Table S15. As for the carpal bones, very few tarsal bones were recovered from the VCS
675 (one cuneiform and two cubonaviculars). The lack of comparative samples and the scarcity of the material do
676 not allow us to perform proper comparison with other bovid populations.

677 *Cuneiform*^{3/4} The only cuneiform (IPS92965) recovered from VCS comes from EVT10. It is complete,
678 although slightly damaged, and resembles in size and shape those of *Bison* and *Bos* (Sala, 1986: Figs 32, 33).

679 *Central tarsal bone*^{3/4} The two specimens from EVT10 are quite similar to each other. IPS92957 is
680 slightly fragmented in some portions of the proximal and distal surfaces, whereas IPS92958 is complete. The
681 articular facets for the astragalus are ovoid, with the medial facet being slightly larger than the lateral. Overall,
682 their morphology is typical of *Bison* and *Bos*. The comparison with the material of *B. schoetensacki* from Isernia
683 shows that the VCS specimens are quite similar to those from the Italian site.

684

685 4.2.14. Metatarsals

686 *Description*^{3/4} The metatarsals are less abundant and morphologically more homogeneous than the
687 metacarpals in the VCS collection (Fig. 6d-f; Table 6). Half of the specimens are lacking the distal epiphysis and
688 most of them are damaged, but four specimens (IPS92934, IPS92931, IPS107634, and IPS92932) are very well
689 preserved.

690 The medial articular facet is posteriorly concave and shows an irregular pit joined to the posterior
691 margin. The lateral facet is higher and relatively flat. They are separated by a well-developed ridge. Three
692 specimens (IPS92932, IP92933, and IPS92934) show a small bulge in the middle of the medial margin,
693 posteriorly to the medial facet (particularly developed in IPS92932). The posterior articular facet is small,
694 antero-posteriorly short, strongly inclined toward lateral margin, and of variable maximum length. A secondary
695 facet for the articulation with the second metatarsal is present at the postero-medial corner of the proximal
696 epiphysis. There is a small crest along the postero-lateral corner of the articular surface. Two specimens
697 (IPS92932 and especially IPS92932) have a markedly slenderer diaphysis than the rest of the sample. A very
698 small and narrow proximal foramen is still visible only in IPS92931, IPS92936, IPS92937, IPS92938, and

699 IPS107634. The anterior side of the bone is characterized by the well-marked and deep vascular groove. In
700 their distal portion, the edges of the groove are shaped as sharp ridges. There is a secondary, shallower groove
701 located on the dorso-lateral aspect of the proximal portion of the shaft in most of the specimens (although it
702 is very faint in IPS92932 and IPS92932). An elliptical distal foramen is present in all the specimens. In the distal
703 epiphysis, the margins of the intertrochlear space are subparallel to distally convergent. As in the metacarpals,
704 the epitrochlear tubercles are well developed, so that the width at the level of the tubercles is about the same
705 as that measured between the outer trochlear margins. The only notable feature in the posterior side of the
706 proximal epiphysis is the pointed medial corner. Distally next to it, IPS92930 and IPS92932 show a small circular
707 facet, which is also present (although less marked) in IPS107634, corresponding to the posterior articular facet
708 for the second metatarsal. The large proximal foramen is located inside a deep subcircular depression distal
709 to the posterior margin of the proximal epiphysis. The proximal diaphysis is delimited by two crests, the medial
710 being usually stronger than the lateral, which do not extend beyond the proximal third of the shaft. The
711 posterior surface of the diaphysis is slightly concave to flat in its proximal half, where two very shallow
712 longitudinal grooves are present. These two grooves disappear toward the distal portion, which is completely
713 flat. The distal foramen is distinct and elliptical. As in the metacarpals, on the anterior side, proximally to each
714 trochlear crest, two depressions develop, with the outer one being larger and deeper than the inner. The distal
715 epiphysis is slightly curved posteriorly. The lateral and medial trochlear pits are deep and proximally
716 surrounded by radial rugosities. The two trochlear ridges are subparallel relative to the medial and lateral
717 margins of the distal end and converge anteriorly.

718 *Remarks and comparisons* As for the metacarpals, the metatarsals have often been considered
719 diagnostic for large bovids in the literature (Table S28). In the proximal articular surface, the angle between
720 the lateral and medial facets is lower in *Bos* (13–22°) than in *Bison* (22–40°; Schertz 1936a; Sala, 1986; Sher,
721 1997), even if the measurement can be somewhat biased depending on the methods (Sher, 1997). The VCS
722 sample most closely resembles *Bison* in this regard (20–30°). The anterior contact between the two proximal
723 facets is different in *Bos* and *Bison* (Brugal, 1985; Gee, 1993). In *Bos* there is no contact between these two
724 facets, often divided by a narrow channel. In *Bison*, the facets are confluent forming, in most of the cases, a
725 small but sharp ridge (Gee, 1993). In the VCS metatarsals, the two facets are in contact and a clear ridge is

726 present in all the specimens. Nevertheless, the major difference in metatarsal morphology between *Bos* and
727 *Bison* lies at the distal half of the bone. As for the metacarpals, the VCS metatarsals display the typical
728 morphology of *Bison* s.l., where the contact between the diaphysis and the distal epiphysis is medio-laterally
729 inflated (Sala, 1986; Sher, 1997)—so that medio-lateral width at this level is similar or even larger than than
730 that between the trochlear margins—whereas in *Bos* the medial and lateral margins of the distal end are
731 strongly divergent (Table S29).

732 *Bison* can readily be distinguished from *Leptobos* given the possession of larger and stouter
733 metatarsals, but given the considerable variation within *Bison* s.l. it is difficult to find reliable differences
734 among different species (Table S28). The “stoutness” diagram (Fig. 9b) shows that *B. priscus* and *B.*
735 *schoetensacki* have generally heavily-built metatarsals with wider ends compared to other samples, despite
736 considerable variation; in contrast, *B. menneri* has much slenderer metatarsals, while those of *B. (Eobison)*
737 spp. are both smaller and slenderer. Most of the VCS sample displays an intermediate size and slender built,
738 except for two specimens (IPS107634 and IPS92937 from EVT12) that are particularly large and massive, and
739 a quite slender specimen (IPS114553 from EVT7). The ANOVA shows that, although there are some differences
740 between syn-Jaramillo (EVT10 and EVT12) and post-Jaramillo (CGRD7 and EVT7) subsamples, these are not
741 significant for seven out of the eight analyzed variables (Table 4). The “stoutness” diagram and PCAs further
742 confirm that, despite the rather homogeneous morphology of the whole sample, a change from stouter to
743 slenderer metatarsals can be recognized from EVT10-EVT12 to CGRD7-EVT7. The MANOVA on five variables
744 confirms that the relative proportions of the VCS metatarsal sample are not characterized by significant
745 differences (Table 4).

746 As for the metacarpals, the PCAs enable the distinction of various groups of *Bison* s.l. despite
747 considerable overlap. In the first PCA (Fig. 10c, Table S30), based on seven shape variables, PC1 (40%
748 variance), positive scores are mainly influenced by msLmax and, to a lesser extent, msDET, whereas negative
749 scores are mostly driven by msDW, msPEW, and msDEW. In turn, PC2 (21% variance) is mainly determined
750 by msDEW and msDET (positive scores) and msDW, and to a lesser extent Lmax (negative scores). The VCS
751 sample is rather scattered in the diagram. The most massive specimens (IPS107634 and IPS92937),
752 characterized by a relatively stout appearance (short and wide bones), overlap with the bulk *B. priscus* form

753 UK and Taubach (negative PC1 scores). The VCS slender specimens (possibly females) overlap with the more
754 gracile *B. (Eobison)* group and *B. menneri*, which feature positive PC1 values due to their relatively long and
755 narrow diaphysis.

756 In the second PCA (Fig. 10d, Table S31), PC1 (39% variance) is almost totally influenced positively by
757 reMLmax, separating long metatarsals (positive scores) from short ones (negative scores). PC2 (25% variance),
758 on the contrary, separates metatarsals with more massive diaphysis (high positive values of reDT and reDW)
759 from those with a stouter distal epiphysis. The VCS metacarpals partially overlap with *B. menneri* from
760 Untermaßfeld, *B. (Eobison) cf. degiulii* from the Mygdonia Basin, and *B. priscus* from UK, highlighting the high
761 variation of these bones in the VCS sample. The meager comparative data for *B. schoetensacki* do not allow us
762 to further assess the variation of this species. The MANOVA indicates that our sample differs significantly only
763 from the extremely slender samples from Venta Micena and Untermaßfeld (Table. S32). This result obtained
764 for the metatarsals highlight less differences between taxa than the same analyses carried out on metacarpals
765 (see Section 4.2.9), pointing out that the bison hindlimbs are more variable.

766

767 4.2.15. Phalanges

768 *Proximal phalanges* ^{3/4} The proximal phalanges are overall well preserved and morphologically very
769 similar (Fig. S4; Table S33). The abaxial and interdigital margins are parallel so that the width of the phalanx is
770 similar throughout its length. The abaxial tuberosity is more developed than the interdigital one; in IPS14977
771 and IPS92925, the former constitutes a large bulging prominence. Between these tuberosities and the two
772 small sesamoid facets, there are two tubercles separated by a depression of variable depth. A depression,
773 developed mediolaterally, is present in the proximal part of the phalanx, between the posterior tuberosities
774 and the proximal end. In the proximal articulation, the interdigital glenoid cavity is higher and narrower than
775 the abaxial one. The abaxial sesamoid facet is larger and flatter than the interdigital one.

776 *Intermediate phalanges* ^{3/4} See Fig. S4 and Table S33. The shaft of the phalanx is stout and massive.
777 The interdigital surface is concave, while the abaxial is convex. In the proximal articulation, the abaxial glenoid
778 cavity is slightly larger than the interdigital, and both are inclined dorsally and interdigitally. Below the articular

779 surface there is a small depression. The outline of the distal articular trochlea is triangular, with the abaxial
780 lobe larger than the interdigital; the groove that divides the two lobes is inclined dorsally and interdigitally.

781 *Distal phalanges* ³⁴ See Figure S4 and Table S33. In dorsal view, the abaxial margin is convex and the
782 interdigital is almost straight. Proximally, the two glenoid cavities are similar in size and inclined dorsally and
783 interdigitally, aligned obliquely relative to the sagittal plane. Posteriorly to them, a small subtriangular,
784 interdigitally-oriented sesamoid facet is visible. Below the sesamoid facet, there is a deep oblique groove,
785 delimited by a small crest. The abaxial surface is convex while the interdigital one is slightly concave.

786 *Remarks and comparison (Phalanges)* ³⁴ The phalanxes of *Leptobos*, *Bison* and *Bos* are quite similar and
787 no morphological differences were found. Discriminating between forelimb and hindlimb phalanxes, also
788 taking in account the sexual dimorphism in bovids, is not easy. Generally, the forelimb proximal phalanges are
789 shorter and more compact than the hindlimb ones (Revilliod et Dottrens, 1946), which are longer and relatively
790 slenderer (Sala, 1986); shorter and wider according to Sher (1997). The intermediate phalanxes are slightly
791 longer but considerably wider in the forelimbs than in the hindlimbs (Sala, 1986; Sher, 1997). According to Sala
792 (1986) the forelimb distal phalanxes are shorter and broader compared to the hindlimb ones, whereas Sher
793 (1997) states that, on the contrary, the forelimb distal phalanges are longer than the hindlimb ones. The fact
794 that in most cases the phalanges are found isolated make this discrimination difficult, which is further
795 aggravated by the fact that phalangeal measurements are seldom published and not all the authors agree in
796 how to distinguish the manual and pedal phalanges (e.g. Sala, 1986 and Sher, 1997). Regarding the sample
797 from VCS, the lack of comparative measurements, the scarcity of the material, and the lack of associated
798 specimens make it impossible to reliably discriminate between fore and hind phalanges or between male and
799 female specimens.

800

801 **5. Results**

802 *5.1. The VCS sample: taxonomy and morphological variation*

803 Based on the qualitative and quantitative comparisons reported above, it is possible to confidently
804 refer all described remains from the VCS to the same species (Table 4). The analyses performed on the
805 metapodials suggest that two morphotypes are recognizable, characterized by slightly different proportions

806 probably due to ecophenotypic variation (see Section 6.1.). The study performed on the 220 remains allow us
807 to refer the large bovid from VCS to the genus *Bison*. Moreover, the large size and the stout morphology of
808 the limb bones support their assignment to subgenus *Bison*, which includes the largest species of the genus.
809 Some features, such as the relatively slender limbs, most closely resemble the early members of this subgenus,
810 namely *B. menneri* and *B. schoetensacki*, which are first recorded during the Epivilafranchian. The VCS bison
811 differs from the roughly coeval *B. menneri* in the markedly stouter limb bones, as well as the shorter and wider
812 metapodials (in particular, the metacarpals). The steppe bison *B. priscus* is characterized by even more robust
813 proportions (Fig. 9). The partial overlap in metapodial dimensions between the larger and stouter specimens
814 from the VCS and the smaller and slenderer specimens of *B. priscus* probably reflects sexual size dimorphism
815 in the two samples, with male individuals from VCS displaying a similar size to female individuals of *B. priscus*.

816 In sum, the morphological characters of the VCS bison allow the referral of this sample to *Bison*
817 *schoetensacki*, which was the most common bison species in Europe during the Middle Pleistocene, although
818 it originated during the latest Early Pleistocene (Flerov, 1975, 1979). The chronostratigraphic distribution of *B.*
819 *schoetensacki* might span from ca. 1.1 to 0.5 Ma (Grange et al. 2018). *Bison schoetensacki* has been regarded
820 as an early member of the lineage that ultimately led to the steppe bison and extant European wisent (Palacio
821 et al., 2017), but this needs to be clarified further. Although *B. schoetensacki* is quite common in the European
822 fossil record, only a few localities have yielded a large number of fossils, hindering a more detailed assessment
823 of its phylogenetic relationships.

824 The VCS sample is the largest collection of *B. schoetensacki*, together with that from Isernia, thus
825 substantially improving our knowledge on the anatomy of this species and allowing us to provide the
826 reconstruction depicted in Fig. 11. Moreover, almost all the fossils from VCS were recovered from layers dated
827 between 1.1 and 0.86 Ma, thus offering a broader chronological perspective on the morphology of this species,
828 which was likely influenced by major paleoenvironmental changes in the study area (see Section 6.1).

829

830 5.2. *The Leptobos etruscus–Leptobos vallisarni lineage*

831 *Bison* probably evolved in Asia from a derived species of *Leptobos* (Pilgrim, 1947; Tong et al., 2016).
832 Among the described species of the latter genus, *L. etruscus* from the Late Villafranchian of Europe is the

833 largest and one of the most derived, showing some cranial features that closely resemble those of *Bison* s.l.
834 (Masini, 1989; Bukhsianidze, 2005; Masini et al., 2013). The postcranial skeleton of *L. etruscus* is well known
835 thanks to the large collections from Senèze (France), Olivola and Upper Valdarno (Italy). Its metapodials are
836 particularly slender (length reaching 26.5 mm and epiphysis width not exceeding 70 mm; Table S16), being
837 similar in size to those of *B. (Eobison)* (Fig. 10). Other postcranial bones (e.g., radii, astragali) are overall smaller
838 and slenderer than those of *Bison* s.l. (Fig. 10).

839 *Leptobos vallisarni*, which is up to date the only *Leptobos* species reported both in Europe and Asia, is
840 characterized by even more derived features (Masini, 1989). This large-sized species was described by Merla
841 (1949) on the basis of a partial cranium from the Early Pleistocene of the Upper Valdarno, but two almost
842 complete skulls from the Gonghe Basin (central China) testify to the wide geographic distribution of this taxon
843 (Zheng et al., 1985). Unfortunately, the postcranial skeleton of *L. vallisarni* is poorly known. The very rich
844 sample from the late Villafranchian of Pietrafitta (central Italy), which is attributed to *L. aff. vallisarni* (Masini,
845 1989; Gentili and Masini, 2005) and also includes a large number of metapodials, displays a derived cranial
846 morphology that resembles that of *Bison* s.l.—thereby rendering the attribution to *Leptobos* unreliable. A few
847 metapodials from the Upper Valdarno, housed in the Natural History Museum of the University of Florence,
848 have been attributed to this species (Masini, 1989; Masini et al., 2013), but our analysis of the collection
849 suggests that they might had been mixed with material of other *Leptobos* species. For this reason, we refrain
850 from making further assumptions about the limb proportions of *L. vallisarni* until a complete revision of the
851 European *Leptobos* spp. postcranial collections is undertaken.

852

853 5.3. *Early Bison species*

854 The early occurrences of *Bison* s.l. correspond to *B. (E.) palaeosinensis* and *B. (E.) sivalensis* from Asia.
855 While many authors agree on an Asian origin of *Bison* s.l. (e.g., Flerov, 1972; Sala, 1986; Sher, 1997), there is
856 still no consensus on the chronology. The earliest known remains are referred to *B. (E.) cf. sivalensis* from the
857 Upper Siwaliks (northern Pakistan), dated to 3.3–2.6 Ma (Khan et al., 2010). These fossils mostly consist of
858 cranial material, and therefore we did not include them in our comparative analyses. However, the remains
859 attributed to *B. (E.) sivalensis*, apart from the lost holotype cranium, are too fragmentary to confirm that they

860 belong to a single species, particularly in the light of their unclear stratigraphic provenance (Kostopoulos et
861 al., 2018).

862 In turn, *B. (E.) palaeosinensis* is a small-sized and primitive species from the Early-Middle Villafranchian
863 of Asia, whose taxonomic status has been much debated (Teilhard de Chardin and Piveteau, 1930; Skinner and
864 Kaiser, 1947; Tong et al., 2016). The three incomplete crania and several postcranial bones of this species
865 come from different sites of Yushe and Nihowan Basins (China). Our analyses reveal that the metacarpals
866 were short and relatively slender, falling within the *B. (Eobison)* range (Fig. 9). One metacarpal from Nihowan
867 (NIH113; Masini, 1989) displays a slender morphology that fits with *L. etruscus* (Fig. 9), whereas the remaining
868 metacarpals are and being most similar to those of *Bison* sp. from Venta Micena and *B. (Eobison) degiulii* from
869 the Italian Peninsula (Fig. 9). The metatarsals, radii and astragali are small and slender, largely overlapping with
870 *Leptobos* but not with *Bison* s.s.

871 The earliest record of *Bisons* s.l. from Europe corresponds to the small and primitive species *B. (Eobison)*
872 *georgicus*. The remains of this species come from the Late Villafranchian site of Dmanisi (Georgia; ca. 1.77 Ma)
873 and consist of a single neurocranium with horn cores and several postcranial bones (Bukhsianidze, 2005). Our
874 analyses shown that two metacarpals (GNM D2288, GNM D2812) display slender proportions similar to those
875 of *L. etruscus*, whereas another (GNM D3426) is clearly stouter and matches instead the variation of *B.*
876 *(Eobison)* spp. and also overlaps to some extent with *B. schoetensacki* (Fig. 10). The slenderer specimens are
877 about 8% longer than but more than 12% narrower distally than the stouter one. Given that, often, female
878 *Bison* metacarpals are shorter and narrower than those of males (Schertz, 1936a), the aforementioned
879 differences might simply be explained by sexual dimorphism. On the other hand, two complete radii from
880 Dmanisi (GNM D2962, GNM D2165) do not display the elongated and slender morphology of *L. etruscus* but
881 closely resemble that of *Bison* s.l. Taking into account the age of the site, Dmanisi might record the co-
882 occurrence of the last *Leptobos* and earliest of *Bison* s.l. with transitional characters, as already suggested by
883 Kostopoulos et al. (2018), but additional fossils would be required to adequately test such a possibility.

884 A large bovid from Venta Micena (southern Spain; ca. 1.6 Ma) was attributed to *Bison* sp. due to its
885 clearly "bisontine" size and proportions (Moyà Solà, 1987). The metapodials are shorter than those of *L.*
886 *etruscus* but slenderer than those of late forms of *Bison* s.s., resembling the samples of the *B. (E.) degiulii* and

887 *B. (E.) palaeosinensis* (Fig. 9). In metacarpal proportions (Fig. 9a), two specimens (VM-9033 and VM-925) at
888 the upper range of the Venta Micena sample overlap with those of *L. etruscus* from Olivola and Senèze. The
889 rest of the Spanish sample is otherwise quite homogeneous, albeit clearly showing differences attributable to
890 sexual dimorphism in the size and robusticity of the metacarpals. The metatarsals similarly plot with the
891 smaller and slenderer forms (i.e., *Leptobos* and *Eobison*; Fig. 9b). The PCAs, irrespective of the variables used,
892 indicate that the metapodials of the Venta Micena bovid are intermediate between *Leptobos* and *Bison* s.s.,
893 partially overlapping with the former (Fig. 10). The three most complete radii from Venta Micena are quite
894 short and slender, being the smallest ones in our comparative sample (Fig. 9c). The identification of the bovid
895 postcranials from Venta Micena is further complicated by the attribution of cranial remains to both *Bison* sp.
896 and *Hemibos* aff. *gracilis*, of Asian origin (see Martínez-Navarro et al., 2011). A revision of the cranial and
897 postcranial bovid material from Venta Micena is pending, but our morphometric analyses indicate that the
898 metapodials fit well with the morphology of *B. (Eobison)* (Figs. 9–10). On geographic and chronological
899 grounds, the Venta Micena sample might be referable to *B. (E.) degiulii*, but more in-depth analyses would be
900 required to confirm such an attribution.

901 Current knowledge of *B. (E.) degiulii* is limited. The type material includes the partial cranium of an
902 elder individual (holotype) and six metapodials (five metacarpals and one metatarsal) from the latest
903 Villafranchian of Pirro Nord (southern Italy; ca. 1.6–1.4 Ma; Masini, 1989). Masini (1989) also attributed to
904 this species one metacarpal and one metatarsal from Capena (central Italy, Late Villafranchian) and three
905 metacarpals from Sainzelles (southern France, Late Villafranchian, Brugal, 1995). As noted above, the
906 metacarpals of *B. (E.) degiulii* are quite similar to those from Venta Micena, albeit they are slightly shorter
907 and stouter (Fig. 9). The bovid sample from the Mygdonia Basin (Greece), mainly including metapodial
908 remains and a few cranial elements from Kalamoto, Tsiotra Vryssi, Krimni, and Apollonia (dated to between
909 1.7 and 1.2 Ma), was attributed to *B. (E.) cf. degiulii* by Kostopoulos et al. (2018). The marked morphological
910 variation among metapodials was interpreted as the result of an increasing size and stoutness trend in
911 relation to progressive climate deterioration throughout the Late Villafranchian (Kostopoulos et al., 2018).
912 Several metacarpals from the younger locality of Apollonia (ca. 1.2–1.1 Ma) resemble male specimens of *B.*
913 *schoetensacki* in size and robusticity, but most of the sample displays the typical proportions of *B. (Eobison)*,

914 and only two (AUTH APL-677, AUTH KRM) are slightly slenderer and more *Leptobos*-like (Fig. 9). The PCAs
915 performed Maniakas and Kostopoulos (2017a) and Kostopoulos et al. (2018) showed considerable overlap
916 among *Bison* s.l. species, only distinguishing “slender” from “stout” forms. They revealed proportion
917 similarities between the Mygdonia bovid remains and those of *B. menneri* from Untermassfeld, as well as
918 between the latter and *Bison* sp. from Venta Micena. These similarities are also evident from our “stoutness”
919 and Log_{10} ratio diagrams (Fig. 9), which show that *B. menneri* and *B. (Eobison)* spp. mostly differ in size but
920 not in proportions. Kostopoulos et al. (2018) questioned the inclusion of *B. degiulii* into subgenus *Eobison*
921 based on some derived characters of the holotype and the cranium KLT-638 from Kalamoto. If the whole
922 sample from the Mygdonia basin belongs to a single species (Kostopoulos et al., 2018), the postcranial
923 remains further display a mosaic of derived and primitive features, because some metacarpals from
924 Apollonia (AUTH APL-745, AUTH APL-414, AUTH APL-578, AUTH APL-446, and AUTH APL-95) resemble in
925 robusticity the male specimens of *B. schoetensacki* from Mosbach, Durfort, Cromer Forest-bed, and VCS (Fig.
926 9). Nevertheless, our PCAs, ANOVAs and Log_{10} ratio diagrams confirm that, despite some overlap, the
927 Mygdonia sample is distinct from “priscoid” forms and show that, on average, the Greek metacarpals are
928 characterized by relatively shorter and slenderer proportions (Fig. 9e–g, Fig. 10a–b, Table S21). Such results
929 suggest suggeststhat the assignment to *B. (E.) cf. degiulii* by Kostopoulos et al. (2018) is well supported, at
930 least until a more detailed revision of this species is undertaken.

931 Two additional species of *B. (Eobison)* are poorly known. *Bison (E.) tamanensis* from the Taman
932 Peninsula and *B. (Eobison) suchovi* from central Ukraine, erected without a diagnosis by Verestchagin (1959)
933 and Alekseeva (1967), respectively. Both these late Early Pleistocene Eastern European species have a debated
934 taxonomic history and are described on quite scanty fossil material (see Kostopoulos et al., 2018 and
935 references therein). In the light of these issues the taxonomic status of this species cannot be properly
936 assessed and is not discussed in this paper.

937 Unlike the above, *B. menneri* is a well-known species from the German site of Untermassfeld (ca. 1.0
938 Ma; MIS31), being considered one of the earliest members of *Bison* s.s. (Sher, 1997). Bukhsianidze (2020)
939 recently referred this species to the subgenus *Bison (Poephagus)* based on purported closer cranial similarities
940 with extant yaks. The postcranial morphology of *B. menneri* has adequately been characterized (the holotype

941 itself, IQW 1982/17948, is a male metacarpal; Sher, 1997). The species is described as a long-legged bovid with
942 tall appearance, as well as a relatively small head and short horns (Sher, 1997; van Asperen and Kahlke, 2017;
943 Bukhsianidze, 2020). Among large bovids, *B. menneri* has the longest and most slender metacarpals, and
944 displays a mixture of *Bison*-like and, to a lesser extent, *Bos*-like features in the limb bones (Sher, 1997;
945 Bukhsianidze, 2020). The extremely elongated metapodials are similar in proportions to those of *Leptobos* and
946 *B.* (*Eobison*) (Fig. 9a–b), with considerable overlap with the latter in our PCAs (Fig. 10). Nevertheless, Sher
947 (1997) ruled out the possibility that the Untermassfeld bovid could represent a boreal variant of a
948 Mediterranean/Asian *Eobison* species, due to its large size and metapodial built. The most complete skull
949 displays some primitive characters for the bison lineage, such as not very tubular orbits, elongated postcornual
950 portion of the cranium, and horn cores very backwardly orientated. According to Bukhsianidze (2020) these
951 elements are shared with the yak lineage (subgenus *Poephagus*). From the site of Untermassfeld, a juvenile
952 skull and a single metacarpal (IQW 1983/19 253 (Mei. 18 773)) are not referable to the aforementioned
953 species (Bukhsianidze, 2020); indeed, IQW 1983/19 253 (Mei. 18 773) resembles in stoutness the more
954 “priscoid” form *B. schoetensacki* (Fig. 9), although the scanty remains do not enable a specific attribution.
955 *Bison menneri* has also been reported from the North Sea seabed “Het Gat” site (Mol et al., 2003) and,
956 tentatively (*B. cf. menneri*), from layer TE9c of Sima del Elefante (Spain) (Huguet et al., 2017) and from
957 Cimichioi-III and Hadjimus (Moldova) (Croitor, 2016).

958 The three species from east Europe and Asia: *Adjiderebos cantabilis*, *Probison kushkunensis* and
959 *Probison dehmi* (Dubrovo and Burchak-Abramovich, 1986; Burchak-Abramovich, Gadzhiev and Vekua, 1980;
960 Shani and Khan, 1968) are known for isolated cranial remains. Their affinities and relationships with *Bison* s.l.
961 group are still matter of debate, however their transitional morphology from *Leptobos* to *Bison* could shed
962 lights on the first forms of primitive bison.

963

964 5.4. Other samples of *Bison schoetensacki*

965 5.4.1. *Le Vallonnet*

966 The bison remains from *Le Vallonnet* (southeastern France, ca. 1.2–1.1 Ma), which is one of the few
967 European localities that record the earliest Epivillafranchian (de Lumley et al., 1988; Mouillé, 1992; Mouillé et

968 al., 2006; Michel et al., 2017), were attributed to *B. schoetensacki* by Mouillé (1992). The metapodials from Le
969 Vallonnet are characterized by large size and quite slender proportions, resembling material of *B.*
970 *schoetensacki* from the type locality of Mauer, and partially overlapping with the specimens from Mosbach
971 and Durfort (Fig. 9). Sexual dimorphism is particularly pronounced in the Le Vallonnet metacarpal sample, with
972 the putative female specimens (MPRM A8 B2 326 and MPRM B9 BJ7 346) being located on the left portion of
973 the stoutness diagram due to their slenderer morphology (Fig. 9a). Both the Le Vallonnet and the Mauer
974 samples partially overlap with that of *B. menneri* from Untermassfeld, which they resemble in the elongated
975 diaphysis and relatively narrow distal epiphysis, despite the larger diaphysis (Fig. 9a). Other postcranial bones
976 from Le Vallonnet, such as astragali and humeri, are within the size range of *Bison* s.s., even though the
977 astragali are slightly stouter than in other samples of *B. schoetensacki* (Fig. 9d). The two complete metatarsals
978 (MPRM B6278(G) and MPRM E7C186(D)) from Le Vallonnet most likely belong to large males, due to their
979 heavily-built morphology. Indeed, B6278(G) is one of the largest specimens in the entire sample of *B.*
980 *schoetensacki* and falls within the range of "priscoid" forms (Fig. 9b). Based on the Log_{10} ratio diagrams, PCAs,
981 and pairwise comparison, the sample of metacarpals from Le Vallonnet is similar to those of *B. schoetensacki*,
982 except for some diaphyseal measurements that appear relatively wider and thicker (Figs 9–10). Overall, the Le
983 Vallonnet sample fits well with the variation of *B. schoetensacki*, and in particular with the large morphotype
984 represented by the Mauer sample thereby confirming the presence of this species before the Jaramillo
985 subchron. Together with the specimens described here from roughly coeval VCS layers (CGRD2), they
986 represent the first occurrences of *B. schoetensacki*, conclusively indicating that *Bison* s.s. was recorded in
987 Europe since the Villafranchian-Epivilafranchian boundary.

988

989 5.4.2. Durfort and La Vassyére

990 The bison sample from Durfort (southwestern France; ca. 1.0–0.5 Ma) was referred to *B. schoetensacki*
991 on the basis of cranial (horn cores) and metapodial features (Brugal, 1995). The metapodials are
992 morphologically intermediate between those of *B. menneri* and *B. priscus*, and resemble the earlier fossils of
993 *B. schoetensacki* from Le Vallonnet at a slightly smaller size (particularly the metacarpals; Fig. 9). The
994 "stoutness" and Log_{10} diagrams and both PCAs (Figs 9–10) indicate that the Durfort sample fits with the

995 variation of *B. schoetensacki*, resembling the stout forms from Mosbach and the VCS—as the male specimens
996 (MNHN 010 D, MNHN 107 G, MNHN 105 G, MNHN 104 G) approach the “priscoid” scatter, and the putative
997 female specimens (MNHN 106 G, MNHN 108 G) overlap with *B. (Eobison)* (Figs 9a, 10a–b). The analysis of
998 metatarsals (Figs 9b, 10c–d) shows the same pattern, with the material from Durfort being intermediate
999 between the “priscoid” and slenderer forms. Our results confirm the attribution of the Durfort sample to *B.*
1000 *schoetensacki*, being characterized by slightly stouter metapodial proportions than the material from Le
1001 Vallonnet and Mauer, and most similar to the VCS bovid (Figs. 9–10). From the Early Pleistocene site of La
1002 Vassyére (southern France; ca. 0.6) several remains of a large bovid were recovered. The fossils were
1003 attributed to *Bison* cf. *schoetensacki* (Brugal and Fosse, 2003). The general morphology and proportions of the
1004 only complete metacarpal fit perfectly with the variation of *B. schoetensacki* (Fig. 9).

1005

1006 *5.4.3. Mauer and Mosbach*

1007 *Bison schoetensacki* was originally described by Freudenberg (1914) on the basis of remains from
1008 Mauer (Germany; Middle Pleistocene, ca. 0.4 Ma). The holotype is a partial cranial vault (which was lost during
1009 World War II; Sala, 1986), but Freudenberg (1914) also referred to the same species other cranial and few
1010 postcranial remains from Mauer and Cromer Forest-bed, and to *B. cf. schoetensacki* an almost complete skull
1011 from Mosbach. Multiple studies on this species have not entirely clarified its diagnostic features (e.g.,
1012 Hilzheimer, 1918; Schertz, 1936a, b; Skinner and Kaisen, 1947; Flerov, 1969; Sala, 1986; Sher, 1997; Drees,
1013 2005). Sala (1986) described the cranial anatomy of *B. schoetensacki* based on the remains from Mauer and
1014 Isernia (Italy; Middle Pleistocene, ca. 0.55 Ma), but for the postcranium only summarized the most important
1015 differences between *Bos* and *Bison*. In contrast, Sher (1997) focused on metapodial proportions and rejected
1016 the common misconception that *B. schoetensacki* was a small-sized *Bison* (Sher, 1997), improving the original
1017 description given by Freudenberg (1914), in which only the relative slenderness of the limbs and the small
1018 horn cores were stressed.

1019 During the last century, the material from Mauer and Mosbach was scattered across more than five
1020 different institutions. We managed to measure some of the specimens, while for others we relied on the few
1021 published measurements (Freudenberg, 1914; Schertz, 1936a, b; Sher, 1997). However, it should be taken into

1022 account that the collections from Mauer/Mosbach might mix two different species, *B. schoetensacki* and *B.*
1023 *priscus* (Schertz, 1936a, b; Sher, 1997). Their stratigraphic context is not clear, especially for Mosbach in which
1024 two different levels with different ages and faunas are recognized (Breda and Marchetti, 2005), and both sites
1025 include layers dated to 0.6–0.5 Ma (Wagner et al., 2010; Kahlke et al., 2011), close to MIS11–9 (0.4–0.3 Ma),
1026 when the first occurrence of the large and stout *B. priscus* is recorded (Kahlke, 1999). According to Schertz
1027 (1936b) and Sher (1997), most of the material from Mosbach and some specimens from Mauer would indeed
1028 belong to *B. priscus*. This idea derives from the assumption that *B. priscus* has long metacarpals, whereas, in
1029 fact, the various well-known populations of *B. priscus* from Eurasia (except the gigantic ones from Taubach,
1030 Romain la Roche and, possibly, Tiraspol) are characterized by very short and extremely stout metacarpals (e.g.,
1031 North Sea, Krasny Yar, Roter Berg, Chumysh, Kiputz IX, among others)—a misconception already remarked by
1032 Van der Made (2017). Furthermore, Sher (1997) did not consider the samples from Le Vallonnet and Durfort,
1033 which based on both morphology and chronology undoubtedly belong to *B. schoetensacki* even if they fall
1034 within the variation of most of the specimens that he attributed to *B. priscus*. The “stoutness” biplot, show
1035 that all the metacarpals from Mauer indeed share the same diagram area with other populations of *B.*
1036 *schoetensacki*, being, altogheter with Le Vallonnet sample, among the slenderest ones; whereas the
1037 metacarpals from Mosbach are characterized by a more pronounced stoutness (Fig. 9). Moreover, based on
1038 the specimens morphologically closer to *B. schoetensacki*, our Log_{10} diagrams indicate that the Mauer sample
1039 fits with the characters of *B. schoetensacki* and that the Mosbach specimens feature slightly stouter
1040 metacarpals than that from Mauer and other *B. schoetensacki* populations (Fig. 9). The more massive, *B.*
1041 *priscus*-like proportions of the Mosbach material further agrees with the derived and “priscoid” cranial
1042 features displayed by some cranial remains from this locality (Sala, 1986). In the two PCAs (Fig. 10), the
1043 Mauer/Mosbach metacarpals cluster in the area occupied by the species *B. schoetensacki* and *B. priscus*, with
1044 the Mauer specimens being recognizable by their slenderer proportions. Overall, our results confirm that the
1045 *Bison* sample from Mosbach display an increased robusticity, suggesting the presence of very large *B. priscus*-
1046 like morphologies in the German site. For this reason, we prefer to use open nomenclature when assigning
1047 Mosbach remains to *B. cf. schoetensacki*.

1048 In turn, the few analyzed metatarsals from Mauer and Mosbach are quite heterogeneous. In the
1049 "stoutness" diagrams (Fig. 9), all the Mosbach metatarsals are long and stout, resembling those of *B. priscus*.
1050 In turn, one of the two metatarsals from Mauer (DMSTD in Schertz, 1936b) fits with the variation of *B.*
1051 *schoetensacki*, whereas the other (MAU402) displays an extremely slender structure, similar to that of *B.*
1052 *menneri*.

1053 A complete revision of the cranial and postcranial material from Mauer and Mosbach would be
1054 required: (1) to clarify the diagnosis of *B. schoetensacki* (especially based on the sample from Mauer, which is
1055 the type locality) and (2) to confirm the possible first co-occurrence with larger "priscoid" forms (in the case
1056 of the larger specimens from Mosbach). An earlier co-occurrence of *B. schoetensacki* and *B. priscus* at Mosbach
1057 cannot be ruled out, as it is consistent with our results, which indicate relatively stout metacarpal proportions
1058 with a wide variation in the sample (Fig. 9). Moreover, it has to be considered that, even if most of the Mosbach
1059 material comes from the upper layers (Mosbach 2) roughly coeval to Mauer and Isernia, its lowermost
1060 sediments are dated to around 1.0 Ma (Koenigswald and Tobien, 1987). Unfortunately, the stratigraphic
1061 provenance of the remains was not recorded. Nonetheless, we disagree with Schertz (1936b) and Sher (1997)
1062 and state that the entire sample from Mauer and, possibly, some of the Mosbach specimens, are attributable
1063 to *B. schoetensacki* and not to *B. priscus*.

1064

1065 5.4.4. *Süssenborn*

1066 Flerov (1969) referred the large bovid remains from Süssenborn (Germany; Middle Pleistocene, ca.
1067 0.6 Ma) to two subspecies of *B. schoetensacki* (*B. schoetensacki schoetensacki* and *B. schoetensacki*
1068 *lagenocornis*) based on cranial characters without any reference to the metapodials. *Bison schoetensacki*
1069 *lagenocornis* was subsequently synonymized with the nominotypical one by Sala (1986), who found that the
1070 roughly coeval *B. schoetensacki* from Isernia displayed a range of cranial morphologies that encompassed the
1071 differences between the two purported subspecies, which were reinterpreted as resulting from sexual
1072 dimorphism.

1073 Sher (1997) concluded that the metacarpals from Süssenborn are quite heterogeneous and probably
1074 referable to more than a single species. Indeed, our results (Fig. 9) indicate that three out of five metacarpals

1075 fall in the range of *B. schoetensacki* from Mosbach, whereas one fits within *B. menneri* from Untermaßfeld,
1076 and the remaining one more closely resembles *Bison* sp. from Venta Micena. However, Sher's (1997)
1077 interpretation was based again on a misinterpretation of the size and proportions of *B. priscus* forelimbs. The
1078 "stoutness" diagram and both the PCAs (Fig. 9) shows that the three stoutest metacarpals from Süssenborn
1079 (IQW 1965/2330, IQW 1965/2325, IQW 1965/2319), referred to *B. priscus* by Sher (1997), fit well within the
1080 variation of male specimens of *B. schoetensacki* from Le Vallonnet, Durfort, and the VCS, while the smallest
1081 specimen from Süssenborn (IQW 1965/2331) is also very close to female specimens of *B. schoetensacki* from
1082 the same sites. The only exception is represented by the metacarpal IQW 1965/2333, here attributed to *B. cf.*
1083 *menneri*, which probably comes from earlier deposits than the rest of the assemblage due to the different type
1084 of preservation from most Süssenborn fossils and its extremely elongate and slender morphology. In turn, the
1085 metatarsals from Süssenborn fit quite well with the available sample of *B. schoetensacki* in the "stoutness" and
1086 the PCAs (Figs 9b, 10c-d). In summary, the bulk metapodials from Süssenborn can be confidently referred to
1087 a stout form of *B. schoetensacki*, very similar to those from the VCS and Durfort.

1088

1089 *5.4.5. Isernia and Cesi*

1090 The site of Isernia La Pineta (southern Italy; 0.58 Ma; Coltorti et al., 2005; Peretto et al., 2015) has
1091 yielded a rich sample of *B. schoetensacki* cranial and postcranial remains (Sala, 1986), although no complete
1092 long bones are preserved due to carcass exploitation by hominins (Sala, 1983). The distal epiphysis of some
1093 metapodials (e.g., IS.F.1979.t.3q(1) and IS.I.q.73.t.3(1)) has large mediolateral and anteroposterior diameters,
1094 resembling the proportions of heavily-built forms of *B. schoetensacki*. On the other hand, complete astragali
1095 and calcanei fit well with those of *Bison* s.s. and are overall larger than those of earlier populations of *B.*
1096 *schoetensacki* from Durfort and the VCS (Tables S25, S27). We therefore conclude that the rich sample from
1097 Isernia attests to the presence of a stout form of *B. schoetensacki* in Italy during the earliest Middle
1098 Pleistocene, exhibiting some postcranial features akin to the "priscoid" forms. Among the few remains of *Bison*
1099 from the early Middle Pleistocene site of Cesi (central Italy; Ficcarelli et al., 1997) the most informative is a
1100 complete metacarpal. The size and proportions fit with the ones observed in the *B. schoetensacki* sample in

1101 both the stoutness diagram and the PCA (Fig. 9), confirming that in the early Middle Pleistocene this species
1102 was already populating the Italian Peninsula.

1103 *5.4.6. Cromer Forest-bed, Boxgrove, and Westbury*

1104 The bovids from various sites of the Cromer Forest-bed Formation (eastern UK), Boxgrove and
1105 Westbury (western UK) collectively encompassing the whole early Middle Pleistocene (ca. 0.7–0.4 Ma; Breda
1106 et al., 2010), have been described by several authors (Freudenberg, 1914; Sala, 1986; Breda et al., 2010). Two
1107 horn cores (M/6559 and M/1426) from an unknown locality were attributed to *B. schoetensacki* (Freudenberg,
1108 1914; Flerov, 1969; Sala, 1986), and according to the latest review (Breda et al., 2010) multiple bovids would
1109 be recorded by teeth and a few postcranial remains in the Forest-bed Formation: *B. cf. schoetensacki*, *B.*
1110 *priscus*, and cf. *Bos primigenius*.

1111 The “stoutness” diagram (Fig. 9a) indicates that the metapodials from most of these sites (Boxgrove,
1112 Trimingham, Sidestrand, Ostend, and Palling) fit with the general proportions of stouter *B. schoetensacki* from
1113 Süßenborn, Durfort, Mosbach, and the VCS, whereas the three metacarpals from the yellow breccia of
1114 Westbury-sub-Mendip are stouter and more closely resemble *B. priscus*, as already suggested by Breda et al.
1115 (2010).

1116 The only available complete radius, which comes from Pakefield, fits with the variation of both *B.*
1117 *schoetensacki* and *B. menneri*, while the one from the younger site of Boxgrove falls far from these taxa and
1118 more closely resembles in length and stoutness those of *B. priscus* (Fig. 9a). The two radii from Westbury also
1119 overlap the borders of the “priscoid” variation (Fig. 9c). We therefore conclude that the material from the
1120 Cromer Forest-bed Formation most likely probably belongs to *B. schoetensacki*, whereas the assignment of
1121 the small sample from Boxgrove is more debatable, being attributed here to *Bison* sp. Finally, the Westbury
1122 sample is referred to *B. cf. priscus* due to the stoutness of both radii and metapodials.

1123 *5.4.7. Châtillon-Saint-Jean and Siréjol cave*

1124 Mourer- Chauvire (1972) described a large number of bovid remains from the late Middle Pleistocene
1125 site of Châtillon-Saint-Jean (France). The author referred to *B. schoetensacki* the smaller and slender
1126 postcranial specimens and to *B. priscus* the larger and stouter ones. Our morphometric analyses on the
1127 metacarpals question these attributions. On the whole, the Châtillon-Saint-Jean assemblage is characterized

1128 by the presence of a large bison featuring quite large metacarpals (Fig. 9) and long and very wide diaphysis
1129 (Fig. 10) fitting with the variation of *B. priscus*. The presence of two morphologically distinct groups is here
1130 interpreted as the result of intraspecific differences (i.e., sexual dimorphism) in the same sample of *B. priscus*
1131 (Fig. 9, Table S34), confirming the interpretation of Brugal (1985). The size and stoutness of the Châtillon-Saint-
1132 Jean bison metacarpals resemble those recorded for the very large-sized *B. priscus* from Romain-la-Roche,
1133 referred to *B. priscus* together with the Taubach sample (Flerov, 1976; Vercoutère and Guérin, 2010),
1134 and for the bison from Tiraspol, referred to *B. schoetensacki* by Flerov (1972); and then to *B. aff. priscus* by
1135 Sher (1997).

1136 The sample from the Late Pleistocene cave of Siréjol (France), attributed to *B. schoetensacki* (Guérin
1137 and Philippe, 1971), then reported to *B. priscus* with a nov. ssp. (Brugal, 1985, 1999) is characterized by
1138 relatively short and robust metacarpals. The “stoutness” and Log₁₀ ratio diagrams (Fig. 9) as well as the PCA
1139 (Fig. 10) show that the distal and proximal epiphysis width is larger (relative to total length) than in *B.*
1140 *schoetensacki*, fitting with the variation of *B. priscus*. Nonetheless, the bison from Siréjol is distinguishable
1141 from latest Pleistocene *B. priscus* based on the significantly narrower metacarpal diaphysis compared with the
1142 distal and proximal epiphysis (especially the specimens n°100 000+658, n°100 000+664, n°100 000+665, n°100
1143 000+667, n°100 000+668; Figs. 9–10). This latter difference is particularly interesting in the light of recent
1144 molecular studies (Palacio et al., 2017; Grange et al., 2018), which recognize the Siréjol specimens as
1145 genetically distinct from *B. priscus* and close to the extant *B. bonasus*. Further discoveries from the same site
1146 and/or coeval sites are needed to investigate the intriguing presence of another bison species in the European
1147 Late Pleistocene, hitherto only suggested by molecular data.

1148

1149 **6. Discussion**

1150 *6.1. Metapodials variation within Bison schoetensacki*

1151 The metacarpal IPS14917 from CGRD2 (ca. 1.1 Ma) is quite long and slightly slenderer than the rest of
1152 the sample, which comes from younger layers (ca. 1.0–0.86 Ma). The “stoutness” diagram and Log₁₀ ratio
1153 diagrams (Fig. 9a-e) show that IPS14917 fits with the size and proportions of *B. schoetensacki* from the type
1154 locality of the species, Mauer, and the pre-Jaramillo cave site of Le Vallonnet (ca. 1.2 Ma). The Mauer fauna is

1155 characterized by taxa typical of forest environments (Soergel, 1914; Breda and Marchetti, 2005; Kahlke et al.,
1156 2013), the palynological study performed on the fossiliferous layers of Le Vallonnet suggest that the site might
1157 have been a tree refugia in a period of relatively dry and cold phase. The stout metapodials from EVT10-EVT12
1158 exhibit more “priscoid” proportions, similar to (but overall smaller than) the metapodials of the steppe-
1159 adapted Late Pleistocene *B. priscus mediator*. From EVT12, two slenderer metacarpals were also recovered,
1160 interpreted as the only female metacarpals of the collection. The EVT7-CGRD7 metacarpals are characterized
1161 by less stout limb proportions, similar to the remains from the sites of Durfort, Süssenborn, and Cromer forest-
1162 bed, all sites featuring a mixture of open and forested landscapes (Brugal, 1995; Stuart and Lister, 2001; van
1163 Asperen and Kahlke, 2011).

1164 The lowermost layers of VCS (CGRD2-CGRD4) span from 1.1 to 1.0 Ma (Madurell-Malapeira et al.,
1165 2010). Paleobotanical data indicate that the VCS pre-Jaramillo period was characterized by a relatively warm-
1166 temperate and humid paleoenvironment with a mixture of habitats dominated by wooden landscapes, as
1167 suggested by the abundance of arboreal taxa (Mijarra et al., 2007). This fits with the aforementioned
1168 paleoenvironmental reconstructions of the nearly coeval and geographically close site of Le Vallonnet and of
1169 the younger site of Mauer. The dental wear pattern of the large herbivore remains from the VCS sin-Jaramillo
1170 layers (1.0–0.99 Ma; EVT10-EVT12) points to a generally abrasive diet, suggesting an environment with a
1171 significant predominance of open dry grasslands (Strani et al., 2019). This might explain the stouter and
1172 “priscoid” metapodials unearthed from these layers. The same study, performed on the post-Jaramillo layers
1173 of VCS dated to 0.86–0.78 Ma (EVT7-CGRD7), suggests an increase of average humidity and a relative
1174 expansion of forested habitats, in accordance with the study of the micromammal fauna (Lozano-Fernandez
1175 et al., 2015; Strani et al., 2019). This fits with the Durfort, Cromer Forest-bed, and Süssenborn inferred
1176 paleoenvironments mentioned above. In sum, the metapodial proportions of the VCS *Bison* sample, though
1177 characterized by an overall homogeneous morphology, shows a certain degree of variation when sub-samples
1178 from different stratigraphic contexts are compared. This variation shows a remarkable correlation with the
1179 dominant paleoenvironment conditions reconstructed along the composite section, with an increase of limbs
1180 stoutness corresponding to more arid conditions and slenderness to more humid ones, also tracing the trend
1181 observed in other *B. schoetensacki* samples. A similar interpretation has been even anticipated by Flerov

1182 (1979), who stated that the slenderer and taller forms of *Bison* are better adapted to closed and forested
1183 environments as opposite to the stouter ones, which are more suited to open and arid conditions. This idea is
1184 furtherly confirmed by the extremely slender *B. menneri* from Untermaßfeld and the massive but very tall *B.*
1185 *priscus priscus* from Taubach and Romain-la-Roche, all sites characterized by a mixture of close and open
1186 habitats (Sher, 1997; Argant, 2010; van Asperen and Kahlke, 2011). On the contrary, *B. priscus mediator*,
1187 featuring the typical “priscoid” proportions with short and large metapodials, was one of the most
1188 representative taxa of the so-called Mammoth Steppe fauna during the Late Pleistocene (Kahlke, 1999).

1189

1190 *6.2. The metapodial morphology of Bison schoetensacki*

1191 Our comparative analysis indicate that the metacarpals are the most useful postcranial skeletal
1192 elements for distinguishing the different species of *Bison* s.l. Most of the metacarpals attributable to *B.*
1193 *schoetensacki* are characterized by the following features (ranges based on all the samples attributed to *B.*
1194 *schoetensacki* in Table 16): total length between 225–270 mm, ratio of distal width to total length between
1195 27–34%, ratio of midshaft width to total length between 16–21%, and ratio of proximal width to total length
1196 between 28–36%. In early Middle Pleistocene sites with uncertain chronology and potentially
1197 redeposited/mixed material, such as Mauer, Mosbach, and Süssenborn, some metacarpals fall outside the
1198 aforementioned variation ranges and are not considered in this discussion. With the exception of these
1199 remains and the clearly different *B. menneri* from Untermaßfeld, all the remaining bison samples from
1200 Epivillafranchian-early Middle Pleistocene European sites are distinguishable from earlier and later samples,
1201 and are here referred to *B. schoetensacki*.

1202 Our morphometric data show some morphometric variation both among samples from different localities,
1203 especially for the metacarpals (Fig. 9). This variation is probably due to ecophenotypic changes in limb
1204 robusticity and size through time and space in a single wide-ranging and long-lasting species (see Section 6.1.).
1205 However, excluding these small intraspecific differences, our results show that all the putative *B. schoetensacki*
1206 samples are showing no significant differences. After 0.5 Ma, with the first occurrence of the massive *B.*
1207 *priscus*, it is virtually impossible to discern female *B. priscus* from male *B. schoetensacki* individuals based on
1208 postcranial material, leading to possibly erroneous taxonomic attributions in sites where the two species

1209 purportedly co-occur, particularly in the Middle and Late Pleistocene (e.g., Chatillon-Saint-Jean and Sirejol
1210 cave; Mourer-Chauvire, 1972), but determined as male and female of *B. priscus* (Brugal, 1999; Grange et al.,
1211 2018). This is also relevant in the light of molecular studies (Palacio et al., 2017; Grange et al., 2018; Vershinina
1212 et al., 2019) indicating the presence of various Late Pleistocene *Bison* lineages in Eurasia, which are not easily
1213 distinguishable on morphometric grounds.

1214 *6.3. Sexual dimorphism*

1215 Fifteen complete metacarpals from the sites of Mauer, Le Vallonnet, Durfort, EVT12 of VCS,
1216 Trimingham, and Süssenborn are slenderer and overall smaller than the rest of the sample attributed to *B.*
1217 *schoetensacki* with values of DEW/Lmax% less than 30 (Figs. 9–10). These metacarpals are, here, attributed to
1218 females, indicating a significant degree of sexual dimorphism, as it is frequently observed in large bovids like
1219 bison. To quantify the magnitude of these differences and to assess if it is similar to those recorded for extant
1220 species, we applied the equations by Schertz (1936a) (see Section 3) to all the available samples in which
1221 putative males and females were recognized (*B. schoetensacki* from VCS layer EVT12, Durfort, and Süssenborn;
1222 *B. menneri* from Untermaßfeld; *B. priscus* from Châtillon-Saint-Jean, North Sea, and Krasny Yar; extant *B.*
1223 *bonasus*, and *B. bison*; Table S34). The results obtained for all analyzed EVT12 show that the sample has similar
1224 values to those of the extant and fossil *Bison* species (except for an unusual high value for DW).

1225 In most of the studied localities, including VCS, males represent the majority of the metacarpal record
1226 (e.g., 75% in VCS, 53% in Le Vallonnet, 67% in Durfort, 81% in Taubach, 56% in North Sea), apparently in
1227 contrast with what is observed in extant gregarious large mammals, in which female individuals are normally
1228 more abundant (Gower et al., 2019). This imbalance in the frequency of sex distribution has been reported for
1229 several fossil collections of large mammals, including carnivores such as *Ursus*, and female-herd-based
1230 herbivores such as *Mammuthus* and *Bison* (Pečnerová et al., 2017; Gower et al., 2019). This might be explained
1231 by (1) bias in the fossil collection (e.g., focused on larger remains, especially in historical times), (2) taphonomic
1232 reasons (e.g., greater resistance of larger and more massive skeletal remains against destructive taphonomic
1233 agents), (3) different behaviors between the two sexes (i.e., segregation of males) and/or (4) seasonality factor
1234 for the bone accumulation. Gower et al. (2019) genetically sexed both cranial and postcranial bones belonging

1235 to 186 fossil individuals of *Bison* spp. from several Holarctic sites and found that the sample was composed by
1236 ca. 75% of males, a percentage very similar to that estimated for the VCS sample.

1237

1238 *6.4. Final remarks on the postcranial differences among Leptobos and Bison*

1239 Metatarsals are less diagnostic due to their greater variation, but their distal end is nevertheless useful
1240 to distinguish large and stout *Bison* s.s. from the slenderer *Leptobos* and *B. (Eobison)*. Of the most common
1241 variables used in the literature, only a few are useful to discriminate among *Bison* species (Fig. 10), particularly
1242 metapodial total length, robustness of diaphysis and distal epiphysis width (Scott and Barr, 2014), despite
1243 some overlap. These differences in the proportions of metapodials, and the appendicular skeleton in general,
1244 are often linked to ecophenotypic variation in bovids, and must be therefore taken with caution when making
1245 taxonomic attributions or inferring phylogenetic relationships (Brugal, 1999; Scott and Barr, 2014).

1246 The astragalus is also often used as a diagnostic element for large bovids. The geometric morphometric
1247 analysis of astragali performed by Maniakas and Kostopoulos (2017b) on a large sample of *Bison* suggests that
1248 the shape of this bone is strongly (but not only) related to habitat preferences. Although there are some
1249 differences between the *Bos* and *Leptobos/Bison*, astragalus is not diagnostic enough for reliable taxonomic
1250 distinction between *Leptobos* and *Bison*. Size and proportions of the talus may help in distinguishing large and
1251 stout *Bison* s.s. from small and slender *Leptobos* and *B. (Eobison)*, but the overlap between the ranges of
1252 variation is significant. In our opinion, the radius is one of the more useful long bones to distinguish *Leptobos*
1253 and *Bison*, and also different species of *Bison* s.l. In particular, *B. menneri* and *B. (Eobison)* have significantly
1254 slenderer radii than *B. priscus*, while *B. schoetensacki* is characterized by intermediate proportions (Fig. 9).
1255 Finally, phalanges, carpals, and tarsals (other than the astragalus) can only give some hints on the overall size
1256 and built, but are too homogeneous among large bovids to have any taxonomic value. Similarly, humeri and
1257 tibiae are taxonomically uninformative within the *Leptobos/Bison* group.

1258 Postcranial differences between *Leptobos* and *Bison* almost exclusively relate to dimensions and
1259 proportions. Some of these morphometric differences are also reflected in the identification of distinct groups
1260 within *Bison* s.l., which in some cases correspond to specific taxa. In particular, our results allow us to clearly
1261 distinguish among *B. (Eobison)* (Dmanisi, Venta Micena, Pirro Nord, Capena, Mygdonia Basin), *B. menneri*

1262 (Untermassfeld), *B. schoetensacki*, and early *B. priscus*. In turn, the last two species are very polymorphic,
1263 which results in the identification of local samples with peculiar postcranial proportions and/or dimensions,
1264 e.g., *B. schoetensacki* "slender" (CGRD2 of VCS, Mauer, Le Vallonnet) and "stout" (EVT7, EVT 10, EVT 12, and
1265 CGRD7 of VCS, Durfort, Süssenborn, Cromer Forest-bed, possibly Isernia and Mosbach) forms; *B. p. priscus*
1266 (Taubach, Romain-la-Roche, Tiraspol, Châtillon-Saint-Jean) and *B. p. mediator* (North Sea, Habarra, Kiputz IX
1267 and others) subspecies. At least for the case of *B. schoetensacki* (a deeper look into *B. priscus* is out of the
1268 scope of this manuscript) these differences might be related to ecophenotypic changes related to
1269 paleoenvironmental conditions (Section 6.1). At the state of the art, we are unable to establish, at least for *B.*
1270 *schoetensacki*, whether these differences can be the result of ecophenotypic variation within the same
1271 species, or whether they can correspond to different taxa or evolutive trend. From the late Middle Pleistocene
1272 onwards, the second hypothesis could find indirect support in the recognition of different haplotypes in the
1273 ancient DNA of European bison (Palacio et al., 2017), which to date do not correspond to species defined on
1274 a morphological basis. Regarding *B. priscus*, the two putative subspecies *B. p. priscus* and *B. p. mediator* which,
1275 until now, had been distinguished on the basis of cranial features and size, display substantial differences in
1276 proportions also in the metapodials (especially metacarpals; Grange et al., 2018; Fig. 9).

1277

1278 7. Conclusions

1279 The described bison sample from the VCS is attributed to *B. schoetensacki*. The records of this species in
1280 the lower layers of CGR and the roughly coeval site of Le Vallonnet in France represent the first occurrences
1281 of *Bison* s.s. in Europe, dating to the beginning of the Epivilafranchian (ca. 1.2–1.1 Ma). *Bison schoetensacki*
1282 can therefore be considered a biochronological marker for the beginning of this biochron (Kahlke et al.,
1283 2007; Bellucci et al., 2015), in association with the first occurrence of *Megaloceros savini* (see Madurell-
1284 Malapeira et al., 2019) and the reappearance of *Sus strozzi* in Europe after the latest Villafranchian "suid
1285 gap" (Cherin et al., 2020). According to our results, *B. schoetensacki* was widely distributed across Eastern
1286 and Central Europe (from UK to Italy, and from Iberia to Germany) between 1.2 and 0.6–0.5 Ma,
1287 representing the most common large bovid during the Epivilafranchian and early Middle Pleistocene. In the
1288 absence of sufficiently complete cranial remains, the morphometric analysis on postcranial bones (especially

1289 metapodials) represents the most powerful tool for diagnosing Pleistocene bovine taxa. In particular,
1290 metapodial proportions enable a reliable distinction among the genera *Leptobos*, *Bison*, and *Bos*, as well as
1291 among different *Bison* species. For the two most polymorphic and geographically widespread species,
1292 namely *B. schoetensacki* and *B. priscus*, it is even possible to distinguish several morphotypes, whose
1293 biological meaning (local ecophenotypic variation vs taxonomic differences) should be subject to further
1294 research. The relatively wide range of morphometric variation exhibited by the VCS sample of *B.*
1295 *schoetensacki* may be related to ecophenotypic changes and/or local adaptations in response to
1296 environmental changes that affected the VCS area during the Epivillafranchian (Strani et al., 2019). In
1297 particular, these changes may be related to the important ecological transitions that occurred during the
1298 EMPT. Moreover, the increased size and robusticity observed in the long bones from the VCS intermediate
1299 layers (EVT10 and EVT12) represent the earliest record of “priscoid” characters in *Bison* s.s. at ca. 1.0 Ma.

1300

1301 Acknowledgments

1302 This work is funded by the Agencia Estatal de Investigación–European Regional Development Fund of the
1303 European Union (CGL2016-76431-P and CGL2017-82654-P, AEI/FEDER-UE) and the Generalitat de Catalunya
1304 (CERCA Program). LS is supported by the FI AGAUR fellowship (ref. 2020 FI_B1 00131) funded by the Secretaria
1305 d’Universitats i Recerca de la Generalitat de Catalunya and the European Social Fund. D.M.A. and J.M.M. are
1306 members of consolidated research group 2017 SGR 116 (AGAUR, Generalitat de Catalunya). We would like to
1307 thank Marzia Breda for sending us measurements of the UK bovids; Marisa Blume and Oliver Sandrock for
1308 measurements of the bovids from Mosbach and Mauer; Lionel Cavin and Corinne Charvet for sending us
1309 measures of the bovids from Romain-la-Roche; Paola Romi (Soprintendenza Archeologia Belle Arti e Paesaggio
1310 dell’Umbria) for the possibility to study the Pietrafitta bovid collection at the MPLB; Benedetto Sala and Claudio
1311 Berto for the possibility to study the Isernia bovid collection at the UNIFE and MPPPL; Alessandro Blasetti for
1312 the possibility to study the Cesi bovid collection at the MuPA; Elisabetta Cioppi and Luca Bellucci for the
1313 possibility to study the Valdarno bovid collection at the IGF. Comments by Marzia Breda and an anonymous
1314 reviewer helped to significantly improve the manuscript.

1315 References

1316 Agadzhanyan, A.K., Vislobokova, I.A., Shunkov, M.V. and Ulyanov, V.A., 2017. Pleistocene mammal fauna of
1317 the Trlica locality, Montenegro. *Fossil Imprint* 73, 93–114.

1318 Alekseeva, L.I., 1967. To the history of subfamily Bovinae during the Pleistocene in the European USSR. In:
1319 *Paleontologiya, geologiya i poleznye iskopaemye Moldavii* Vyp. 2. Shtiintsa, Kishinev, pp. 123–127 (in
1320 Russian).

1321 Alekseeva, L.I., 1977. Theriofauna of the Early Anthropocene of Eastern Europe. *Trudy Geol. Inst. Akad.* 300,
1322 1–214 (in Russian).

1323 Ambert P., Brugal J.P., Houles N., 1996. Le maar du Riège (Hérault, France): géologie, paléontologie,
1324 perspectives de recherches. *C. R. Acad. Sc. Paris* 322, 125–132.

1325 Argant, J., 2010. Palynologie des coprolithes d'hyène de Romain-la-Roche (Doubs, France): apport
1326 paléoenvironnemental. *Rev. Paléobiol.* 29, 473–476.

1327 Asperen van, E.N., Kahlke, R.D., 2017. Dietary traits of the late early Pleistocene *Bison menneri* (Bovidae,
1328 Mammalia) from its type site Untermaßfeld (Central Germany) and the problem of Pleistocene
1329 'wood bison'. *Quat. Sci. Rev.* 177, 299–313.

1330 Ayrolles P., 1973. Essai de distinction des genres *Bos* et *Bison* d'après deux métacarpiens. *Etudes*
1331 *préhistoriques* 7, 13–15.

1332 Bellucci, L., Sardella, R. and Rook, L., 2015. Large mammal biochronology framework in Europe at Jaramillo:
1333 the Epivilafanchian as a formal biochron. *Quat. Int.* 389, 84–89.

1334 Bibikova, V.I., 1958. Some distinguishing features in the bones of the genera *Bison* and *Bos*. *Bull. Mosk.*
1335 *Obschetschestwa Isp. Privoda NS Otdel Biol.* 63, 23–35.

1336 Breda, M., Collinge, S.E., Parfitt, S.A., Lister, A.M., 2010. Metric analysis of ungulate mammals in the early
1337 Middle Pleistocene of Britain, in relation to taxonomy and biostratigraphy: I: Rhinocerotidae and
1338 Bovidae. *Quat. Int.* 228, 136–156.

1339 Brugal J.P., -1983. Application des analyses multidimensionnelles à l'étude systématique du squelette des
1340 membres des Grands Bovidés Pléistocènes (Grottes de Lunel-Viel, Hérault); Perspectives évolutives.
1341 Ph.D. Dissertation, Université Aix-Marseille II.

1342 Brugal, J.-P., 1985. Le *Bos primigenius* Boj., 1827 du Pléistocène moyen des grottes de Lunel-Viel (Hérault).
1343 Bull. Mus. Anthr. Préh. Monaco 28, 7–62.

1344 Brugal, J.-P., 1995. Le bison (Bovidae, Artiodactyla) du Pléistocène moyen ancien de Durfort (Gard, France).
1345 Bull. Mus. Natl. Hist. Nat. 16C 2–4, 349–381.

1346 Brugal, J.P., 1999. Etude des populations de grands Bovidés européens: intérêt pour la connaissance des
1347 comportements humains au Paléolithique. In: Brugal, J.P., David, F., Enloe, J.G., Jaubert, J. (Eds.), Le
1348 Bison: gibier et moyen de subsistance des hommes du Paléolithique aux Paléoindiens des Grandes
1349 Plaines, Ed. APDCA, Antibes (1999), pp. 85–104.

1350 Brugal J.P., Fosse P. 2005. Les grands bovidés (*Bison* cf. *schoetensacki*) du site pléistocène moyen de La
1351 Vayssière (Aveyron, France). In: Crégut-Bonouvre, E. (Ed.), Les Ongulés Holarctiques du Pliocène et
1352 du Pléistocène Quaternaire H.S. 2, 75–80

1353 Bukhsianidze, M., 2005. The fossil Bovidae of Dmanisi. Ph.D. Dissertation, Università degli Studi di Ferrara.

1354 Bukhsianidze, M., 2020. New Results on Bovids from the Early Pleistocene site of Untermaßfeld. In: Kahlke,
1355 R.D. (Ed.), Das Pleistozän von Untermaßfeld bei Meiningen (Thüringen). Teil 4. Habelt-Verlag, Bonn,
1356 pp. 1169–1195.

1357 Burchak-Abramovich, N.I., Gadzhiev, D.V., Vekua, A.K., 1994. On a new Pleistocene Bovine from Eastern
1358 Georgia. Teriologii Paleoteriologija 253-261. (in Russian).

1359 Caloi, L., Palombo, R., 1980. La fauna quaternaria di Venosa, i Bovidi. Boll. Geol. It. 100, 101–140.

1360 Cherin, M., D'Allestro, V., Masini, F., 2019. New bovid remains from the Early Pleistocene of Umbria (Italy)
1361 and a reappraisal of *Leptobos merlai*. J. Mamm. Evol. 26, 201–224.

1362 Cherin, M., Alba, D.M., Crotti, M., Menconero, S., Mouillé, P.É., Sorbelli, L., Madurell-Malapeira, J., 2020. The
1363 post-Jaramillo persistence of *Sus strozzii* (Suidae, Mammalia) in Europe: New evidence from the
1364 Vallparadís Section (NE Iberian Peninsula) and other coeval sites. *Quat. Sci. Rev.* 233, 106–234.

1365 Clark, P.U., Archer, D., Pollard, D., Blum, J.D., Rial, J.A., Brovkin, V., Mix, A.C., Pisias, N.G., Roy, M., 2006. The
1366 middle Pleistocene transition: characteristics, mechanisms, and implications for long-term changes
1367 in atmospheric pCO₂. *Quat. Sci. Rev.* 25, 3150–3184.

1368 Coltorti, M., Feraud, G., Marzoli, A., Peretto, C., Ton-That, T., Voinchet, P., Bahain, J.J., Minelli, A.,
1369 Hohenstein, U.T., 2005. New 40Ar/39Ar, stratigraphic and palaeoclimatic data on the Isernia La
1370 Pineta Lower Palaeolithic site, Molise, Italy. *Quat. Int.* 131, 11–22.

1371 Croitor, R., 2010. Critical remarks on genus *Bison* (Bovidae, Mammalia) from Pleistocene of Moldova. *Revista*
1372 *Archeologica* 5, 172–188. (in Russian)

1373 Croitor R., 2016. Genus *Bison* (Bovidae, Mammalia) in Early Pleistocene of Moldova. In: Coropceanu E. (Ed.),
1374 *Materialele Conferinței științifici ce naționale cu participare internațională “Mediul și dezvoltare*
1375 *durabilă”, Ediția a III-a, Chisinau*, pp. 14–20.

1376 David, A.I., Svistun, V.I., 1981. Bison remains from Upper Pliocene and Lower Pleistocene deposits of
1377 Moldova and South Ukraine. In: *Biostratigraphy of Anthropogene and Neogene of South-West of*
1378 *USSR. Shtiintsa*; Kishinev pp. 3–15. (in Russian)

1379 Delpech F., 1972. Fouilles de sauvetage dans le gisement magdalénien de Fongaban. Commune de Saint-
1380 Emilion (Gironde), 3ème partie: la Faune. *L'Anthropologie* 76, 615–629.

1381 Lumley, H. de, Kahlke, H.D., Moigne, A.M., Mouillé, P.É., 1988. Les faunes de grands mammifères de la grotte
1382 du Vallonnet. *L'Anthropologie* 92, 465–495.

1383 Demirel, F.A., Mayda, S., 2014. A new early Pleistocene mammalian fauna from Burdur Basin, SW Turkey.
1384 Russ. J. Theriol. 13, 55–63.

1385 Drees, M., 2005. Sexual dimorphism in Pleistocene *Bison priscus* (Mammalia, Bovidae) with a discussion on
1386 the position of *Bison schoetensacki*. Senck. Leth. 85, 153–157.

1387 Duvernois, M. P., 1990. - Les *Leptobos* (Mammalia, Artiodactyla) du Villafranchien d'Europe occidentale. Doc.
1388 Lab. Géol., Lyon, 113, 1–213 pp.

1389 Ficcarelli, G., Abbazzi, L., Albianelli, A., Bertini, A., Coltorti, M., Magnatti, M., Masini, F., Mazza, P.,
1390 Mezzabotta, C., Napoleone, G., Rook, L., 1997. Cesi, an early Middle Pleistocene site in the Colfiorito
1391 Basin (Umbro-Marchean Apennine), central Italy. J. Quat. Sci. 12, 507–518.

1392 Fischer, K.H., 1965. Bisonreste (*Bison schoetensacki voigtstedtensis* ssp. n.) aus den altpaläozänen Tonen
1393 von Voigtstedt in Thüringen. Paläontol. Abh. A Paläozool. 2, 364–377.

1394 Flerov, K.K., 1969. Die Bison-Reste aus den Kiesen von Süßenborn bei Weimar. Paläontol. Abh. 3, 489–520.

1395 Flerov, C.C., 1972. The Most Ancient Bisons and the History of Genus *Bison*. In: Teriologiya, vol 1. Nauka,
1396 Novosibirsk, pp. 81–86 (in Russian).

1397 Flerow, K.K., 1975. Die Bison-reste aus den travertinen von Weimar-ehringsdorf. Abh. Zentr. Geol. Inst. 23,
1398 171–199.

1399 Flerov, K.K., 1979. Morphology, systematic, evolution, ecology. In: Sokolov, E.V. (Ed.), European Bison.
1400 Nauka, Moscow, pp. 9–127 (in Russian).

1401 Freudenberg, W., 1914. Die Säugetiere des älteren Quartärs von Mitteleuropa. Geol. Paleont. Abh. NF 12,
1402 533–549.

1403 Froese, D., Stiller, M., Heintzman, P.D., Reyes, A.V., Zazula, G.D., Soares, A.E., Meyer, M., Hall, E., Jensen, B.J.,
1404 Arnold, L.J., MacPhee, R.D., 2017. Fossil and genomic evidence constrains the timing of bison arrival
1405 in North America. Proc. Natl. Acad. Sci. USA 114, 3457–3462.

1406 Gee, H., 1993. The distinction between postcranial bones of *Bos primigenius* Bojanus, 1827 and *Bison priscus*
1407 Bojanus, 1827 from the British Pleistocene and the taxonomic status of *Bos* and *Bison*. J. Quat. Sci. 8,
1408 79–92.

1409 Gentili, S., Masini F., 2005. An outline of Italian Leptobos and a first sight on *Leptobos* aff. *vallisarni* from
1410 Pietrafitta (early pleistocene, Perugia) Quaternarie Hors Series, 2, 81–89

1411 Geraads, D., 1992: Phylogenetic analysis of the tribe Bovini (Mammalia: Artiodactyla). Zoological Journal of the
1412 Linnean Society 104, 193–207.

1413 Gower, G., Fenderson, L.E., Salis, A.T., Helgen, K.M., van Loenen, A.L., Heiniger, H., Hofman-Kamińska, E.,
1414 Kowalczyk, R., Mitchell, K.J., Llamas, B., Cooper, A., 2019. Widespread male sex bias in mammal fossil
1415 and museum collections. Proc. Natl. Acad. Sci. USA 116, 19019–19024.

1416 Grange, T., Brugal, J.P., Flori, L., Gautier, M., Uzunidis, A., Geigl, E.M., 2018. The evolution and population
1417 diversity of bison in Pleistocene and Holocene Eurasia: Sex matters. Divers. 10, 65.

1418 Gromov, I.M., Baranova, G.I. (Eds.), 1981. Catalogue of Mammals of the USSR (Pliocene-Recent). Nauka,
1419 Leningrad, pp. 1–456 (in Russian).

1420 Hammer, Ø., Harper, D.A., Ryan, P.D., 2001. PAST: Paleontological statistics software package for education
1421 and data analysis. Paleontol. Electron. 4, 1–9.

1422 Head, M.J., Gibbard, P.L., 2005. Early-Middle Pleistocene transitions: an overview and recommendation for
1423 the defining boundary. Geol. Soc. London Special Publications 247, 1–18.

1424 Hilzheimer, M., 1918. Dritter Beitrag zur Kenntnis der Bisonten. Arch. Naturg. 84, 41–87.

1425 Huguet, R., Vallverdú, J., Rodríguez-Álvarez, X.P., Terradillos-Bernal, M., Bargalló, A., Lombera-Hermida, A.D.,
1426 Menéndez, L., Modesto-Mata, M., Van der Made, J., Soto, M., Blain, H.A., 2017. Level TE9c of Sima
1427 del Elefante (Sierra de Atapuerca, Spain): A comprehensive approach. Quat. Int. 433, 278–295.

1428 Jungers, W.L., Falsetti, A.B., Wall, C.E., 1995. Shape, relative size, and size-adjustments in morphometrics.
1429 Yrbk. Phys. Anthropol. 38, 137–161.

1430 Kahlke, R.D., 1999. The History of the Origin, Evolution and Dispersal of the Late Pleistocene *Mammuthus*-
1431 *Coelodonta* Faunal Complex in Eurasia (large mammals). Fenske Companies, Rapid City.

1432 Kahlke, R.-D., 2007. Late Early Pleistocene European large mammals and the concept of an Epivillafranchian
1433 biochron. In: Kahlke, R.-D., Maul, L.C., Mazza, P. (Eds.), Late Neogene and Quaternary Biodiversity
1434 and Evolution: Regional Developments and Interregional Correlations. Volume II. Proceedings of the
1435 18th International Senckenberg Conference (VI International Palaeontological Colloquium in
1436 Weimar). *Cour. Forsch.-inst. Senck.* 259, 265–278.

1437 Kahlke, R.D., García, N., Kostopoulos, D.S., Lacombat, F., Lister, A.M., Mazza, P.P., Spassov, N. and Titov, V.V.,
1438 2011. Western Palaearctic palaeoenvironmental conditions during the Early and early Middle
1439 Pleistocene inferred from large mammal communities, and implications for hominin dispersal in
1440 Europe. *Quat. Sci. Rev.* 30, 1368–1395.

1441 Khan, M.A., Kostopoulos, D.S., Akhtar, D.S., Nazir, M., 2010. Bison remains from the upper Siwaliks of
1442 Pakistan. *N. Jahrb. Geol. Palaontol. Abh.* 258, 121–128.

1443 Kostopoulos, D.S., Maniakas, I., Tsoukala, E., 2018. Early bison remains from Mygdonia Basin (Northern
1444 Greece). *Geodiversitas* 40, 283–319.

1445 Von Koenigswald, W., Tobien, H., 1987. Bemerkungen zur Altersstellung der pleistozänen Mosbach-Sande
1446 bei Wiesbaden. *Geologisches Jahrbuch Hessen* 115, 227–237.

1447 Lehman U., 1949. Der Ur in diluvium Deutschlands und seine verbreitung. *Neues Jb. Miner. Abh.* 90, 163–
1448 266.

1449 Lopatin, A.V., Vislobokova, I.A., Lavrov, A.V., Startsev, D.B., Gimranov, D.O., Zelenkov, N.V., Maschenko, E.N.,
1450 Sotnikova, M.V., Tarasenko, K.K. and Titov, V.V., 2019. The Taurida Cave, a new locality of Early
1451 Pleistocene vertebrates in Crimea. *Dokl. Biol. Sci.* 485, 40–43.

1452 Madurell-Malapeira, J., Minwer-Barakat, R., Alba, D.M., Garcés, M., Gómez, M., Aurell-Garrido, J., Ros-
1453 Montoya, S., Moyà-Solà, S., Berástegui, X., 2010. The Vallparadís section (Terrassa, Iberian Peninsula)
1454 and the latest Villafranchian faunas of Europe. *Quat. Sci. Rev.* 29, 3972–3982.

1455 Madurell-Malapeira, J., Alba, D. M., Minwer-Barakat, R., Aurell-Garrido, J., & Moyà-Solà, S., 2012. Early
1456 human dispersals into the Iberian Peninsula: A comment on Martínez et al. (2010) and Garcia et al.
1457 (2011). *J. of Hum. Evol.*, 62, 169–173.

1458 Madurell-Malapeira, J., Ros-Montoya, S., Espigares, M.P., Alba, D.M., Aurell-Garrido, J., 2014. Villafranchian
1459 large mammals from the Iberian Peninsula: paleobiogeography, paleoecology and dispersal events. *J.*
1460 *Iber. Geol.* 40, 167–178.

1461 Madurell-Malapeira, J., Alba, D.M., Espigares, M.P., Vinuesa, V., Palmqvist, P., Martínez-Navarro, B., Moyà-
1462 Solà, S., 2017. Were large carnivores and great climatic shifts limiting factors for hominin
1463 dispersals? Evidence of the activity of *Pachycrocuta brevirostris* during the Mid-Pleistocene
1464 Revolution in the Vallparadís Section (Vallès-Penedès Basin, Iberian Peninsula). *Quat. Int.* 431, 42–52.

1465 Madurell-Malapeira, J., Sorbelli, L., Bartolini Lucenti, S., Rufí, I., Prat-Vericat, M., Ros-Montoya, S., Espigares,
1466 M.P., Martínez-Navarro, B., 2019. The Iberian latest Early Pleistocene: glacial pulses, large
1467 carnivores and hominins. In: Martínez- Navarro, B., Palmqvist, P., Espigares, M.P., Ros-Montoya, S.
1468 (Eds.), *Libro de Resúmenes XXXV Jornadas de la Sociedad Española de Paleontología*, pp. 155–159.

1469 Maniakas, I., Kostopoulos, D.S., 2017a. Morphometric-palaeoecological discrimination between *Bison*
1470 populations of the western Palaearctic. *Geobios* 50, 155–171.

1471 Maniakas, I., Kostopoulos, D.S., 2017b. Assessing astragalar morphology and biomechanics in western
1472 Palaearctic *Bison* populations with geometric morphometrics. *C. R. Palevol* 16, 783-794.

1473 Martin, T., 1987. Artunterschiede an den Langknochen großer Artiodactyla des Jungpleistozäns
1474 Mitteleuropas. *Cour. Forsch-inst. Senck.* 96, 1–121.

1475 Martínez-Navarro, B., Pérez-Claros, J.A., Palombo, M.R., Rook, L., Palmqvist, P., 2007. The Olduvai buffalo
1476 *Pelorovis* and the origin of *Bos*. *Quat. Res.* 68, 220–226.

1477 Martínez-Navarro, B., Ros-Montoya, S., Espigares, M.P., Palmqvist, P., 2011. Presence of the Asian origin
1478 Bovini, *Hemibos* sp. aff. *Hemibos gracilis* and *Bison* sp., at the early Pleistocene site of Venta Micena
1479 (Orce, Spain). *Quat. Int.* 243, 54–60.

1480 Masini, F., 1989. I bovini villafranchiani dell'Italia. Ph.D. Dissertation, Università di Modena-Bologna-Firenze-
1481 Roma.

1482 Masini, F., Palombo, M.R., Rozzi, R., 2013. A reappraisal of the Early to Middle Pleistocene Italian Bovidae.
1483 *Quat. Int.* 288, 45–62.

1484 Merla, G., 1949. I *Leptobos* Rütim. italiani. *Palaeontogr. Ital.* 46, 41–155.

1485 Michel, V., Shen, C.-C., Woodhead, J., Hu, H.-M., Wu, C.-C., Mouillé, P.-É., Khatib, S., Cauche, D., Moncel, M.-
1486 H., Valensi, P., Chou, Y.-M., Gallet, S., Echassoux, A., Orange, F., de Lumley, H., 2017. New dating
1487 evidence of the early presence of hominins in Southern Europe. *Sci. Rep.* 7, 10074.

1488 Mijarra, J.M.P., Burjachs, F., Manzaneque, F.G., Morla, C., 2007. A palaeoecological interpretation of the
1489 lower–middle Pleistocene Cal Guardiola site (Terrassa, Barcelona, NE Spain) from the comparative
1490 study of wood and pollen samples. *Rev. Palaeobot. Palynol.* 146, 247–264.

1491 Minwer-Barakat, R., Madurell-Malapeira, J., Alba, D.M., Aurell-Garrido, J., De Esteban-Trivigno, S., Moyà-Solà,
1492 S., 2011. Pleistocene rodents from the Torrent de Vallparadís section (Terrassa, northeastern Spain)
1493 and biochronological implications. *J. Vertebr. Paleontol.* 31, 849–865.

1494 Mol, D., Post, K., Reumer, J.W.F., de Vos, J., Laban, C., 2003. Het Gat: preliminary note on a Bavelian fauna
1495 from the North Sea with possibly two mammoth species. *Deinsea* 9, 253–266.

1496 Mourer-Chauvire, C., 1972. Etude de nouveaux restes de vertébrés provenant de la carrière Fournier à
1497 Châtillon-Saint-Jean. III. Artiodactyles, chevaux, oiseaux. *Quaternaire* 9, 271–305.

1498 Mouillé, P.E., 1992. Les grands mammifères du Pléistocène inférieur de la grotte du Vallonnet (Roquebrune-
1499 Cap-Martin, Alpes-Maritimes). Étude paléontologique des Carnivores, Équidés, Suidés et Bovidés.
1500 Ph.D. Dissertation, Muséum national d'Histoire naturelle, Paris.

1501 Mouillé, P.É., Lacombat, Echassoux, A., 2006. Apport des grands mammifères de la grotte du Vallonnet
1502 (Roquebrune-Cap-Martin, Alpes-Maritimes, France) à la connaissance du cadre biochronologique de
1503 la seconde moitié du Pléistocène inférieur d'Europe. *L'Anthropologie* 110, 837–849.

1504 Moyà-Solà, S., 1987. Los bóvidos (Artiodactyla, Mammalia) del yacimiento del Pleistoceno inferior de Venta
1505 Micena (Orce, Granada, Espana). *Paleontol. Evol. Mem. Esp.* 1, 181–236.

1506 Palacio, P., Berthonaud, V., Guérin, C., Lambourdière, J., Maksud, F., Philippe, M., Plaire, D., Stafford, T.,
1507 Marsolier-Kergoat, M.C., Elalouf, J.M., 2017. Genome data on the extinct *Bison schoetensacki*
1508 establish it as a sister species of the extant European bison (*Bison bonasus*). *BMC Evol. Biol.* 17, 48.

1509 Pečnerová, P., Díez-del-Molino, D., Dussex, N., Feuerborn, T., von Seth, J., van der Plicht, J., Nikolskiy, P.,
1510 Tikhonov, A., Vartanyan, S., Dalén, L., 2017. Genome-based sexing provides clues about behavior and
1511 social structure in the woolly mammoth. *Curr. Biol.* 27, 3505–3510.

1512 Peretto, C., Arnaud, J., Moggi-Cecchi, J., Manzi, G., Nomade, S., Pereira, A., Falguères, C., Bahain, J.-J.,
1513 Grimaud-Hervé, D., Berto, C., Sala, B., Lembo, G., Muttillo, B., Gallotti, R., Thun Hohenstein, U.,
1514 Vaccaro, C., Coltorti, M., Arzarello, M., 2015. A human deciduous tooth and new $^{40}\text{Ar}/^{39}\text{Ar}$ dating
1515 results from the Middle Pleistocene archaeological site of Isernia La Pineta, Southern Italy. *PLoS ONE*
1516 10, e0140091.

1517 Pilgrim, G.E., 1947. The evolution of the buffaloes, oxen, sheep and goats. *Zool. J. Linn. Soc. Lond.* 41, 272–
1518 286.

1519 Prat F., 1968. Observations sur quelques ossements découverts dans la Basse Terrasse de l'Oise à Moru
1520 (Rhuis, Oise). In *La Préhistoire, Problèmes et Tendances*. CNRSParis, pp. 337–348

1521 Revilliod P., Dottrens E., 1946, La faune néolithique de la couche profonde de St-Aubin. Etude préliminaire
1522 des phalanges osseuses de *Bos taurus domesticus*, *Revue Suisse de Zoologie*, Genève, 53, 739–774.

1523 Rook, L., Martínez-Navarro, B., 2010. Villafranchian: the long story of a Plio-Pleistocene European large
1524 mammal biochronologic unit. *Quat. Int.* 219, 134–144.

1525 Sala, B., 1986. *Bison schoetensacki* Freud. from Isernia La Pineta (early Mid-Pleistocene – Italy) and revision
1526 of the European species of bison. *Palaeont. It.* 74, 113–170.

1527 Schertz, E., 1936a. Zur Unterscheidung von *Bison priscus* Boj. und *Bos primigenius* Boj. an Metapodien und
1528 Astragalus, nebst Bemerkungen über einige diluviale Fundstellen. *Seckenbergiana* 18, 37–71.

1529 Schertz, E., 1936b Der Geschlechts-Unterschied an Metapodien von Bison. *Senckenbergiana* 18, 357–381.

1530 Scott, R.S., Barr, W.A., 2014. Ecomorphology and phylogenetic risk: implications for habitat reconstruction
1531 using fossil bovids. *J. Hum. Evol.* 73, 47–57.

1532 Shapiro, B., Drummond, A.J., Rambaut, A., Wilson, M.C., Matheus, P.E., Sher, A.V., Pybus, O.G., Gilbert,
1533 M.T.P., Barnes, I., Binladen, J., Willerslev, E., 2004. Rise and fall of the Beringian steppe bison.
1534 *Science* 306, 1561–1565.

1535 Sher, A.V., 1997. An Early Quaternary *Bison* population from Untermaßfeld: *Bison menneri* sp. nov. In:
1536 Kahlke, R.D. (Ed.), *Das Pleistozän von Untermaßfeld bei Meiningen (Thüringen). Teil 2*. Habelt-Verlag,
1537 Bonn, pp. 101–180.

1538 Simpson, G.G., 1941. Large Pleistocene felines of North America. *Am. Mus. Novit.* 1136, 1–27.

1539 Skinner, M.R., Kaisen, O.C., 1946. The fossil *Bison* of Alaska and preliminary revision of the genus. *Bull. Am.*
1540 *Mus. Nat. Hist.* 89, 123–256.

1541 Soubrier, J., Gower, G., Chen, K., Richards, S.M., Llamas, B., Mitchell, K.J., Ho, S.Y., Kosintsev, P., Lee, M.S.,
1542 Baryshnikov, G., Bollongino, R., 2016. Early cave art and ancient DNA record the origin of European
1543 bison. *Nat. Commun.* 7, 13158.

1544 Stampfli, H.R., 1963. Wisent, *Bison bonasus* (Linné) 1758, Ur, *Bos primigenius* Bojanus, 1827, und Hausrind
1545 *Bos taurus* (Linné) 1758. In: J. Boessneck, J.-P. Jéquier, H.R. Stampfli (Eds.), *Burgäschisee-Süd, Teil 3:*
1546 *Die Tierreste, 2. Acta Bernensia, Beiträge zur prähistorischen, klassischen und jüngeren Archäologie*
1547 *II. Verlag Stämpfli & Cie, Bern*, pp. 117–196.

1548 Strani, F., DeMiguel, D., Alba, D.M., Moyà-Solà, S., Bellucci, L., Sardella, R., Madurell-Malapeira, J., 2019. The
1549 effects of the “0.9 Ma event” on the Mediterranean ecosystems during the Early-Middle Pleistocene
1550 transition as revealed by dental wear patterns of fossil ungulates. *Quat. Sci. Rev.* 210, 80–89.

1551 Stuart, A.J. and Lister, A.M., 2001. The mammalian faunas of Pakefield/Kessingland and Corton, Suffolk, UK:
1552 evidence for a new temperate episode in the British early Middle Pleistocene. *Quat. Sci. Rev.* 20,
1553 1677–1692.

1554 Teilhard de Chardin, P., Piveteau, J., 1930. Les mammifères fossiles de Nihowan (Chine). *Ann. Paleontol.* 19,
1555 1–134.

1556 Tong, H.W., Chen, X., Zhang, B., 2016. New fossils of *Bison palaeosinensis* (Artiodactyla, Mammalia) from the
1557 steppe mammoth site of early Pleistocene in Nihewan Basin, China. *Quat. Int.* 445, 450–468.

1558 Van der Made, J., Rosell, J., Blasco, R., 2017. Faunas from Atapuerca at the Early–Middle Pleistocene limit:
1559 The ungulates from level TD8 in the context of climatic change. *Quat. Int.* 433, 296–346.

1560 Vershinina, A.O., Kapp, J.D., Soares, A.E.R., Heintzman, P.D., Lowson, C., Cassatt-Johnstone, M., Shidlovskiy,
1561 F.K., Kirillova, I.V., Shapiro, B., 2019. Ancient DNA analysis of a Holocene bison from the Rauchua
1562 River, Northwestern Chukotka, and the existence of a deeply divergent mitochondrial clade. *Zool. J.*
1563 98, 1091–1099.

1564 Verestchagin, N.K., 1959. The Mammals of the Caucasus. A History of the Fauna. Academia Nauk, Leningrad
1565 (translated from Russian; Israel Program for Scientific Translations, Jerusalem 1967).

1566 Wagner, G.A., Kröbtschek, M., Degering, D., Bahain, J.J., Shao, Q., Falguères, C., Voinchet, P., Dolo, J.M.,
1567 Garcia, T., Rightmire, G.P., 2010. Radiometric dating of the type-site for *Homo heidelbergensis* at
1568 Mauer, Germany. *Proc. Natl. Acad. Sci. USA* 107, 19726–19730.

1569 Zheng, S.H., Wu, W.Y., Li, Y., Wang, G.D., 1985. Late Cenozoic mammalian faunas of Guide and Gonghe
1570 Basins, Qinghai Province. *Vert. PalAs.* 23, 89–134 (in Chinese).

1572

1573

1574

1575

1576

1577

1578

1579

1580

1581

1582

1583

1584

1585

1586

1587

1588 **Figure captions**

1589 **Fig. 1.** a, Quaternary time scale showing the chronological/biochronological distribution of the studied taxa in
1590 Europe and the most important Early-Middle Pleistocene sites mentioned in the text. b, Map of Europe with
1591 the location of some of the sites mentioned in the text. c, Focus on the Black Sea area. d, Geographic location
1592 of the studied sites of Cal Guardiola and Vallparadís Estació in the town of Terrassa (Iberian Peninsula).
1593 Abbreviations: Ma, million years ago; GC, geochronology; LMA, Land Mammal Age; C, glacial/interglacial
1594 cyclicity; MS, magnetostratigraphy; CF, Cava Filo (Italy); CBF, Cromer Forest-Bed sites (United Kingdom); Ce,
1595 Cesi (Italy); CSL, Châtillon-Saint-Jean (France); Dma, Dmanisi (Georgia); Dur, Durfort (France); Isen, Isernia La
1596 Pineta (Italy); KIX, Kiputz IX (Spain); Mau, Mauer (Germany); MB, Mygdonia Basin sites (Greece); Mos, Mosbach
1597 (Germany); Olv, Olivola (Italy); Pf, Pietrafitta (Italy); Pir, Pirro (Italy); RIR, Romain-la-Roche (France); Se, Senèze
1598 (France); Si, Siréjol cave (France); Sus, Süssenborn (Germany); Tau, Taubach (Germany); Tir, Tiraspol (Ukraine);
1599 Unt, Untermassfeld (Germany); Val, Le Vallonnet (France); VCS, Vallparadís Composite Section (Spain); VM,
1600 Venta Micena (Spain); We, Westbury (United Kingdom).

1601

1602 **Fig. 2.** Some of the measurements taken on postcranial bones in this work: a, radioulna in anterior (1), lateral
1603 (2) proximal (3) and distal (4) views; b, ulna in lateral (1) and anterior (2) views; c, tibia in distal view; d,
1604 calcaneum in anterior (1), medial (2) and posterior (3) views; e, cubonavicular in distal (1) and anterior (2)
1605 views; f, semilunar in proximal (1) and anterior (2) views; g, astragalus in anterior (1), lateral (2) and medial (3)
1606 views; h, cuneiform in distal (1) and medial (2) views; i, pyramidal in lateral (1) and proximal (2) views; j,
1607 unciform in proximal (1) and lateral (2) views; k, scapula in lateral (1) and distal (2) views; l, phalanx in proximal
1608 (1), distal (2) and anterior (3) views; m, distal phalanx in anterior view; n, metacarpal in anterior (1), posterior
1609 (2), proximal (3) and distal (4) views; o, metatarsal in proximal view; p, humerus in lateral (1), posterior (2),
1610 anterior (3) and distal (4) views; q, thoracic vertebra in anterior (1) and lateral (2) views. Abbreviations as in
1611 Table 1.

1612

1613

1614 **Fig. 3.** Dentognathic remains of *Bison schoetensacki* from the Vallparadís Composite Section: a, left dp4
1615 IPS93008 in occlusal (1) and lingual (2) views; b, left p4 IPS93015 in occlusal (1) and lingual (2) views; c, right
1616 m1 IPS93027 in occlusal view; d, left m2 IPS93044 in occlusal view; e, left m3 IPS92989 in occlusal (1) and
1617 buccal (2) views; f, left P2 IPS92986 in occlusal (1) and buccal (2) views; g, left P3 IPS92998 in occlusal (1) and
1618 buccal (2) views; h, right P4 IPS13557 in occlusal (1) and buccal (2) views; i, left M1 IPS93029 in occlusal (1)
1619 and buccal (2) views; j, left M2 IPS93005 in occlusal (1) and lingual (2) views; k, right M2 IPS93032 in occlusal
1620 (1) and lingual (2) views; l, right M3 IPS20182 in occlusal (1) and lingual (2) views; m, left maxillary fragment
1621 with M2–M3 IPS92993 in occlusal view. Scale bar: 30 mm.

1622

1623 **Fig. 4.** Craniodontal and postcranial remains of *Bison schoetensacki* from the Vallparadís Composite Section:
1624 a, left hemimandible with m1–m3 IPS92973 in occlusal (1) and lingual (2) views; b, juvenile mandible with dp2–
1625 dp4 IPS92968 in left lateral (1) and occlusal (2) views; c, horn core IPS92970 in dorsal (1), ventral (2), and
1626 anterior/posterior (undetermined laterality) (3) views; d, right scapula IPS107637 in distal (1) and lateral (2)
1627 views. Scale bars: 50 mm.

1628

1629 **Fig. 5.** Forelimb remains of *Bison schoetensacki* from the Vallparadís Composite Section: a, distal fragment of
1630 left humerus IPS107620 in anterior (1) and posterior (2) views; b, distal fragment of right humerus IPS50672
1631 in anterior (1) and posterior (2) views; c, left radioulna IPS107617 in anterior (1), medial (2), posterior (3), distal
1632 (4), and proximal (5) views; d, right radius IPS39893 in anterior (1), lateral (2), posterior (3), and distal (4) views
1633 and associated right ulna in anterior (5) and lateral (6) views. Scale bar: 100 mm.

1634

1635 **Fig. 6.** Metapodials of *Bison schoetensacki* from the Vallparadís Composite Section: a, left metacarpal IPS14917
1636 (male) in anterior (1), proximal (2), distal (3) and posterior (4) views; b, left metacarpal IPS107635 (male) in
1637 anterior (1), proximal (2), distal (3) and posterior (4) views; c, left metacarpal IPS92910 (female) in anterior (1),
1638 proximal (2), distal (3) and posterior (4) views; d right metatarsal IPS92934 (male) in anterior (1), proximal (2),
1639 distal (3) and posterior (4) views; e, right metatarsal IPS107634 (male) in anterior (1), proximal (2), distal (3)

1640 and posterior (4) views; f, right metatarsal IPS92932 (female) in anterior (1), proximal (2), distal (3) and
1641 posterior (4) views. Scale bar: 100 mm.

1642

1643 **Fig. 7.** Hindlimb remains of *Bison schoetensacki* from the Vallparadís Composite Section: a, right tibia
1644 IPS107618 in posterior (1), medial (2), lateral (3), distal (4) and anterior (5) views; b, left tibia IPS92942 in
1645 posterior (1), medial (2), lateral (3), distal (4) and anterior (5) views. Scale bar: 100 mm.

1646

1647 **Fig. 8.** Tarsals of *Bison schoetensacki* from the Vallparadís Composite Section. a, left astragalus IPS92953 (male)
1648 in anterior (1), posterior (2), and lateral (3) views; b, right astragalus IPS92952 (female) in anterior (1), posterior
1649 (2), and lateral (3) views; c, right calcaneum IPS92945 (female) in medial (1), lateral (2), posterior (3), and
1650 anterior (4) views; d, right calcaneum IPS13936 (male) in medial (1), lateral (2), posterior (3), and anterior (4)
1651 views. Scale bar: 50 mm.

1652

1653 **Fig. 9.** a-d, Bivariate plots of maximum length (Lmax) vs distal end width (DEW) / maximum length (Lmax) %
1654 to evaluate stoutness of metacarpals (a), metatarsals (b), radii (c), and astragali (d) in several *Leptobos* and
1655 *Bison* s.l. species. e, \log_{10} ratio diagrams of seven selected metacarpal variables, in which the VCS bison is
1656 compared with *Leptobos etruscus*, *B. (Eobison)* spp., and *B. menneri* (1), *B. schoetensacki* from several sites (2),
1657 and *B. priscus* from several sites (3).

1658

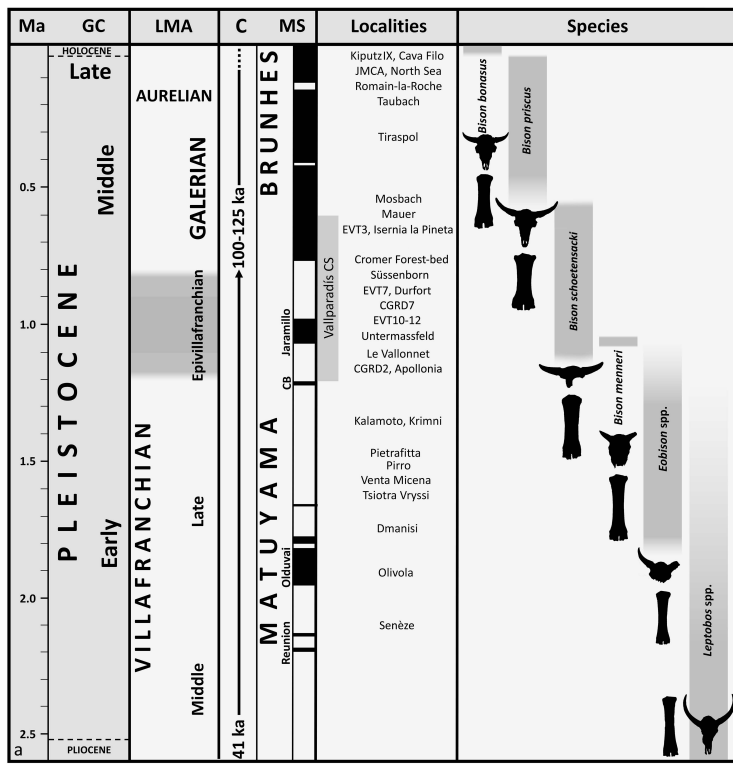
1659 **Fig. 10.** Bivariate plots of the first two principal component (PC) scores resulting from principal components
1660 analyses of metacarpal (a) and metatarsal (b) variables, based on the seven variables used in this study (1), as
1661 well as in those used by Scott and Barr (2004) (2). Significant PCs with variance and coefficient of variables are
1662 in Tables S19, S20, S30, S31. Abbreviations as in Table 2.

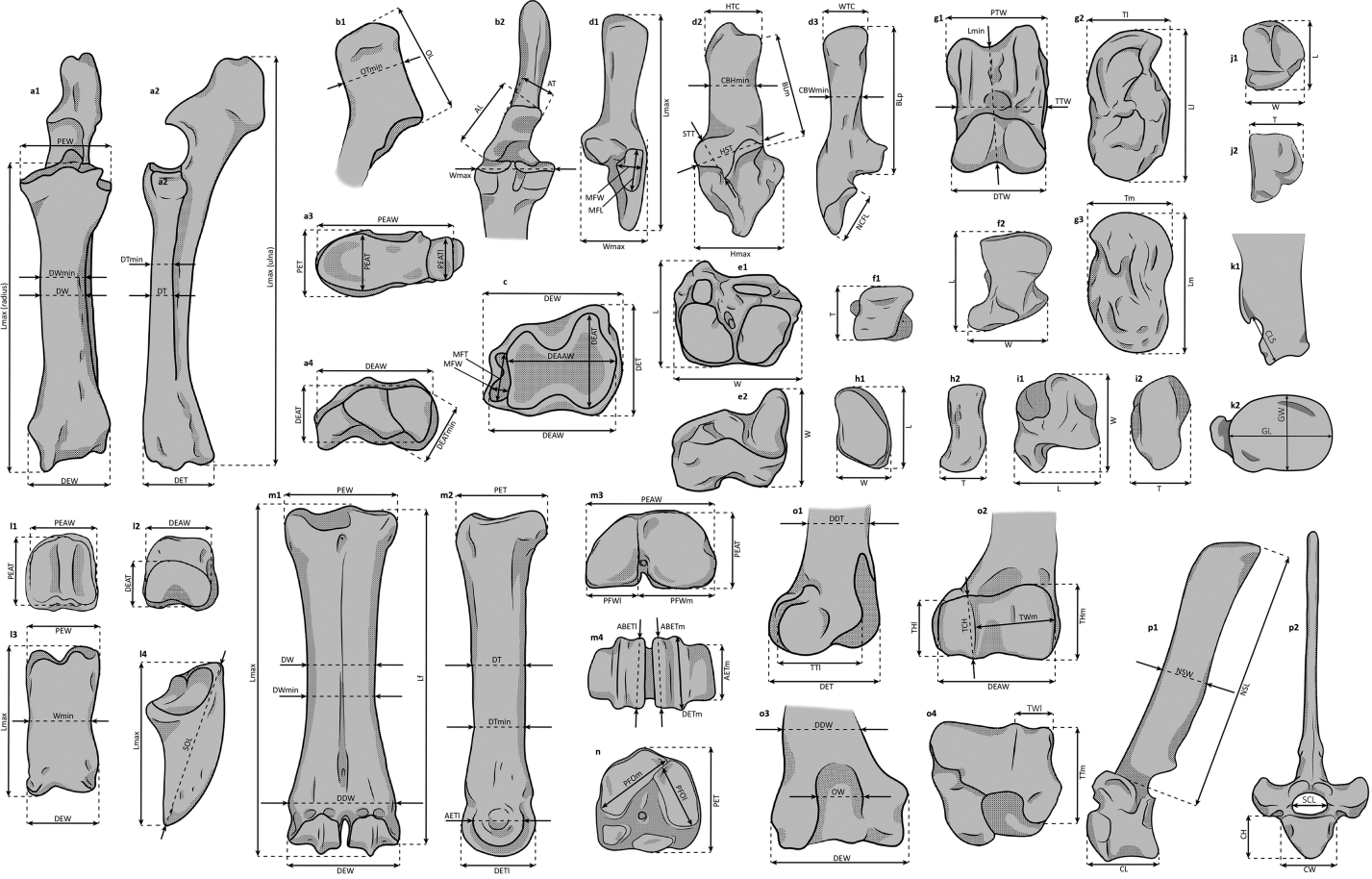
1663

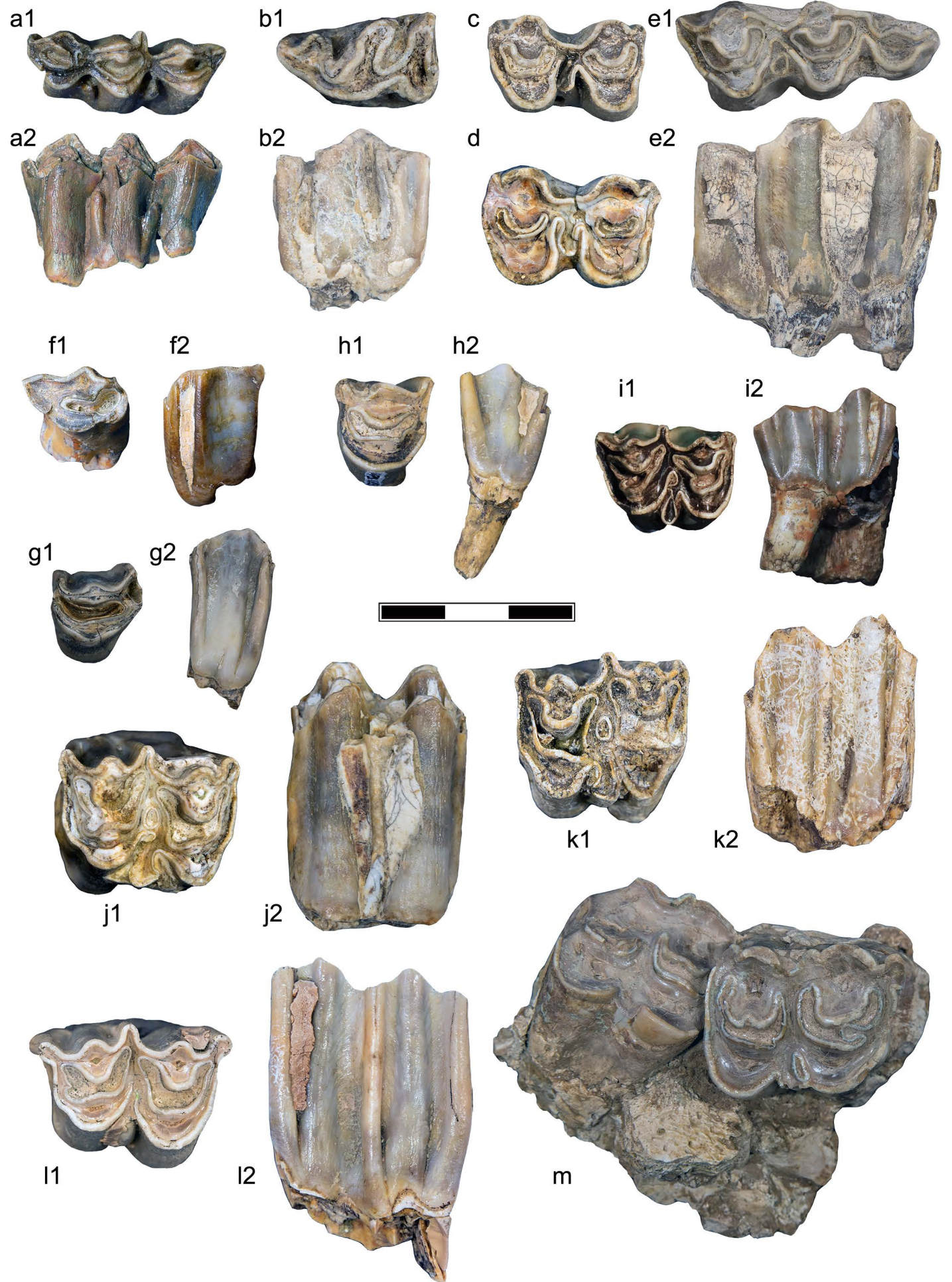
1664 **Fig. 11.** Reconstruction of the skeleton (a) and external appearance (b) of an adult male of *Bison schoetensacki*
1665 based on the remains recovered from VCS and other European sites. Scale bar: 300 mm.

1666

1667 Fig. 12. Comparison of metacarpals among *Leptobos* and *Bison* s.l. species. a, *Leptobos etruscus* male IGF 2452
1668 (1) and female IGF 2471 (2) from Olivola (Italy); b, *Bison (Eobison) palaeosinensis* IVPP V 22655 from
1669 Shanshenmiaozui (China; taken from Tong et al., 2016); c, *Bison (Eobison)* sp., male IPHES VM 83.C-3.G-85 (1)
1670 and female IPHES VM 83.C-3.G-7.11 (2) from Venta Micena (Spain; taken from Moyà-Solà, 1987); d, *Bison*
1671 (*Eobison*) *georgicus* males GNM D2812 (1) and GNM D2288 (2) from Dmanisi (Georgia; taken from
1672 Bukhsianidze, 2005); e, *Bison (Eobison)* cf. *degiulii* male AUTH KLT-646 (1) and female AUTH APL-373 (2) from
1673 Mygdonia Basin (Greece; taken from Kostopoulos et al., 2018); f, *Bison schoetensacki* males MNHN DUR-105
1674 (1), MNHN DUR-107 (2) and female MNHN DUR-106 (3) from Durfort (France); g, *Bison schoetensacki* males
1675 IPS14917 (1), IPS13928 (2), IPS14815 (3), IPS13547 (4), IPS92907 (5), IPS92912 (6), IPS92911 (7), IPS107635
1676 (8), IPS107636 (9) and females IPS107626 (10), IPS107626 (11) from VCS (Spain); h, *Bison schoetensacki* males
1677 MPRM A8 B1 3748 (1), MPRM A7 AH14 8424 (2), MPRM E7 C 242 (3), MPRM C6 359 (4), MPRM C4 CE13 209
1678 (5), MPRM C6 200 (6) and females MPRM A8 B2 326 (7); MPRM B9 BJ7 346 (8) from Le Vallonnet (France); i,
1679 *Bison schoetensacki* HLMD-Mau-401 from Mauer (Germany; kindly provided by Marisa Blume and Oliver
1680 Sandrock); j, *Bison menneri* male IQW 1980/15235 (1) and female IQW 1980/16658 (2) from Untermaßfeld
1681 (Germany; taken from Sher, 1997); k, *Bison schoetensacki* HLMD-Mb-433 (1), HLMD-Mb-435 (2) HLMD-Mb-
1682 785 (3) from Mosbach (Germany; kindly provided by Marisa Blume and Oliver Sandrock); l, *Bison priscus* males
1683 NAS F-3072 (1), NAS F-1155 (2), NAS F-1275 (3) and females NAS F-1353 (4), NAS F-1339 (5), NAS F-1348 (6)
1684 from Siberia (Russia; taken from Kirilova et al., 2015); m, *Bison priscus*: MCM BOV 1520 M 13-34 Ro 87 from
1685 Romain-la-Roche (France; kindly provided by Lionel Cavin and Corinne Charvet). Scale bar: 100 mm.
1686

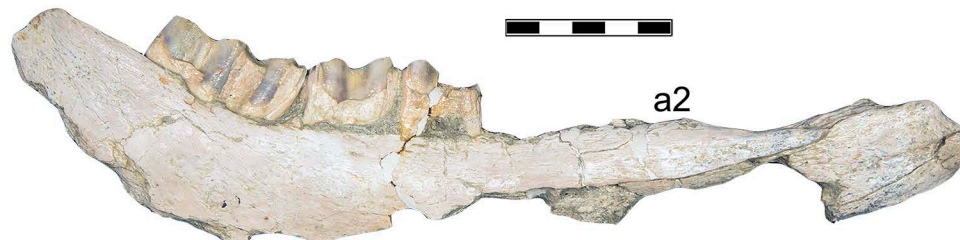








a1



a2



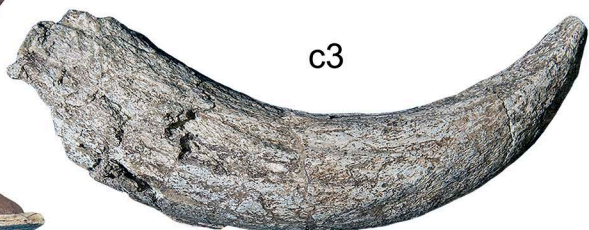
b1

c1

c2



c3



b2



d1



d2





a1



a2



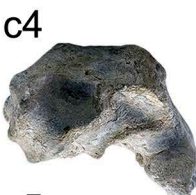
c1



c2



c3



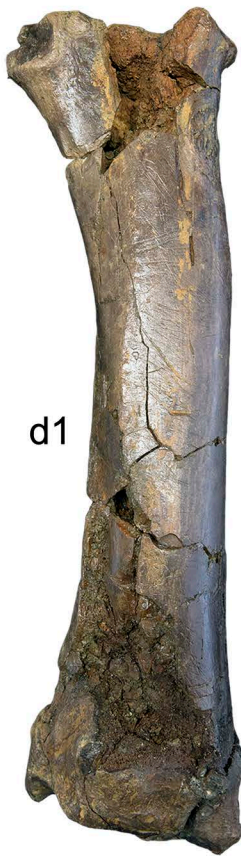
c5



b1



b2



d1



d2



d3

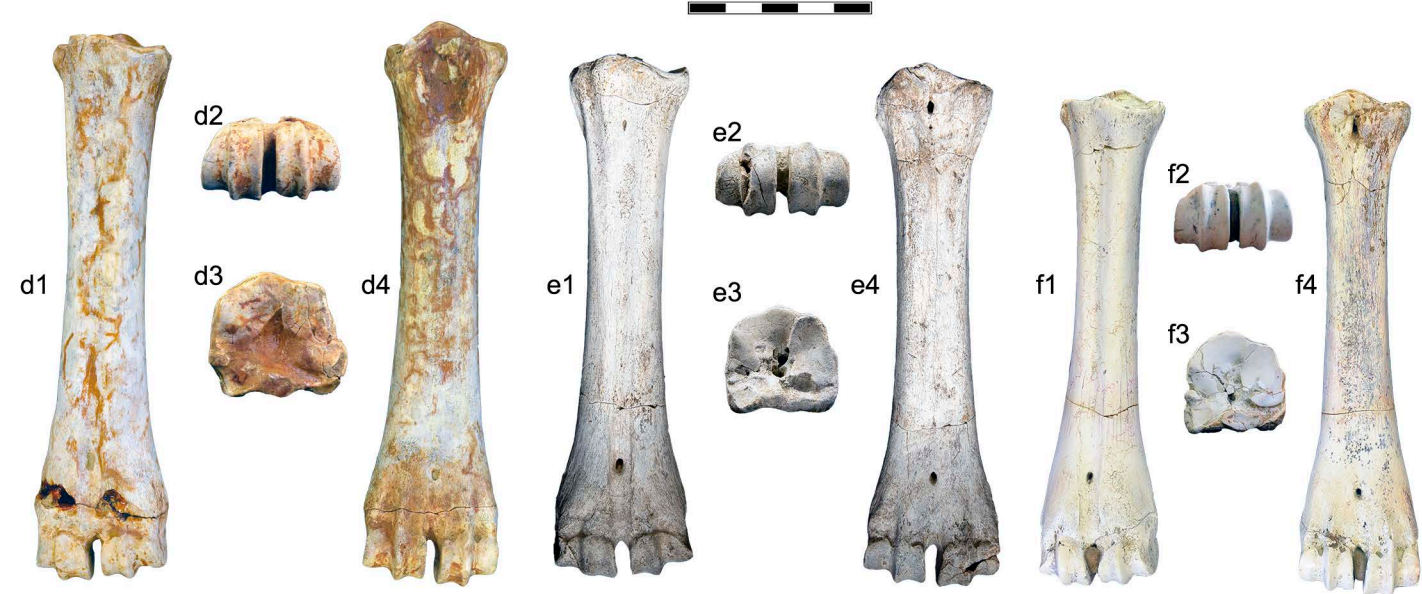
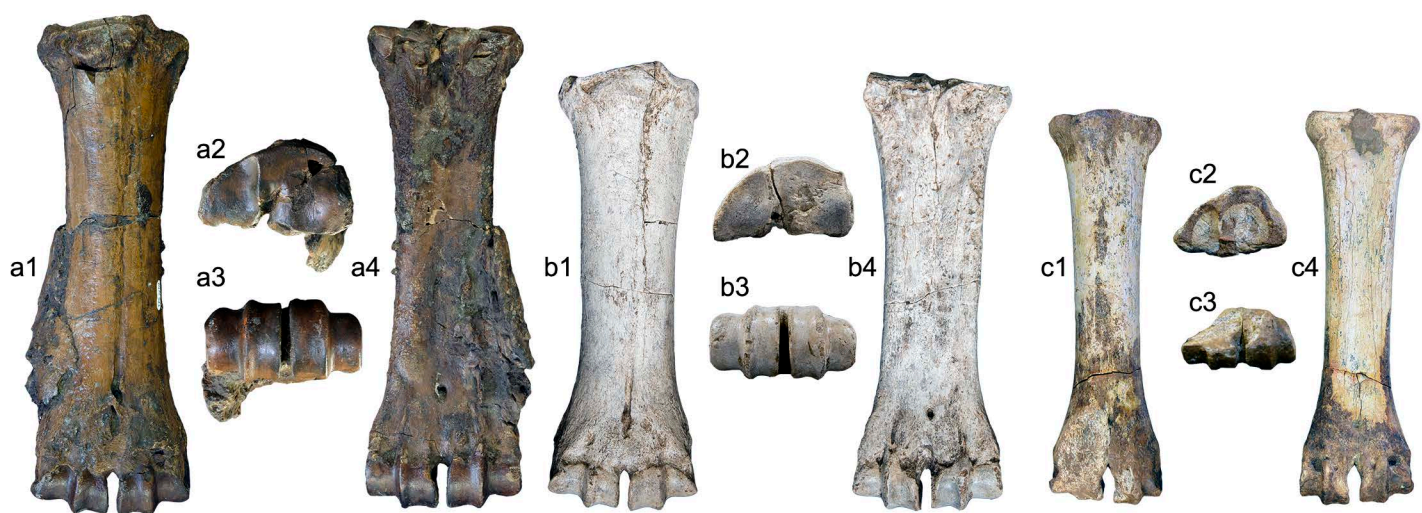


d4



d5





a1



a2



a3



b1



b2



b3



c1



c2



c3



c4



d1



d2

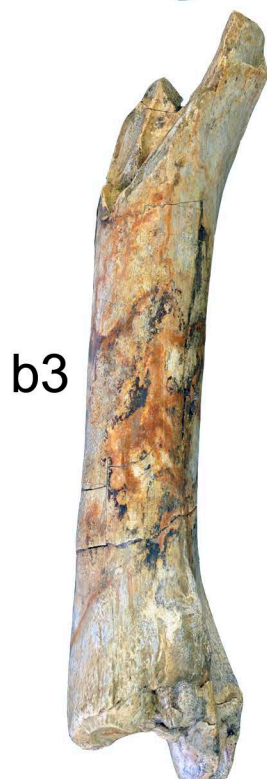
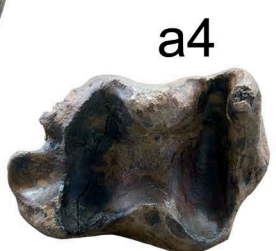


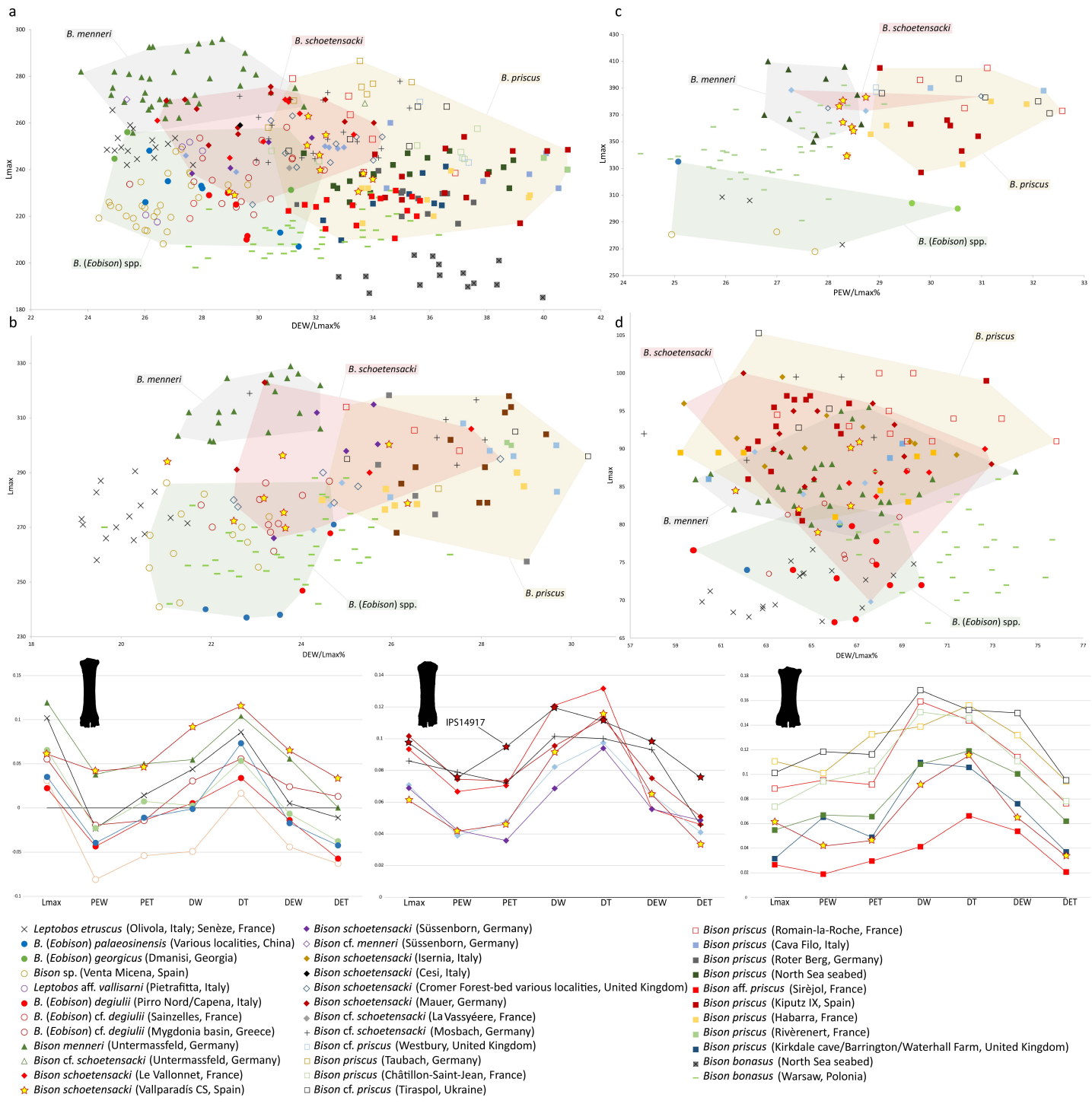
d3



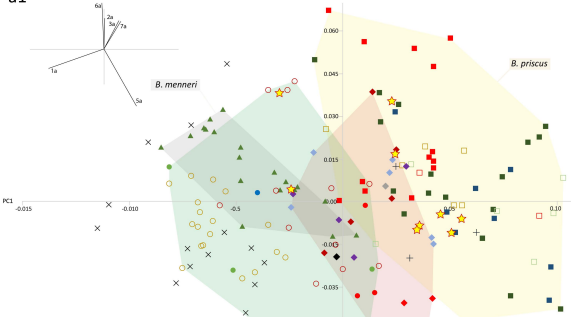
d4



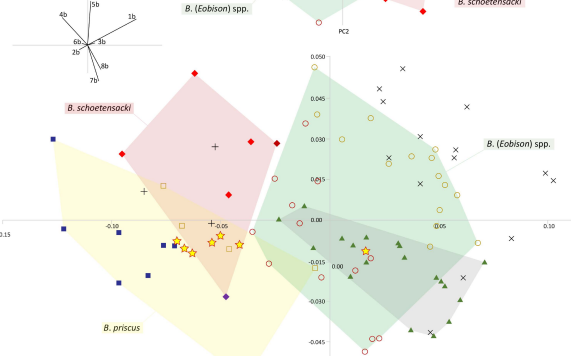




a1

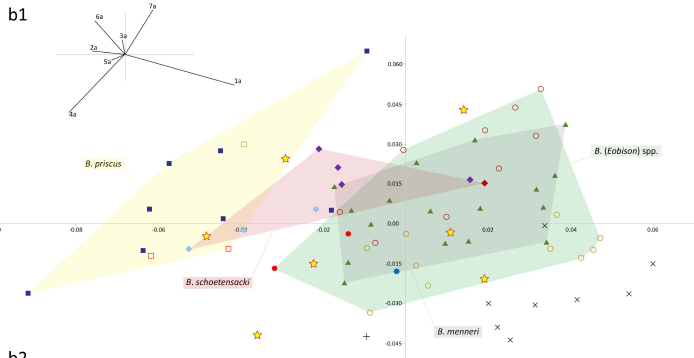


a2

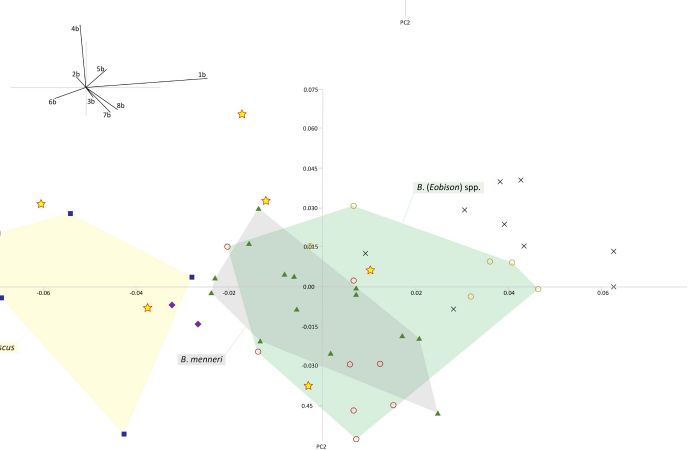


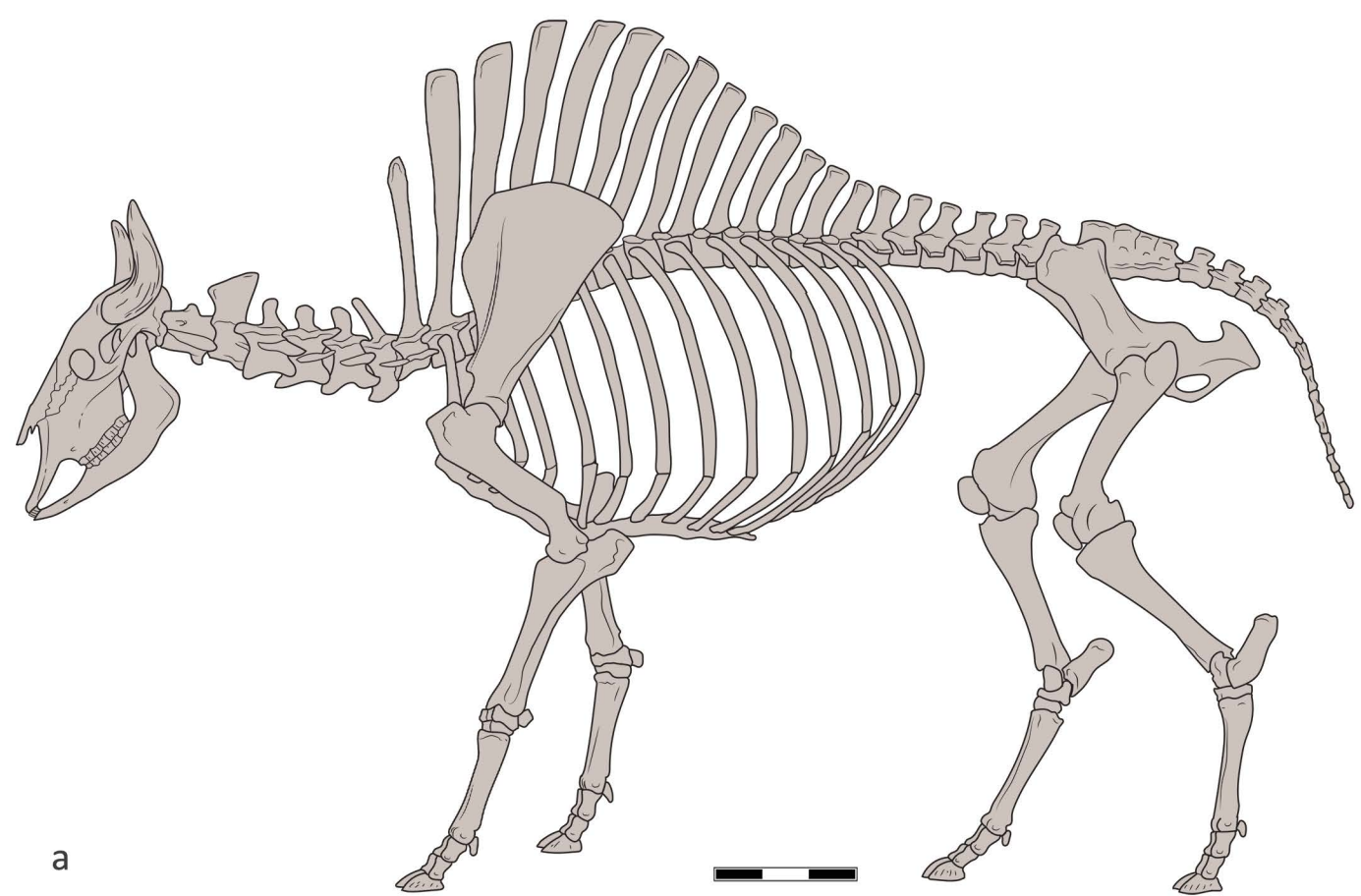
- × *Leptobos etruscus* (Oliva, Italy; Senèze, France)
- *B. (Eobison) paleoasiensis* (Various localities, China)
- *B. (Eobison) georgicus* (Omanis, Georgia)
- *Bison* sp. (Venta Micena, Spain)
- *B. (Eobison) deguillii* (Pirro Nord/Capena, Italy)
- *B. (Eobison) cf. deguillii* (Mygdonia basin, Greece)
- ▲ *Bison menneri* (Untermassfeld, Germany)
- *Bison schoetensacki* (Le Vallonnet, France)
- ★ *Bison schoetensacki* (Vallparadís CS, Spain)
- △ *Bison schoetensacki* (Durfort, France)
- ◆ *Bison schoetensacki* (Suisse/Born, Germany)
- ◆ *Bison schotensacki* (Cesi, Italy)
- ◆ *Bison schotensacki* (Mauer, Germany)
- ◆ *Bison cf. schotensacki* (La Vassière, France)
- + *Bison cf. schotensacki* (Mosbach, Germany)
- *Bison priscus* (Taubach, Germany)
- *Bison priscus* (Châtillon-Saint-Jean, France)
- *Bison priscus* (Romain-la-Roche, France)
- *Bison priscus* (North Sea seabed)
- *Bison aff. priscus* (Siréjol, France)
- *Bison priscus* (Kirkdale Cave/Barrington/Waterhall Farm, United Kingdom)

b1



b2





a



b

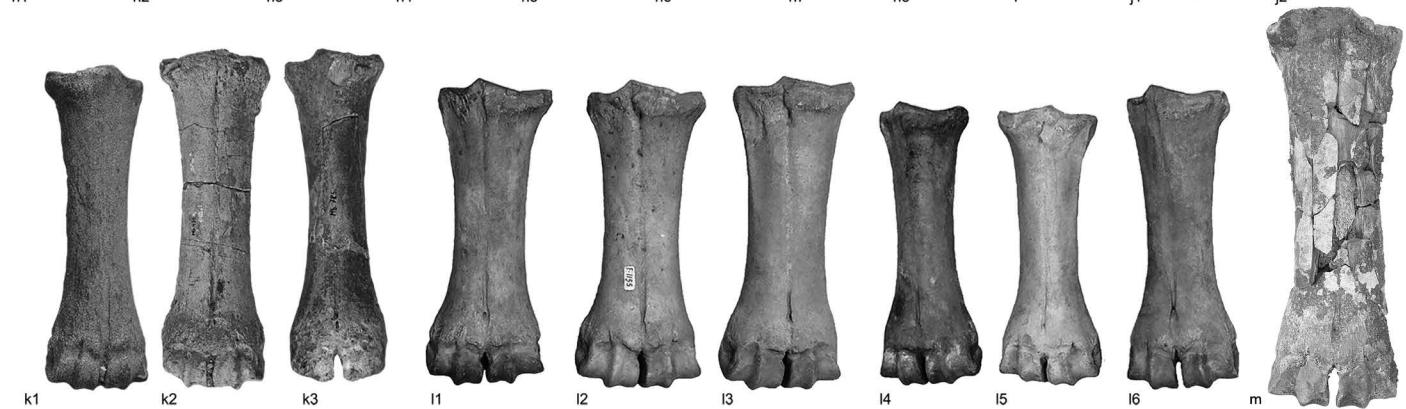
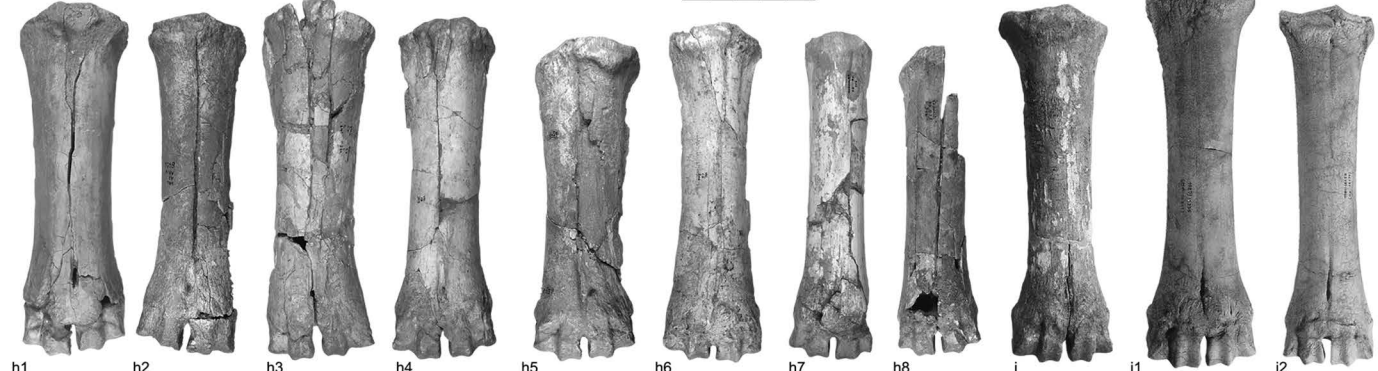


Table 1. Abbreviations of the measurements taken and shown in Fig. 2.

Abbreviation	Measurement taken
ABETl	Abaxial emicondyle thickness (lateral emicondyle)
ABETm	Abaxial emicondyle thickness (medial emicondyle)
AETm	Axial emicondyle thickness (medial emicondyle)
AL	Articular surface length
AT	Articular surface thickness
BLm	Calcaneum minimum length (medial view)
BLp	Calcaneum body length (posterior view)
CBHmin	Calcaneum body minimum height
CBWmin	Calcaneum body minimum width
CH	Centrum height
CL	Centrum length
CW	Centrum width
DDT	Distal diaphysis thickness
DDW	Distal diaphysis width
DEAAW	Distal epiphysis astragalus articulation width
DEAT	Distal end articular thickness
DEATmin	Distal end articular thickness (without the distal end of ulna)
DEAW	Distal end articular width
DET	Distal end thickness
DETI	Distal end thickness (lateral trochlear crest)
DETm	Distal end thickness (medial trochlear crest)
DEW	Distal end width
DT	Diaphysis thickness (midshaft)
DTmin	Diaphysis minimum thickness
DW	Diaphysis width (midshaft)
DWmin	Diaphysis minimum width
GL	Glenoid cavity length
GPL	Glenoid process length
GW	Glenoid cavity width
Hmax	Maximum height
HST	Height at sustentaculum tali level
HTC	Height of tuber calcanei
L	Length
LI	Lateral length
Lmax	Maximum length
Lmin	Minimum length
MFL	Malleolar facet length
MFW	Malleolar facet width
NCFL	Cubonavicular articular facet length
NSL	Neural spine length
NSW	Neural spine width
OL	Olecranon length
OTmin	Olecranon minimum thickness

OW	Olecranon fossa width
PEAT	Proximal end articular thickness
PEATI	Lateral facet articular thickness (proximal end)
PEAW	Proximal end articular width
PET	Proximal end thickness
PEW	Proximal end width
PFOI	Metatarsal proximal articular facet oblique diameter (lateral facet)
PFOm	Metatarsal proximal articular facet oblique diameter (medial facet)
PFWI	Metacarpal proximal articular facet width (lateral facet)
PFWm	Metacarpal proximal articular facet width (medial facet)
SCW	Spinal canal width
SOL	Oblique length of the sole
STT	Sustentaculum tali thickness
T	Thickness
TCH	Trochlea crest height
THI	Lateral trochlear height
THm	Medial trochlear height
TI	Lateral thickness
TTI	Trochlea thickness (lateral epicondyle)
TTm	Trochlea thickness (medial epicondyle)
TTW	Intertrochlear width
TWI	Trochlear lateral articulation width
TWm	Trochlear medial articulation width
Wmax	Maximum width
Wmin	Minimum width
WTC	Width of tuber calcanei

Con formato: Español (España)

Con formato: Español (España)

Table 2. Shape variables used for the principal component analysis. Abbreviations: DETI, distal epiphysis thickness (lateral trochlear crest); DETm, distal epiphysis thickness (medial trochlear crest); DEW, distal epiphysis width; DT, diaphysis thickness (midshaft); DW, diaphysis width (midshaft); Lmax, maximum length; MGSV, metapodial global size variable (for the equation see Section 3); ms, Mosimann shape variable; PET, proximal epiphysis thickness; PEW, proximal epiphysis width; re, relative.

Selected Mosimann shape variables	Fig. 10a	Relative dimension variables, after Scott and Barr (2014)	Fig. 10b
msLmax = Log(Lmax/GM)	1a	reLmax = Log(Lmax/MGSV)	1b
msPET = Log(PET/GM)	2a	reDW = Log(DW/MGSV)	2b
msPEW = Log(PEW/GM)	3a	reDT = Log(DT/MGSV)	3b
msDT = Log(DT/GM)	4a	reDETI = Log(DETI/MGSV)	4b
msDW = Log(DW/GM)	5a	reDETm = Log(DETm/MGSV)	5b
msDETm = Log(DETm/GM)	6a	reDEW = Log(DEW/MGSV)	6b
msDEW = Log(DEW/GM)	7a	rePEW = Log(PEW/MGSV)	7b
		rePET = Log(PET/MGSV)	8b

Table 3. Measurements (mm) of the teeth of *Bison schoetensacki* from Vallaradís Estació (EVT) and Cal Guardiola (CGR) layers. Abbreviations: L, length; W, width.

ID Specimen	Layer	Tooth	L	W
IPS92968	EVT12	dp2	11.4	7.1
IPS92968	EVT12	dp3	19.6	10.3
IPS14965	CGRD7	dp4	29.4	16.0
IPS92968	EVT12	dp4	32.5	14.1
IPS92997	EVT7	dp4	25.0	12.8
IPS93008	EVT7	dp4	31.0	14.3
IPS92977	EVT7	dp4	20.3	13.2
IPS93015	EVT7	p4	20.5	12.4
IPS93045	EVT7	p4	17.4	11.7
IPS93056	EVT7	p4	19.4	11.3
IPS93027	EVT7	m1	24.8	15.7
IPS93042	EVT7	m1	24.6	17.0
IPS92973	EVT7	m1	25.0	16.5
IPS92977	EVT7	m1	23.9	15.1
IPS93009	EVT7	m2	25.3	16.1
IPS93014	EVT7	m2	24.0	17.2
IPS93019	EVT7	m2	26.2	18.4
IPS93030	EVT7	m2	24.8	17.1
IPS93044	EVT7	m2	27.7	18.7
IPS92973	EVT7	m2	24.7	18.6
IPS92977	EVT7	m2	28.5	17.6
IPS92990	EVT7	m2	26.8	24.5
IPS93043	EVT7	m3	41.9	17.6
IPS92977	EVT7	m3	38.2	16.3
IPS92973	EVT7	m3	41.7	18.4
IPS92987	EVT7	m3	46.5	18.4
IPS92989	EVT7	m3	40.3	16.7
IPS92986	EVT7	P2	16.3	13.0
IPS92996	EVT10	P3	19.4	16.2
IPS92998	EVT7	P3	13.8	19.9
IPS13557	CGRD7	P4	14.7	19.2
IPS92995	EVT10	P4	15.6	21.8
IPS93013	EVT3	P4	19.5	21.4
IPS93020	EVT7	P4	15.8	21.7
IPS92992	EVT10	M1	25.2	25.6
IPS93016	EVT6	M1	27.2	24.2
IPS93017	EVT6	M1	24.7	25.9
IPS93029	EVT7	M1	21.9	26.8
IPS93036	EVT7	M1	21.0	23.8
IPS93047	EVT7	M1	20.6	23.4
IPS92988	EVT7	M2	25.8	25.3
IPS92991	EVT10	M2	28.1	28.8

IPS92994	EVT10	M2	26.9	27.6
IPS93005	EVT7	M2	27.6	28.2
IPS93003	EVT7	M2	24.9	25.1
IPS93022	EVT7	M2	29.3	21.2
IPS93032	EVT7	M2	28.3	27.3
IPS93034	EVT7	M2	23.3	23.7
IPS93038	EVT7	M2	25.7	26.1
IPS20182	CGRD7	M3	30.6	26.0
IPS92993	EVT10	M3	30.4	27.6
IPS92994	EVT10	M3	31.0	27.5
IPS93007	EVT7	M3	27.3	24.7
IPS93011	EVT7	M3	28.0	24.3
IPS93018	EVT7	M3	27.8	26.0
IPS93021	EVT7	M3	29.1	25.7
IPS93023	EVT7	M3	23.5	25.0
IPS93028	EVT7	M3	32.3	24.5
IPS93033	EVT7	M3	27.0	26.5

Table 4. Univariate and multivariate analyses of variance of M2 and M3, metacarpals, and metatarsals from the two main VCS chronologies: 1.07–0.99 Ma (EVT10-12) and 0.86–0.78 (CGRD7-EVT7) (only complete metapodials included). Values with $p < 0.05$ are in bold. Abbreviations: DET, distal epiphysis thickness (maximum); DEW, distal epiphysis width; DT, diaphysis thickness (midshaft); DW, diaphysis width (midshaft); F, F statistic; L, length; Lmax, maximum length; p , significance; PET, proximal epiphysis thickness; PEW, proximal epiphysis width; W, width.

Molars ANOVA		
Variable	F	p
M2: W/L%	0.5891	0.4719
M3: W/L%	0.05129	0.8273
Metacarpals ANOVA		
Variable	F	p
Lmax	18.55	0.00259
PEW	0.03753	0.849
PET	0.1259	0.728
DW	2.737	0.1263
DT	1.765	0.2109
DEW	2.107	0.19
DET	1.017	0.3467
DEW/Lmax%	0.04082	0.8456
Metacarpals MANOVA		
	F	p
	4.009	0.1412
Metatarsals ANOVA		
Variable	F	p
Lmax	0.06263	0.8107
PEW	1.466	0.2513
PET	3.524	0.08726
DW	0.004166	0.9497
DT	0.898	0.3637
DEW	5.131	0.0641
DET	3.995	0.1021
DEW/Lmax%	7.579	0.03316
Metatarsals MANOVA		
	F	p
	2.049	0.3597

Table 5. Measurements (mm) and descriptive statistics of the metacarpals of *Bison schoetensacki* from Vallparadís Estació (EVT) and Cal Guardiola (CGR) layers.

Abbreviations: ABETI, abaxial emicondyle thickness (lateral emicondyle); ABETm, abaxial emicondyle thickness (medial emicondyle); AETI, axial emicondyle thickness (lateral emicondyle); AETm, axial emicondyle thickness (medial emicondyle); DETI, distal epiphysis thickness (lateral trochlear crest); DETm, distal epiphysis thickness (medial trochlear crest); DEW, distal epiphysis width; DDW, distal diaphysis width (above the epiphysis); DT, diaphysis thickness (midshaft); DW, diaphysis width (midshaft); F, female; L, left; Lf, functional length; Lmax, maximum length; M, male; PET, proximal epiphysis thickness; PEW, proximal epiphysis width; PFWI, proximal articular facet width (lateral facet); PFWm, proximal articular facet width (medial facet); R, right.

ID Specimen	Layer	Side	Sex	Lmax	Lf	PEW	PET	DW	DT	DDW	DEW	DETm	DETI	PFWI	PFWm	ABETm	ABETI	AETm	AETI
IPS796	CGRD7	R	M			75.0		50.4	34.6					43.5	29.7				
IPS13547	CGRD7	R	M	254.7	243.9	81.3	47.6	52.9	33.6	78.6	82.4	43.7	43.8	43.3	35.9	32.8	30.1	39.8	38.5
IPS13911	CGRD2	L	M					53.9	36.6										
IPS13928	CGRD7	R	M	250.2	239.4	79.3	47.0	49.55	30.0	72.6	79.3	45.9	43.6	45.9	32.6	36.7	33.8	39.9	39.4
IPS14102	CGRD7	R	F			70.6	42.1							39.0	27.3				
IPS14702	CGRD7	L	F?			73.5	42.2							40.4	29.5				
IPS14815	CGRD7	L	M	242.5		77.0	46.3	51.8	34.6			37.5		44.4	28.0				
IPS14917	CGRD2	L	M	262.7	251	83.9	51.5	52	33.4	78.5	83.4	45.4	41.4	49.7	31.2	33.1	29.9	40.7	40.3
IPS14985	CGRD7	R	M			83.0	50.2							46.1	31.4				
IPS15002	CGRD7	R	M			79.0	46.9	46.5	46.6					44.2	30.8				
IPS92905	CGRD7	R	M											46.2					
IPS92907	EVT10	L	M	230.3	220.9	83.2	47.0	50.2	33.4	75.2	77.1	41.7	41.7	46.2	28.7	31.6	30.5	37.5	37.0
IPS92909	EVT12	R	M			85.1	49.0	48.7	33.4	74.0				45.2	31.2				
IPS92910	EVT12	L	F	230.5	223.6	67.7	41.3	38.42	29.9	62.8	66.7	36.5	36.5	37	24.1		25.7		
IPS92911	EVT7	R	M	246	232.4	78.2	45.3	50.3	33	74.4	79.1			44.3	34.1	29.6	28.4		
IPS92912	EVT7	R	M	239.5	230.4	77.3	45.5	49.3	32.5	74.6	77.0	41.2	41.6	43.1	32.1	32.9	30.7	39.6	38.0
IPS92913	EVT12	L	M			75.8	45.6							42.9	31.5				
IPS107626	EVT12	L	F	228.9		69.5	44.5	36.3	27.9		66.8	35.3	35.0			29.2	26.3	32.3	32.8
IPS107635	EVT12	L	M	238.0	224.01	78.3	45.8	50.4	32.9	75.8	80.1	42.5	41.9	42.1	34.2	32.5	29.9	40.8	39.9

IPS107636	EVT12	R	M	235.7	224.7	79.0	45.0	50.7	33.5	75.6	80.2	42.4	42.6	42.2	31.9	32.2	30.6	40.5	39.0
		Mean		241.7	232.3	77.6	46.1	48.8	33.7	74.2	77.2	41.2	40.9	38.6	39.2	31.6	28.8	37.9	38.4
		Minimum		228.9	220.9	67.7	41.3	36.3	27.9	62.8	66.7	35.3	35	32.7	29	25	20.8	29.5	32.8
		Maximum		262.7	251	85.1	51.5	53.9	46.6	78.6	83.4	45.9	43.8	42.6	43.1	36.7	33.8	40.8	40.3
		SD		10.8	10.4	5.0	2.7	5.0	4.14	4.4	5.9	3.7	3.1	4.2	5.8	3.1	3.5	4.1	2.5
		N		11	9	18	17	15	15	10	10	10	9	7	5	10	11	9	8

Table 6. Measurements and descriptive statistics of the metatarsals of *Bison schoetensacki* from Vallparadís Estació (EVT) and Cal Guardiola (CGR) layers.

Abbreviations: ABETI, abaxial emicondyle thickness (lateral emicondyle); ABETm, abaxial emicondyle thickness (medial emicondyle); AETI, axial emicondyle thickness (lateral emicondyle); AETm, axial emicondyle thickness (medial emicondyle); DETI, distal epiphysis thickness (lateral trochlear crest); DETm, distal epiphysis thickness (medial trochlear crest); DEW, distal epiphysis width; DDW, distal diaphysis width (above the epiphysis); DT, diaphysis thickness (midshaft); DW, diaphysis width (midshaft); F, female; L, left; Lf, functional length; Lmax, maximum length; M, male; PET, proximal epiphysis thickness; PEW, proximal epiphysis width; PFOI, proximal articular facet oblique diameter (medial facet); PFOm, proximal articular facet oblique diameter (lateral facet); R, right.

ID Specimen	Layer	Side	Sex	Lmax	Lf	PEW	PET	DW	DT	DDW	DEW	DETm	DETI	PFOm	PFOI	ABETm	ABETI	AETm	AETI
IPS92906	EVT7	L	F			54.5	56.5	37.5	42.0					46.5					
IPS92930	CGRD7	R	F	280.5	265.6	58.1	53.2	36.6	34.8	59.0	65.0			37.4	37.6				
IPS92931	EVT7	L	F	269.7	253.0	57.0	56.8	39.4	40.3	62.5	63.8	34.5	35.1	39.3	41.1	25.5			
IPS92932	EVT12	R	F	275.2	258.6	57.3	57.5	34.0	37.9	65.3	65.0	41.4	38.7	40.0	36.9	26.5	25.8	32.2	33.7
IPS92933	EVT7	L	M?			62.6	61.6	42.8	44.3					33.5	52.5	30.7	28.5	35.8	37.3
IPS92934	EVT7	R	M?	296.2	275.3	63.8	59.2	42.2	43.0	72.1	69.9	41.9	41	45.5	43.0				
IPS92935	EVT7	R	M?			63.7	62.0	42.0	40.5					44.5	42.8	31.5	28.9	35.0	40.2
IPS92936	EVT7	L	F					40.3	39.5										
IPS92937	EVT12	R	M	300.2	287.4	68.3	66.0	45.5	45	76.5	78	43.6	41.1	46.0	53.3				
IPS92938	EVT10	L	F			61.0	60.0							41.3	42.0	34.4	32.1	39.1	40.4
IPS92939	EVT7	R	F			59.0	55.5	39.9	40.5					37.5	40.0				
IPS107634	EVT12	R	M	279.0	258.3	60.4	60.0	39.5	42.4	70.7	73.6	42.5	41.9	44.0	40.2				
IPS114552	EVT7	L	F	272.3	268.3	53.0	52.7	36.9	34.2	60.9	61.3	39.5	37.0	37.0	39.0	31.9	30.2	38.7	39.6

IPS114553	EVT7	R	F	293.8	287.4	57.0	55.9	37.7	37.7	63.3	61.8	38.9	44	36.4	30.2	27.7	33.0	32.0	
		Mean		283.4	269.2	59.7	58.2	39.6	40.2	65.8	67.3	40.3	39.1	41.3	42.1	30.1	28.8	35.6	37.2
		Minimum		269.7	253.0	53.0	52.7	34.0	34.2	55.0	61.3	34.5	35.1	33.5	36.4	25.5	25.8	32.2	32.0
		Maximum		300.2	287.4	68.3	66.0	45.5	45.0	76.5	78.0	43.6	41.9	46.5	53.3	34.4	32.1	39.1	40.4
		SD		11.7	13.1	4.2	3.7	3.1	3.3	6.9	6	3.1	2.7	4.2	5.5	3.1	2.2	2.9	3.6
		N		8	8	13	13	13	13	8	8	7	6	13	12	7	6	6	6